DAM BREACH STUDY AND INUNDATION MAPPING OF ELEVEN DAMS OWNED BY OKLAHOMA CITY, OKLAHOMA

By

MOLLY SHIVERS

Bachelor of Science in Engineering Physics-Mechanical Engineering

University of Central Oklahoma

Edmond, Oklahoma

2011

Submitted to the Faculty of the

Graduate College of the

Oklahoma State University

in partial fulfillment of

the requirements for

the Degree of

MASTER OF SCIENCE

May, 2016

DAM BREACH STUDY AND INUNDATION

MAPPING OF ELEVEN DAMS OWNED

BY OKLAHOMA CITY, OKLAHOMA

Thesis Approved:

Dr. Daniel Storm

Thesis Adviser

Dr. Todd Halihan

Dr. Jason Vogel

ACKNOWLEDGEMENTS

This study was done in coordination with the US Geological Survey Oklahoma Water Science Center and the City of Oklahoma City, Oklahoma. I would like to thank Jerrod Smith, *US Geological Survey*, Jason Lewis, *US Geological Survey*, and Trevor Grout for their help with mapping and modeling aspects of this project and in preparation of this thesis. I would also like to thank all other persons who helped in the collection of field data.

Name: MOLLY SHIVERS

Date of Degree: MAY, 2016

Title of Study: DAM BREACH STUDY AND INUNDATION MAPPING OF ELEVEN DAMS OWNED BY OKLAHOMA CITY, OKLAHOMA

Major Field: ENVIRONMENTAL SCIENCE

Abstract: The loss of life and property are a hazard downstream of a reservoir in the event of a dam failure. Inundation mapping of dam failures is required in safety documentation when the dam is considered high hazard. In the past, these maps were created as the result of a catastrophic flood; however, the technology is now available for predictive flood modeling. Eleven dams, operated by Oklahoma City, were selected for inundation mapping and modeled using Hydrologic Engineering Center River Analysis System (HEC-RAS) software to simulate two dam breach scenarios: a 75% Probable Maximum Flood (PMF) and a fair weather (sunny day) flood. The model was calibrated using the Lake Overholser model and daily mean discharge data from the USGS stream-gaging stations. A Manning's roughness coefficient of 0.034 was used for the river channel in the calibrated model. The peak stages of six bridges along Lightning Creek were compared to an indirect step-backwater analysis of the May 8, 1993 flood (Tortorelli, 1996). HEC-RAS modeled maximum surface water difference above the streambed for Lightning Creek were within 55% of the maximum surface water difference above the streambed determined by Tortorelli (1996). The predicted flow was only 36 percent of the flow resulting from the estimated May 1993 flood. HEC-RAS flood models were combined with contour maps to determine the inundated areas downstream of each dam. The resulting maps can be used to create emergency evacuation plans.

TABLE OF CONTENTS

LIST OF TABLES

LIST OF FIGURES

Figure Page

CHAPTER I

INTRODUCTION

The US Federal Emergency Management Agency (FEMA) defined a dam as an artificial structure that impedes the flow of water by impounding, storing, or diverting the water (Federal Emergency Management Agency, 2004). The Oklahoma Water Resources Board (QWRB) classified dams based on size and impounded storage area. Small dams are less than 15 m high and impound less than 12 million m^3. Dams that are between 15 m and 30 m high and impound a storage area of between 12 million and 18.5 million m^3 are classified at intermediate. Large dams impound a maximum of 18.5 million m^3 and are over 30 m high (OWRB, 2013). Both FEMA and OWRB have similar hazard classification, however, OWRB is responsible for classifying all of the dams selected for the study. A dam was considered high hazard if there was a potential for the loss of more than six lives and extensive economic loss in the event of a dam failure. Intermediate hazard dams are those dams which will cause no loss of life, but would result in economic loss, environmental damage, and disruption of use of public facilities. Dams classified as low hazard will not result in the loss of life and only low economic losses in the event of a failure (Oklahoma City, 2012). Dams of intermediate or high hazard are required by OWRB to be routinely regulated (OWRB, 2012).

Dam construction locations and the need to manage hazardous consequences in the event of a failure of one of these dams have resulted in the need for emergency action and response plans. These plans, along with hazardous mitigation planning and dam failure consequences (Federal Emergency Management Agency, 2013) state that dam operators carry the full

responsibility of creating evacuation documentation for the surrounding area near a potentially hazardous dam structure. Evacuation and emergency action plans include maps that display areas downstream of a dam that have the potential to be inundated, or flooded, due to a dam failure.

The objective of this study was to develop and validate inundation maps downstream of eleven high hazard dams in Oklahoma City, Oklahoma and near Atoka, Oklahoma using the one-dimensional (1-D) modeling software HEC-RAS. Inundation maps were developed using HEC-RAS dam-breach modeling software. Each high hazard dam had a breach modeled using two methods, a 75% Probable Maximum Flood (PMF) breach as an overtopping failure and sunny-day breach as a piping failure. The results of this study can be used by the City of Oklahoma City to help develop emergency action plans for the inundated areas modeled downstream of these eleven dams.

CHAPTER II

REVIEW OF LITERATURE

The Federal Emergency Management Agency (FEMA) (2004) defined a hazard significant if there was a "potential to cause loss of life or major damage to permanent structures" in the event that a dam was completely or partially damaged. FEMA began actively enforcing the need for emergency action plans to help lessen the effects of these failures. Unfortunately, most evacuation and safety plans were created as a result of prior dam failures. Such was the case for the Buffalo Creek Dam failure in West Virginia (1972) (Davies et al., 1972), and the Teton Dam failure in Idaho (1976) (Seed & Duncan, 1981). The Buffalo Creek Dam failure resulted in 50 million dollars of property damage, 15 million dollars of highway damage, 500 homes lost, 4,000 homeless, and 118 lives lost in a matter of three hours (Davies et al., 1972). Prior to the Teton Dam failure in 1976, no other dam in the world of that height had failed. The dam failed during the initial filling of the Teton Reservoir and contributed to the loss of 14 lives and approximately 400 million dollars in damage (Seed & Duncan, 1981).

Both the Buffalo Creek Dam and Teton Dam failures were modeled and studied using indirect, or post flood, measurements. Indirect measurements lead to more accurate studies because they were based on actual recorded flood wave elevations. However, indirect measurements can only be performed after a flood has occurred and the water has receded. Advances in technology and the introduction of software programs, such as US Army Corp of Engineers' Hydrologic Engineering Center-1 (HEC-1), HEC-2, Hydrologic Engineering Center-River Analysis System (HEC-RAS), University of Alberta's River 1-D programs, National

Weather Service's Streamflow Synthesis and Reservoir Regulation System (SSARR) and FLDWAV, led to a desire and opportunity to predict floods as a result of dam failure that did not previously exist.

2.1 HEC-1 and HEC-RAS Comparison

HEC-1 was a software program that uses the Modified Puls method centered on the transformation of the continuity equation into a finite difference equation and neglects all dynamic effects of a dam breach flood wave (Singh & Snorrason, 1984). HEC-1 was also used on mainframe computers under the DOS operating system. HEC-2, also developed by the US Army Corp. of Engineers, was released in 1966 as "Backwater Any Cross Section", with the ability to model water surface profiles in irregularly shaped channels, and then released again in 1968 as Water Surface Profiles. Subsequent releases were made in 1971, 1976 and 1988 with updated capabilities, including the simulation of culvert hydraulics (HEC, 1990). One of the only differences that encouraged use of HEC-RAS over HEC-2 is its ability to import and export GIS data; an updated version of HEC-RAS allowed the importation and utilization of three-dimensional cross-section data (Tate & Maidment, 1999).

In a study by Hicks and Peacock (2005), a HEC-RAS model of the Peace River in south-central Florida during the 1987 flood was compared to SSARR and River1-D models. Hicks and Peacock (2005) discovered that the HEC-RAS predicted discharge hydrographs of the flood wave were comparable to the other software programs, and possibly more accurate considering the channel shape was estimated and the HEC-RAS model was not calibrated. HEC-RAS and River1-D models were found to have similar prediction errors, i.e. ± 5%, while HEC-RAS more accurately approximated the wave speed compared to SSARR. The HEC-RAS model did, however, slightly overestimate the maximum water level of the flood wave; however, overestimating was better than underestimating for hazard prediction.

Both the HEC-RAS and FLDWAV models were principally similar because both programs were based on the Saint-Venant equations. Unlike HEC-RAS, the FLDWAV software contained options for modeling mixed-flow regimes, i.e. where the flow changes between supercritical and subcritical flow. HEC-RAS did, though, contain more options for dealing with lateral flows, i.e. tributaries, low-lying wetlands, etc., more realistic cross sections, and was more computationally efficient with inactive flow areas. Zhou, Judge, and Donnelly (2005) found that FLDWAV was capable of modeling complex dam breaches, but was not as "user friendly" as HEC-RAS, which was a windows program with superior pre- and post-processing abilities, flood animation demonstrations, and easier to adjust input modifications.

HEC-RAS was capable of both steady-state and unsteady-state 1-D breach analysis (HEC, 2010a) HEC-RAS computed flood velocities, maximum flood wave levels, flood profiles and possible inundated areas when streamflow, channel geometry, and geometry of bridges or obstructions was available. Based on the Saint-Venant equations, HEC-RAS had three general steps for dam breach analysis: (1) approximation of the manner of failure, (2) calculation of the outflow hydrograph resulting from the dam breach, and (3) flood wave route through the downstream river reach (Fread, 1977). HEC-RAS also provided an option to export spatial information to GIS to estimate the path of the flood wave. Although HEC-RAS predicted the wave along the reach, if GIS was not used, the cross sections were displayed arbitrarily in space and not geographically referenced. By exporting HEC-RAS predictions to GIS, dam breach models can be delineated along the area most likely to be inundated (FEMA, 2004). In the Federal guidelines for inundation maps provided by FEMA (2013), the suggested uses for these maps included dam safety, hazard mitigation, consequence evaluation, and Emergency Action Plans (EAPs).

2.2 Initial and Boundary Condition Modeling

A breach was defined by Fread (1977) as an opening that forms in a failed dam. The water impounded behind the dam escapes through the opening and results in a flood. Unlike floods that are products of excess rainfall and runoff, breach floods propagate downstream rapidly, (Rendon, Ashworth, & Smith, 2012) varying from a few minutes to several hours or days after the breach until the maximum water elevation is reached. Eighty-seven percent of dams in the United States of America (USA) are earthen dams (FEMA, 2013), and thus piping dam failures are a realistic threat due to internal erosion, shifting soil and the formation of cavities and voids (Seed & Duncan, 1981). Other dam failures may result from dam overtopping (Davies et al., 1972; FEMA. 2013) and eroding the backside, or downstream side, of the dam.

Not only is the type of dam failure needed to properly model the system, but also the time to failure and the width of the breach opening. Breach time to failures depend heavily on dam materials. Earthen dams usually reach complete failure in approximately one to two hours, while concrete dams typically have a greater time to failure (Singh & Snorrason, 1984). The dam breach width impacts the output hydrograph and the time to maximum water level and is indirectly related to the flood duration (Ponce et al., 2003). Equations by Van Thun and Gillette (1990) and Froehlich (2008) were developed to predict both time to failure and dam breach widths. Froehlich's method for determining failure time produced the smallest uncertainty compared to other dam breach methods with values ranging from ± 0.6 to ± 1 order of magnitude (Wahl, 2014). Wahl (2014) also found that the uncertainty of Froehlich's method for calculating peak flow (± 0.3 orders of magnitude) was again smaller than the uncertainty of other methods (± 0.5 to ± 1 order of magnitude).

Outflow hydrograph predictions are highly dependent upon the location of the breach within the dam structure, the cross sectional geometry, and Manning's roughness coefficients. Even cross sections in HEC-RAS from Geographic Information System (GIS) derived data are

sensitive to the assumed initial breach locations (Wahl, 2014), because the breach location determines the flood wave path as it propagates downstream. If a breach occurs on one side of a large dam as opposed to the other, there is the possibility that different areas along the cross sections, having different elevations, will be inundated downstream. HEC-RAS has advanced abilities to use digital elevation data to estimate river cross sections; however, these elevation data are often collected several years or decades prior to the modeling study. For example, digital elevation data for a dam breach analysis in South Dakota was developed in 2007, but the study was not completed until 2011 (Hoogestraat, 2011). Cross-sections are currently assumed to be trapezoidal and invariant in HEC-RAS (Walder & O'Connor, 1997), which ignores changes that occur between the time data were collected and the study, and changes that occur during the breach itself.

Manning's roughness coefficients, depicting the channel and floodplain hydraulic roughness, were also assumed invariant in HEC-RAS, disregarding the fact that they were highly irregular and variable (Timbadiya et al., 2011). Timbadiya et al. (2011) found that multiple Manning's roughness coefficients per cross section produced a more accurate model; HEC-RAS allowed up to 20 roughness values per cross section and assumed the same values for similar topographical features. Manning's roughness coefficients for each feature were assumed constant and independent of changes in channel surface, location of weirs or flood retardant structures, or changes in floodplain surfaces, e.g. rural to urban (Timbadiya et al., 2011).

2.3 HEC-RAS Models for Flood Prediction

The US Forest Service (USFS) collaborated with the US Geological Survey (USGS) to simulate floods for five reservoirs in Colorado: Balman Reservoir, Crystal Lake, Manitou Park Lake, McGinnis Lake, and Million Reservoir (Stevens & Hoogestraat, 2013). The simulations were used as a means of classifying the hazard at each dam as high, significant or low. An overtopping failure was selected as the breach method for all five reservoirs using 100- and 500-

year recurrence floods, and the probable maximum precipitation (PMP), the greatest amount of precipitation to fall during an event at a particular location, applied over a 24-hour period. A 100-year recurrence flood is defined as the probability of flow reaching a certain magnitude once in 100 years (USGS, 2016). The same can be said for a 500-year flood. Recurrence floods are based on flow only and occur when the dam is still in place. The Balman Reservoir, Manitou Park Lake, and McGinnis Lake Dams were all classified as low hazard dams due to the low risk of loss of life or property. The Crystal Lake and Million Reservoir Dams hazard classification, however, was deemed significant due to the potential of property loss or damage in the predicted flood areas (Stevens & Hoogestraat, 2013).

A similar study by the USFS was conducted to predict potential floods for four reservoirs located in the Black Hills National Forest, South Dakota. The 100- and 500-year recurrence flood and the 24-hr PMP flood for each reservoir were modeled for Iron Creek Lake, Lakota Lake, Mitchell Lake, and Horsethief Lake (Hoogestraat, 2011). Due to the remote location and lack of permanent structures downstream, Iron Creek Lake, Lakota Lake, and Mitchell Lake were classified as low hazard dams. The fourth reservoir, Horsethief Lake, was classified as a high hazard owing to its location upstream of a major campground and the possible destruction of a major highway (Hoogestraat, 2011). Although three of the four reservoirs were deemed low hazard dams, predicted inundation maps in national parks were useful for determining the potential destruction of protected wildlife habitats and the funds needed for rehabilitation (Rydlund, 2006).

Other agencies in charge of dam operations are also showing interest in this type of modeling, such as the City of Lawton, Oklahoma. Rendon, Ashworth, and Lewis (2012) recently completed an inundation study of Lake Ellsworth and Lake Lawtonka, which were located near Lawton. Two breach scenarios, overtopping due to a PMP event and sunny day, were modeled for the two reservoirs. The predicted inundated areas included wastewater and water treatment plants,

local service offices and several heavily traveled roads (Rendon et al., 2012). The City of Lawton, Oklahoma report was used as a template for the current study area dams owned by the City of Oklahoma City, Oklahoma.

CHAPTER III

METHODOLOGY

Software described in the Review of Literature was all acceptable for predictive flood modeling. However, HEC-RAS was selected due to its ability to utilize the Microsoft Windows® operating system and export predictions to GIS. To comply with the recommendations set forth by FEMA dam safety (FEMA, 2004) and flood inundation map guidelines (FEMA, 2013), inundation maps were needed by the City of Oklahoma City. Physically breaching the targeted dams within Oklahoma City's control was unrealistic; bringing about the necessity for predictive inundation scenarios using the dam-breach software HEC-RAS. The methods below describe the approach taken to model the two "most likely mode[s] of dam failure" (FEMA, 2004) and the subsequent predicted inundation maps that resulted from the dam breach models of eleven selected dam structures owned by Oklahoma City, Oklahoma. All of the dam structures were owned and operated by Oklahoma City and were located within city limits, with the exception of Atoka Reservoir dam, which was located in Southeastern Oklahoma near the town of Atoka.

3.1 Input Data

3.1.1 Reservoir Data

This study was conducted based upon the City of Oklahoma City's need for updated flood hazard plans. The eleven dams were selected by the City of Oklahoma City based on their locations and include: Atoka Reservoir, Dolses Youth Park Lake, Dry Creek Detention Reservoir, Lake Hefner, Lake Overholser, Lightning Creek Holding Pond A, Lightning Creek Holding Pond

C, Northeast (Zoo) Lake, Northwest Oklahoma City Sludge Lagoon, Stanley Draper Lake, and Will Rogers Holding Pond (Figures 1 and 2).

Characteristics of each dam structure are detailed in the following sections with information provided by Phase I Clean Lakes Reports (OWRB, 1978a, b, c, 1979a, b, c, d). Structural information for Atoka Reservoir and Dolese Youth Park Lake was provided by the USGS (2013) and the City of Oklahoma City (2014).

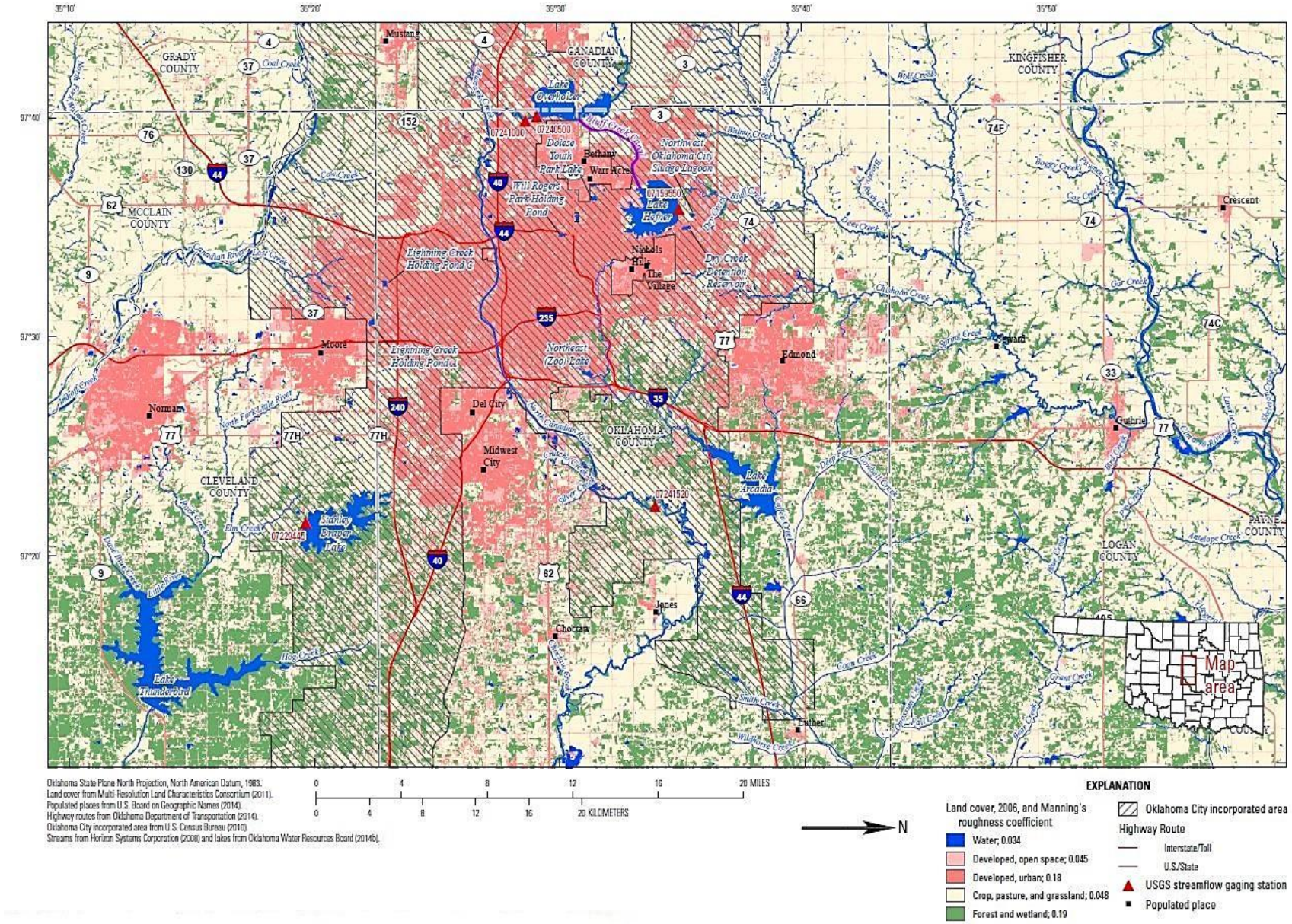

Figure 3.1. Location map of ten of the eleven modeled reservoirs in the Oklahoma City, Oklahoma area, Manning's roughness coefficients, and US Geological Survey stream-gaging stations. Figure Courtesy of US Geological Survey (Shivers et al., 2015).

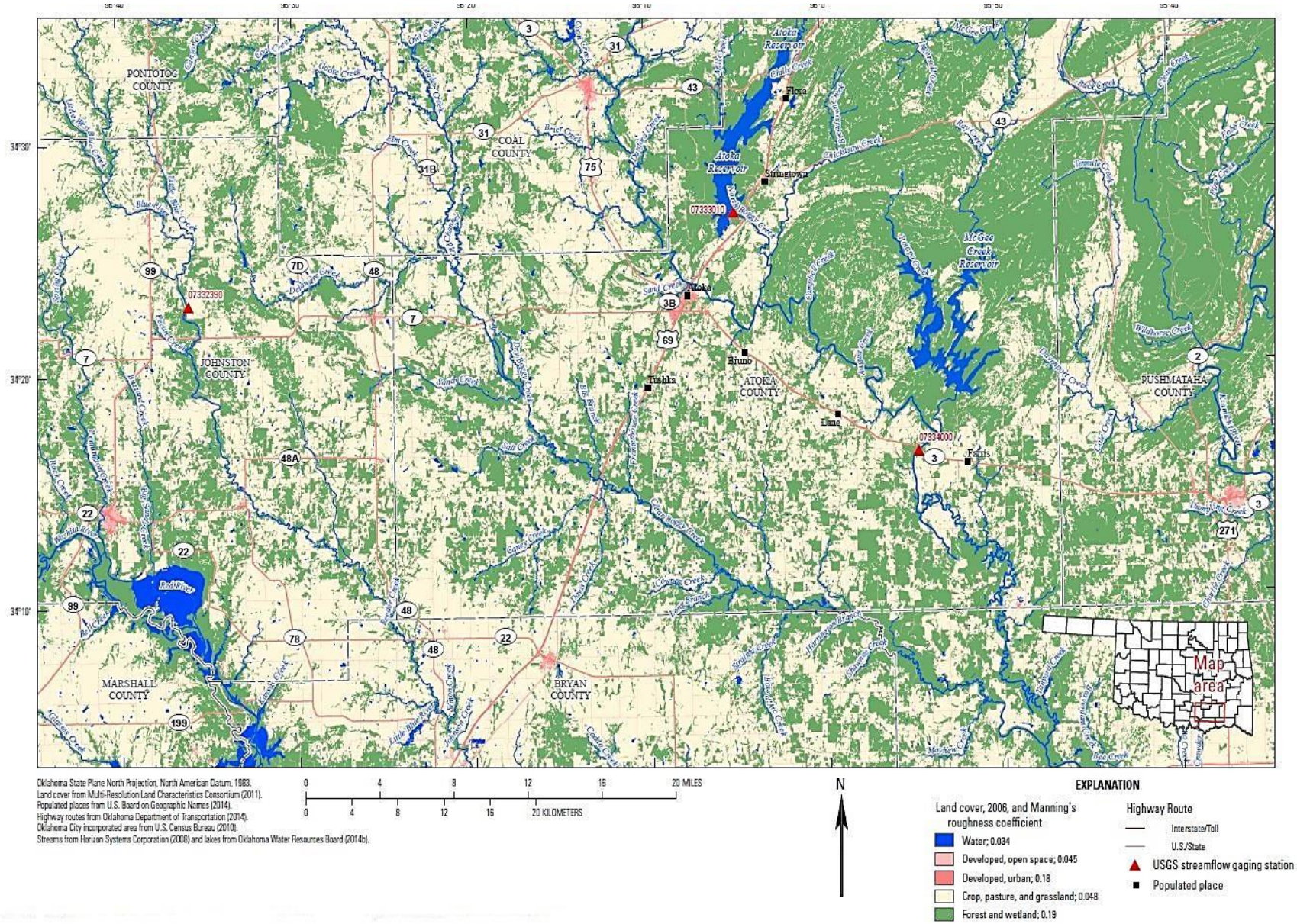

Figure 3.2. Location map of Atoka Reservoir near Atoka, Oklahoma, Manning's roughness coefficients, and current US Geological Survey stream-gaging stations. Figure courtesy of US Geological Survey (Shivers et al., 2015).

3.1.1.1 Atoka Reservoir

Atoka Reservoir was located approximately 161 kilometers (km) (100 miles, mi) southeast of Oklahoma City and six km (4 mi) northeast of Atoka, Oklahoma. The earth-filled dam was constructed in 1959 by the City of Oklahoma City (USGS, 2013) with a maximum pool elevation of 184 meters (m) (602.5 feet, ft.) and a normal pool elevation of 180 m. The reservoir stores 152 million cubic meters (m3) (590 ft.) (North American Vertical Datum of 1988 [NAVD 88]). The 152 million cubic meters (m3) (123,500 acre-feet, acre-ft.) (USGS, 2013) of water stored in Atoka Reservoir was pumped to Stanley Draper Lake by the City of Oklahoma City as a secondary water supply for southern Oklahoma City.

3.1.1.2 Dolese Youth Park Lake

Historically, Dolese Youth Park Lake was a mining site that was donated to Oklahoma City and is now part of a municipal park system. The 79,700 m^2 (19.7-acre) reservoir was impounded by a concrete and earth-filled dam for recreational purposes. In the case of a dam breach, the water from Dolese Youth Park Lake flows north into Lake Hefner (City of Oklahoma City, 2014).

3.1.1.3 Dry Creek Detention Reservoir

The Dry Creek Detention Reservoir was built in 1978 in northwestern Oklahoma City. The elevation at the top of the dam was 353 m (1,157 ft., NAVD 88). Two lateral concrete drains divide the reservoir to carry runoff into a drain on the east side. The earthen dam was supplemented with an auxiliary spillway. The 539 m (1,770 ft.) long by 107 m (350 ft.) wide detention pond was dry for most of the year and collected runoff from the nearby areas (OWRB, 1978a).

3.1.1.4 Lake Hefner

The City of Oklahoma City built Lake Hefner in 1947 as a water source for Oklahoma City. The reservoir was located northwest of downtown Oklahoma City and was filled using

diversion gates on the North Canadian River near Lake Overholser. Lake Hefner dam, a five km (three mi) long earthen structure, stands at an elevation of 34 m (112 ft.) and holds a maximum storage of 132 million m^3 (107,000 acre-ft.) of water (USGS, 2013).

3.1.1.5 Lake Overholser

Lake Overholser was completed in 1917 west of downtown Oklahoma City. The dam was damaged in 1923 and rebuilt in 1924. The dam structure was constructed of concrete with a 384 m (1,260 ft.) long, 19 m (61 ft.) high spillway and a low earthwork five km (three mi) in length. The reservoir was controlled by 23 Tainter gates and an unrestrained spillway (OWRB, 1979a). The maximum storage capacity for Lake Overholser was 21.1 million m^3 (17,100 acre-ft.) (NSVD 88, USGS, 2013). Lake Overholser was supplied by the North Canadian River via a concrete rollover dam almost three km (two miles) north of the spillway.

3.1.1.6 Lightning Creek Holding Pond A

Lightning Creek Holding Pond A was located in south Oklahoma City and was completed in 1977 (OWRB, 1979b). Holding Pond A was constructed to contain runoff during rainfall events and was normally dry. The holding pond has a storage capacity of 667,000 m^3 (541 acre-ft.) and was impounded by an earth-filled dam. A manual release gate regulated a concrete channel during flood events. Holding Pond A was not constructed with a spillway, but had a naturally occurring spillway in the southeast corner that permits water flow above 394 m (1,292 ft.) to circumvent the holding pond (OWRB, 1979b).

3.1.1.7 Lightning Creek Holding Pond C

Completed in 1977, Holding Pond C was constructed to contain runoff during rainfall events. The holding pond had a storage capacity of 231,000 m^3 (187 acre-ft.) and a dam structure that was five meters (16 ft.) above the streambed (City of Oklahoma City, 2014).

3.1.1.8 Northeast (Zoo) Lake

The Northeast (Zoo) Lake was located in northeastern Oklahoma City and was impounded by an earthen dam. The dam structure impounded 987,000 m^3 (800 acre-ft.) of water at an elevation of 335 m (1,098 ft.). The reservoir was built on a tributary of the Deep Fork Creek and was constructed for recreational purposes (OWRB, 1978b).

3.1.1.9 Northwest Oklahoma City Sludge Lagoon

The Northwest Oklahoma City Sludge Lagoon was located north of Lake Hefner and was used by the City of Oklahoma City to recycle and treat water coming from the Lake Hefner treatment plant. The lagoon has a maximum capacity of 497,000 m^3 (403 acre-ft.) with an earthen dam standing 9 m (30 ft.) high (OWRB, 1978c).

3.1.1.10 Stanley Draper Lake

Stanley Draper Lake was located southeast of downtown Oklahoma City and was constructed in 1962 as a water supply for the residents of southern Oklahoma City. The earthen dam had an elevation of 366 m (1,201 ft.) and was about 2,103 m (6,900 ft.) long (OWRB, 1979c). Water was transferred to a treatment plant via an intake tower housing two 1.5 m pipes and an open ditch system. The maximum reservoir capacity for Stanley Draper is 183 million m^3 (148,000 acre-ft.) (USGS, 2013) and received supplemental water from Atoka Reservoir by way of a pipeline.

3.1.1.11 Will Rogers Park Holding Pond

Will Rogers Park Holding Pond was completed in 1967 to impound runoff during flood events. The holding pond remained dry for most of the year and was impounded by an earthen dam 320 m (1,050 ft.) long. A natural spillway along the pond has an elevation of 363 m (1,192 ft.) and was accompanied by paved road that serves as a spillway at an elevation on 364 m (1,195 ft.) A manual gate can also be opened to release water from the 398,000 m^3 (323 acre-ft.) holding pond (OWRB, 1979d).

3.1.2 Hazard Classification

Atoka Reservoir was not within the city limits of Oklahoma City, but was in close proximity to the town of Atoka, Oklahoma, therefore classifying it as high hazard. Lake Hefner, Lake Overholser, and Stanley Draper Lake all contained dams that were considered high hazard due to their location and the height of the dam from the natural streambed. Dolese Youth Park Lake, Lightning Creek Holding Pond A, Lightning Creek Holding Pond C, and Northeast (Zoo) Lake dams were smaller structures, but were located in heavily populated areas and would result in significant loss of life and property in the event of a dam failure. Dry Creek Detention Reservoir and Will Rogers Park Holding Pond were unique in the fact that during sunny day conditions, no water was impounded and the area was used for recreational purposes. However, if failure occurred during a large rainfall event, it would be hazardous to areas downstream. The Northwest Oklahoma City Sludge Lagoon Dam did not meet the height requirement either, but the lagoon was a waste production disposal location and could negatively impact downstream water supplies if a dam failure occurred (FEMA, 2004).

3.1.3 Physical Surveying of Structures and Obstructions

Objects that could impede the course or timing of the flood wave were added to the model to increase the model accuracy. Identified vehicle bridges, railroad bridges, pipelines, and any other transecting structures were physically surveyed and incorporated into the model. The survey included measurements of the width and length of the bridge, the height of the bridge deck, low chord, and handrail. The number of piers, their location in relation to the left and right end of the bridge, and their diameter were also recorded. All measurements obtained were taken using a steel engineer's tape with an accuracy of approximately 0.03 m per 30 m (0.1 ft. per 100 ft.) ("Steel Tape Line Accuracy", n.d.). Photographs were taken upstream and downstream of all identified structures for visual conformation of the structure and cross-sections used in the model.

A Trimble™ Pathfinder ProXH receiver with sub-centimeter accuracy (Trimble Navigation Limited, 2003) was positioned on the center of each structure or obstruction to acquire upstream and downstream elevation data. These elevation data were used to characterize the bridges and obstructions in HEC-RAS. Elevation data recorded by the ProXH was converted using Trimble™ Geomatics Office Software (Trimble Navigation Limited, 2005) to sea level datum with reference to the National Geodetic Survey's network of Continuously Operating Reference Stations network (National Geodetic Survey, 2011). The Trimble™ ProXH must visibly locate orbiting satellites to obtain elevation data; due to this operating limitation, elevations for locations with an obstructed view were achieved near, instead of directly on, the structure.

3.1.4 Stream Centerlines and Cross Sections

The Hydrological Engineering Center Geographical River Analysis System (HEC-GeoRAS) was a toolbox within ESRI ArcGIS™ software that allowed processing and referencing geospatial data (Hydrological Engineering Center, 2011). A bare earth digital elevation model (DEM) was created using light detection and ranging (LiDAR) data, which was used as the base layer. LIDAR was an aerial laser profiling survey that defined elevations of the ground surface and other land or man-made features (Barlow et al., 2008). Oklahoma City provided the LiDAR data, which were collected during leaf-off conditions having a 0.6 and 0.2 m (2.0 and 0.6 ft.) horizontal and vertical accuracy, respectively. Two surveys were completed around Oklahoma City; approximately 357 km^2 (138 mi^2) in 2007 for the City of Norman (City of Norman, 2007) and 1,950 km^2 (752 m^2) in 2004 for Oklahoma City (City of Oklahoma City, 2004). Elevation data for the area surrounding Atoka Reservoir were obtained from a 2007 Interferometric Synthetic aperture radar (IfSAR) survey (Intermap Technologies, Inc., 2014). The DEM was created from approximately 575 km^2 (222 mi^2) of survey data with a horizontal and vertical accuracy of 4 and 2 m (16.4 and 6.6 ft.), respectively. All other elevation data needed to create

the base layer were obtained from the National Elevation Dataset (USGS, 2014) with an accuracy of 10 m (33 ft.) in the horizontal direction and less than 3 m (9.8 ft.) in the vertical direction (Gesch et al., 2014).

Sonar bathymetric survey data were obtained from the Oklahoma Water Resources Board (OWRB) for Arcadia Lake, Atoka Reservoir, Lake Hefner, Lake Overholser, Lake Thunderbird, and Stanley Draper Lake with a vertical accuracy of 0.4 m (1.3 ft.) (OWRB, 2014). Reservoirs in watersheds pertinent to the models that did not have pre-existing bathymetric data were modeled as storage areas in HEC-GeoRAS. A stream base layer was then constructed from the LiDAR, IfSAR, and bathymetric survey data.

Next, a series of line themes starting at the dam structure were created using the HEC-GeoRas toolbox to represent the stream centerline, which identified the path of the stream at the time the survey was completed. The flow path centerlines were used to calculate reach lengths from one cross section to another. Left and right main channel bank lines were also added and used to calculate the wetted perimeter of the river.

Cross-section point elevation data were obtained using HEC-GeoRAS. A cross-section points filter tool was used to reduce the number of points per cross section to less than 500 due to HEC-RAS modeling limitations. The stream cross sections were identified and positioned perpendicular to the stream centerline based on the river geometry and the structure location (Samuels, 1989).

3.2 Model Calibration

Lake Overholser was selected to calibrate the HEC-RAS model since it was the only reservoir with downstream gaging stations. Daily mean discharge data from the USGS stream-gaging stations North Canadian River below Lake Overholser near Oklahoma City, OK (07241000) and North Canadian River at Britton Road at Oklahoma City, OK (07241520) were

used. Steady-state simulations were conducted using 2, 5, 10, 25, 50, 100, and 500-year recurrence interval rainfall events and were compared with measured hydrographs collected using the stream-gaging stations. Manning's roughness coefficients were manually adjusted until the observed stream-gage and the calibrated model peak flow hydrographs agreed within five percent relative error. The calibrated Manning's roughness coefficients were used for all the HEC-RAS models.

3.2 Manning's Roughness Coefficient

Additional graphical themes were added for reservoir storage area for reservoirs without bathymetric surveys and land cover using the HEC-GeoRAS toolbox. The land-use theme was the 2006 National Land Cover Dataset (NLCD) (Multi-Resolution Land Characteristics Consortium, 2011). To simplify the model, land cover data were reduced to five classifications with a Manning's roughness coefficient for each classification to compensate for the HEC-RAS limitation of 20 coefficients per stream cross section. The reduced land cover classifications were used to classify Manning's roughness Coefficient (n) for the river channel and flood plain. Manning's roughness coefficients characterized the amount of friction or resistance to flow created by the channel and floodplain landscape (Acrement & Schneider, 1989), and were estimated using the methods of Barnes (1967), Arcement and Schneider (1989) and Coon (1998).

Calibrated Manning's roughness coefficients were selected based on a sensitivity analysis performed in HEC-RAS of Lake Overholser and the USGS stream gaging stations at North Canadian River below Lake Overholser near Oklahoma City, OK (07241000) and North Canadian River at Britton Road at Oklahoma City, OK (07241520). Calibrated Manning's roughness coefficients were assigned to the other reservoir river channels and floodplains based on the land classification. After topographic data and additional themes were established, these data were exported to HEC-RAS for dam breach modeling. Hec-GeoRAS was used again after

the completion of the dam failure simulation in HEC-RAS for post processing and conversion to readable GIS files for inundation mapping.

3.4 HEC-RAS Modeling

All elements created in HEC-GeoRAS were imported into HEC-RAS, which conducted a 1-D dynamic, unsteady-flow model as well as other river analysis computations. Cross sections numerically labeled by HEC-GeoRAS were imported into HEC-RAS with their associated elevation data. The physical measurements made of each bridge were specified in HEC-RAS. Elevation data collected using the ProXH were also used to determine the height of the bridge deck in relation to the surrounding topography, which was necessary to determine the amount of flow obstructed by the bridges. The dam structures were defined using the Phase I reports provided by Oklahoma City (OWRB, 1978a,b,c, 1979a,b,c,d), which contained original information pertaining to the construction of the dam. This information was corroborated using the elevation data from ProXH.

The two most common modes of dam failure were classified as an overtopping failure and a fair-weather, or sunny day, failure (FEMA, 2013). An overtopping failure occurs when the dam reaches maximum water elevation capacity, which allows the water to flow over the top of the dam structure. This type of failure most often occurs in conjunction with a large rainfall event. However, unlike an isolated precipitation flood event that develops slowly, a dam failure flood occurs rapidly and the flood wave moves quickly downstream (Rendon, Ashworth, & Smith, 2012). The sunny-day flood takes place during non-precipitation events and is the result of a piping or other structural failure. Piping failures most often are caused by errors during construction, mismanagement of the volume of water impounded behind the dam, or structural unsoundness contributing to internal erosion. Internal erosion begins when a tiny hole appears in the dam and continues to enlarge due to the increasing pressure of the water until the entire dam fails (Seed & Duncan, 1981).

Two dam breach methods were used. The first was an overtopping failure based on a Probable Maximum Flood (PMF) defined as the largest possible flood at that location, and modeled when the maximum amount of precipitation possible has fallen. The overtopping breach was modeled using a 75% PMF to comply with OWRB requirements (Oklahoma Water Resources Board, 2011). A second method, a piping failure, was modeled during sunny day conditions, i.e. a simple dam failure at normal reservoir pool capacity with no precipitation. The time to failure and dam breach bottom widths were calculated using two methods, Van Thun and Gillette (1990) and Froehlich (2008). The bottom width of the breach for each dam was calculated using one of the two following equations, Von Thun and Gillette (1990)

$$B = 2.5h_w + C_b \tag{1}$$

where B is the average dam-breach-bottom width, m, h_w is the volume of water above the dam-breach invert at time of failure, m^3, and C_b is an offset factor, which is a function of reservoir volume, or Froehlich (2008)

$$B = C_1 K V_w^{0.32} H_b^{0.04} \tag{2}$$

where C_1 is a constant, 0.27, K is an overtopping multiplier, with 1.3 being used for overtopping and 1.0 being used for a piping failure, V_w is the volume of water above the dam-breach invert at time of failure, m^3, and H_b is the height of the dam breach, m. Breach times to failure were calculated by simultaneous solving the following equations, Von Thun and Gillette (1990)

$$\text{For highly erodible dams } t = B/(4h_w + 61) \tag{3}$$

$$\text{For erosion-resistant dams } t = B/(4h_w) \tag{4}$$

where t is the time to full failure, in hours, and Froehlich (2008)

$$t = C_2 * \sqrt{\frac{V_w}{gH_b^2}} \tag{5}$$

where C_2 is a constant, 63.2, and g is the gravitational acceleration, 9.81 m/s^2.

Along with breach parameters for each reservoir, input hydrographs, initial flows and friction slope boundary conditions for each river reach were required. Input hydrographs for all dams, except Atoka Reservoir and Dolese Youth Park Lake, were based on Phase I dam breach inspection reports (OWRB, 1978a, b, c, 1979a, b, c, d). Lightning Creek Holding Pond C was used as a drainage-area ratio reference site for estimating the 75% PMF flow rates for Dolese Youth Park Lake. The 75% PMF was calculated by multiplying a 0.38 drainage area ratio times the 75% PMF flow for Lightning Creek Holding Pond C (OWRB, 1979c). The USGS gaging station Blue River near Connerville, OK (07332390) had a 420 km^2 (162 mi^2) drainage area, which was similar to the Atoka Reservoir drainage area 443 km^2 (171 mi^2) and thus, was used to estimate the 75% PMF flow rates. The potential peak discharge of Atoka Reservoir was estimated based on Tortorelli and McCabe (2001). The estimated discharge was then combined with a flow hydrograph for the Blue River near Connerville, OK streamflow gaging station.

Initial flows were determined using iterative model runs and were sustained at or lower than 10% of the maximum peak flow of the model as suggested in the BOSS DAMBRK User's Manual (1999). Both Lake Overholser and Atoka Reservoir initial flows were set to 5 and 30% probability, respectively, of flow exceedance recorded at downstream USGS gaging stations (North Canadian River below Lake Overholser near Oklahoma City, OK, 07241000; Muddy Boggy Creek near Farris, OK, 07334000). Friction slope boundary conditions were estimated based on the slope of the channel at the downstream end of the modeled river reach. Input hydrograph sources, initial flow values, and friction slope boundary conditions are given in Table 3.1.

Table 3.1 Hydrologic Engineering Centers River Analysis System (HEC-RAS) input parameters for dam breach modeling for 75% Probable Maximum Flood (PMF) and sunny–day analysis for eleven reservoirs near Oklahoma City, Oklahoma. [m^3/s, cubic meters per second]

Reservoir	Input Hydrograph Source	Initial Stream Flow (m^3/s)	Friction Slope Boundary Condition (m/m)
Atoka Reservoir	Blue River near Connerville	8.50	0.00001
Dolese Youth Park Lake	Drainage area ratio Method	5.66	0.00006
Dry Creek Detention Reservoir	Phase I Report	0.99	0.00010
Lake Hefner	Phase I Report	42.5	0.00004
Lake Overholser	Phase I Report	22.7	0.00040
Lightning Creek Holding Pond A	Phase I Report	1.42	0.00080
Lightning Creek Holding Pond C	Phase I Report	1.42	0.00080
Northeast (Zoo) Lake	Phase I Report	8.50	0.00023
Northwest Oklahoma City Sludge Lagoon	Phase I Report	7.08	0.00090
Stanley Draper Lake	Phase I Report	17.0	0.00200
Will Rogers Park Holding Pond	Phase I Report	5.66	0.00100

HEC-RAS modeled the flood by inundating the stream cross section from the bottom up, i.e. low elevation cross sections were flooded first. However, not all areas of low elevation were connected to the main river reach; these areas of equal or lower elevation than the river channel were ignored by placing fictional levees or ineffective flow lines between them and the main channel. Levees were used to allow the main channel to fill with water before flowing into these low areas, and ineffective flow lines were used near bridge entrances and exits and other structures to simulate the flow constriction at bridge piers. Tributaries were not modeled in HEC-RAS to ensure model stability; the water elevation at the tributary confluences was modified based on the map contour lines to account for backwater effects.

3.5 Sensitivity Analysis

A sensitivity analysis was also conducted for the breach parameters, dam-breach-bottom width and time to full failure, and Manning's roughness coefficients. Dam-breach-bottom width and time of full failure were calculated using Froehlich's and Von Thun and Gillette's equations described earlier. Both sets of parameters for each reservoir were assessed for model stability and the most conservative estimate was used. Manning's roughness coefficients of 0.9 and 1.1 times the modeled values of the 75% PMF Lake Overholser model were used to determine the difference in the maximum water surface elevation and time to peak at each bridge.

3.6 Damage Assessment

A cost of damage assessment was conducted for the sensitivity model inundated area. An average Oklahoma City population density of 2,600 people/km^2 ("Oklahoma City, Oklahoma", n.d.) and 2.55 persons per household ("Quick Facts: Oklahoma City, Oklahoma", 2010-2014) were used to estimate the number of homes per unit area of 1,020 homes/km^2. An estimated cost for a 1.2 m (4 ft.) of water damage, which was the greatest water depth the simulation allowed, was $40,000 assuming a representative 93 m^2 (1000 ft^2) home ("Cost of Flooding", n.d.). The assumption was made that homes in the surrounding area are an average size of 93 m^2 (1000 ft^2).

Therefore, the damage cost per area was estimated as 40.8 million dollars per km^2, which was used to estimate the total damage cost.

3.7 Flood-Inundation Maps

Eleven dam structure failures and the resulting flood wave elevations and locations were predicted using HEC-RAS based on physical measurements of dam structures and bridges combined with aerial light detection and ranging data. Aerial light detection and ranging data use laser surveying technology to determine the location and orientation of an object in space (Hu, 2001).

HEC-GeoRAS was used for post processing of the models and to generate the predicted flood inundation maps. The HEC-RAS models were exported and combined with detailed street and contour maps of Oklahoma City (City of Oklahoma City, 2004; City of Norman, 2007; Intermap Technologies, Inc., 2014; US Geological Survey, 2014) to display locations inundated by the floodwaters.

3.8 May 1993 Flood Comparison

The peak stage predicted at six bridges along Lightning Creek was compared to an indirect step-backwater analysis of the same six bridges by Tortorelli (1996). A flash flood occurred on May 8, 1993 in southwestern Oklahoma City following a three-hour rain event depositing 13 cm (5 in) that flooded several tributaries, including Lightning Creek. This rain event was 0.25 cm (0.1 in) less than the 100- year recurrence rainfall event. The flood peak high-water marks from debris and mud on trees, fence posts, and other structures were documented and compared to the step-backwater analysis using Water Surface Profile Computations (WSPRO) by Tortorelli (1996).

CHAPTER IV

RESULTS AND DISCUSSION

4.1 Method Results

LiDAR elevation data were used for majority of the study, which had accuracy less than 0.3 m. The accuracy using IfSAR was approximately 2.1 m. The lower accurate IfSAR data were used for the Atoka Reservoir model due to the greater terrain slope. Areas of greater terrain slope, i.e. the Atoka model floodplain with average slopes of two percent, yielded greater differences in vertical elevations compared to lesser sloped terrain 0.1 percent for the Oklahoma City area models (Bales and Wagner, 2009). A 0.1 m elevation change at 0.1 and 2 percent yielded an increase in horizontal inundated distance by 5 and 100 m, respectfully. All tables containing peak water-surface elevation display the elevation accurate to a hundredth of a meter for consistency purposes. However, peak water-surface elevations for the Atoka Reservoir model should be considered with ±2.1 m accuracy.

Calculated breach parameters for each method and dam are given in Table 4.1. Each parameter was evaluated using both Froehlich (2008) and Von Thun and Gillette (1990) equations and selected based on model stability. Note that some breach parameters outside of the calculated values were required to stabilize the model. Perimeters for the Atoka Reservoir breach were estimated using the BOSS DAMBRK user's manual (BOSS, 1999) due to the lack of available dam specifications.

Table 4.1. Hydrologic Engineering Centers River Analysis System (HEC-RAS) dam breach parameters used for the selected dams in Oklahoma City, Oklahoma and near Atoka, Oklahoma. [m, meters; hr, hours; values outside of the range of calculated parameters are in bold type]

Reservoir	Breach Parameter Equation	Breach Bottom Width (m)	Time to Failure (hr)
Atoka Reservoir	BOSS DAMBRK User's Manual (1999)	1/2 to 4 time dam height	0.5-4.0
	Selected parameter for modeling	16.0	1.8
Dolese Youth Park Lake	Von Thun and Gillette (1990)	19.1	0.5
	Froehlich (2008)	14.9	0.3
	Selected parameter for modeling	16.9	0.4
Dry Creek Detention Reservoir	Von Thun and Gillette (1990)	62.6	0.9
	Froehlich (2008)	159	2.6
	Selected parameter for modeling	**36.6**	**0.5**
Lake Hefner	Von Thun and Gillette (1990)	118	1.1
	Froehlich (2008)	159	2.6
	Selected parameter for modeling	138	1.9
Lake Overholser	Von Thun and Gillette (1990)	75.0	1.9
	Froehlich (2008)	102	4.3
	Selected parameter for modeling	88.7	3.4
Lightning Creek Holding Pond A	Von Thun and Gillette (1990)	19.4	0.7
	Froehlich (2008)	24.5	0.7
	Selected parameter for modeling	21.9	**0.9**
Lightning Creek Holding Pond C	Von Thun and Gillette (1990)	15.5	0.7
	Froehlich (2008)	19.7	0.7
	Selected parameter for modeling	17.6	0.7
Northeast (Zoo) Lake	Von Thun and Gillette (1990)	38.1	0.5
	Froehlich (2008)	32.2	0.4
	Selected parameter for modeling	35.1	0.5
Northwest Oklahoma City Sludge Lagoon	Von Thun and Gillette (1990)	29.3	0.5
	Froehlich (2008)	25.5	0.4
	Selected parameter for modeling	27.4	0.5
Stanley Draper Lake	Von Thun and Gillette (1990)	130	1.1
	Froehlich (2008)	177	2.5
	Selected parameter for modeling	153	1.6
Will Rogers Park Holding Pond	Von Thun and Gillette (1990)	22.9	0.7
	Froehlich (2008)	21.1	2.4
	Selected parameter for modeling	**8.69**	1.0

Table 4.2. Simplified upland Manning's roughness coefficients (n) for the Hydrologic Engineering Centers River Analysis System (HEC-RAS) models. Calibrated coefficients for each land cover class were determined using a HEC-RAS sensitivity analysis for Lake Overholser along the North Canadian River in Oklahoma City, Oklahoma.

Land Use	Land Cover Class Number	Manning's Roughness Coefficient	
		Initial	Calibrated
Open Water	1	0.03	0.034
Developed Open Space	2	0.035	0.045
Developed Low Intensity Developed Medium Intensity Developed High Intensity	3	0.10	0.18
Barren Land Grassland Pasture Cultivated Crop Land	4	0.04	0.048
Deciduous Forest Evergreen Forest Scrub/Shrub Wetland	5	0.15	0.19

Calibrated Manning's roughness coefficients from the Lake Overholser model were used for all models, i.e. 0.034 for stream channels and 0.045 to 0.19 for the surrounding floodplains. The initial reduced land-cover classifications and corresponding Manning's roughness coefficients are given in Table 4.2.

HEC-RAS can simulate subcritical flow as well as supercritical flow for unsteady flow models. For the majority of the simulated breaches, subcritical flow, i.e. velocities slower than the speed of the wave propagation was maintained by decreasing the Froude number (Fr). The Fr, ranging from 0 to 1, was a dimensionless number characterizing the impact of gravity on fluid motion in open channel flow. However, supercritical flow, with velocities greater than the wave propagation, was common near or directly downstream of a breached dam structure. To reduce flow velocities from supercritical to subcritical, Manning's roughness coefficients were modified to stabilize the model, which more accurately represented observed dam breaches (Zhou et al., 2005).

The Lake Overholser sensitivity analysis produced only minor changes to the inundated area, but did affect the maximum water surface elevation and the time to peak. The model predictions were not used to calibrate Manning's roughness coefficient due to the relatively flat topography in the inundated areas. The maximum water-surface elevation difference from the stream bed for the calibrated Manning's roughness coefficients and Manning's roughness coefficients 0.9 and 1.1 times the calibrated coefficients was less than one percent error. The difference of total inundated area of the sensitivity analysis was also less than one percent. The uncertainty of the sensitivity analysis was less than the uncertainty associated with HEC-RAS modeling, thus indicating that Manning's roughness coefficients were not the primary determining variable. The results of the Manning's roughness coefficient sensitivity model are given in Table 4.4.

The inundated area for the calibrated HEC-RAS Lake Overholser sensitivity analysis model was 2.7, 2.6, and 2.3 km^2 for the 0.9, 1.0, and 1.1 sensitivity models, respectively. Using the total inundated area, the total damage cost due to a dam failure was estimated to be between 94 and 110 million dollars for all three of the Manning's roughness coefficient sensitivity models (Table 4.3). The calculated damage costs were approximated and vary from state to state and home to home, as well as the flood water height inside the structure, which was assumed to be 1.2 m (4 ft.) for this study. For example, a difference in inundated area of less than one percent resulted in a difference of approximately 16 million dollars in damage.

Table 4.3. Total flooded area of the Manning's roughness coefficient sensitivity models and approximated damage cost, assuming 1.2 m water depth in home and 41 million dollars per km^2 of damage. [km^2: square kilometers]

Manning's Roughness Coefficient Model (fraction)	Flooded Area (km^2)	Damage Cost
0.9	2.7	$110,000,000
1.0	2.6	$106,000,000
1.1	2.3	$94,000,000

Table 4.4. Manning's roughness coefficient of the sensitivity model for maximum surface water elevation and time-to-peak for bridges downstream of Lake Overholser in Oklahoma City, Oklahoma. Maximum water surface elevations and time-to-peak are listed for the 75% Probable Maximum Flood (PMF) with three different fractions of Manning's roughness coefficient (1.0, 0.9 and 1.1). [m, meters; hh:mm, hours and minutes of time to peak after dam breach time; maximum surface water elevation data should be considered accurate to 0.1 m based on accuracy of elevation data and modeling uncertainty]

Bridge/Road Name	Manning's Roughness Coefficient (fraction)					
	1.0		0.9		1.1	
	Maximum Surface Water Elevation and Time to Peak					
	(m)	(hh:mm)	(m)	(hh:mm)	(m)	(hh:mm)
Northwest 10th Street	378.8	02:40	378.5	02:30	379.0	02:40
Railroad Bridge	377.0	03:00	376.9	02:50	377.6	03:10
West Reno Avenue	377.0	03:00	377.0	02:50	377.1	03:10
Interstate 40	376.2	03:20	376.0	03:05	376.4	03:45
Council Road	374.0	03:30	374.0	03:10	374.1	04:10
MacArthur Boulevard	372.0	05:20	371.8	04:35	372.3	05:30
Meridian Avenue	370.8	06:00	370.5	05:05	371.0	06:15
Portland Avenue	369.9	06:40	369.6	05:40	370.1	06:50
Interstate 44	369.3	06:50	369.1	05:55	369.5	07:10
May Avenue	368.5	07:10	368.2	06:15	368.7	07:45
Agnew Avenue	367.5	07:40	367.3	06:45	367.7	08:15
Pennsylvania Avenue	366.7	08:10	366.4	07:10	366.9	08:45
Exchange Avenue	365.7	08:40	365.4	07:35	366.0	09:15
Railroad Bridge	365.4	08:50	365.2	07:45	365.6	09:20
Western Avenue	365.1	09:00	364.9	07:50	365.4	09:30
Walker Avenue	364.7	09:00	364.4	07:55	365.0	09:35
Robinson Avenue	364.3	09:10	364.0	08:00	364.6	09:40
Shields Boulevard	364.0	09:10	363.7	08:00	364.3	09:40
15th Street	363.0	09:20	362.7	08:10	363.2	09:50
Pipe Bridge	362.9	09:20	362.7	08:10	363.1	09:50
Railroad Bridge	362.1	09:30	361.9	08:20	362.4	10:53
Lincoln Boulevard	361.8	09:40	361.5	08:30	362.1	10:10
Interstate 35	361.3	09:40	361.1	08:30	361.5	10:15
Eastern Avenue	360.7	09:50	360.5	08:40	360.9	10:25
Reno Avenue	359.7	09:50	359.5	08:45	359.8	10:30

Table 4.4. (Cont.). Manning's roughness coefficient of the sensitivity model for maximum surface water elevation and time to peak for bridges downstream of Lake Overholser in Oklahoma City, Oklahoma. Maximum water surface elevations and time to peak are listed for the 75% Probable Maximum Flood (PMF) with three different fractions of Manning's roughness coefficient (1.0, 0.9 and 1.1). [m, meters; hh:mm, hours and minutes of time to peak after dam breach time; maximum surface water elevation should be considered accurate to 0.1 m based on accuracy of elevation data and modeling uncertainty]

Bridge/Road Name	Manning's Roughness Coefficient (fraction)					
	1.0		0.90		1.1	
	Maximum Surface Water Elevation and Time to Peak					
	(m)	(hh:mm)	(m)	(hh:mm)	(m)	(hh:mm)
Interstate 40 Eastbound	358.7	09:50	358.7	08:45	358.8	10:30
Interstate 40 Westbound	358.6	09:50	358.6	08:45	358.7	10:30
Railroad Bridge	357.5	11:00	357.3	09:50	357.7	11:20
4th Street	357.3	11:00	357.2	09:55	357.5	11:30
10th Street	356.7	11:20	356.6	10:15	356.9	11:40
23rd Street	355.9	11:30	355.9	10:25	356.0	11:55
36th Street	354.6	12:20	354.4	11:05	354.8	12:35
Midwest Boulevard	352.0	12:50	351.9	11:35	352.2	13:15
63rd Street	350.4	13:20	350.2	12:05	350.5	13:40
Britton Road	349.2	13:30	349.2	12:10	349.2	13:55
Hefner Road	346.7	14:10	346.5	12:50	346.8	14:45
122nd Street	344.7	14:50	344.5	13:30	344.9	15:20
Hiwassee Road	343.2	15:10	342.9	13:50	343.4	15:45
Britton Road	338.5	16:10	338.3	14:35	338.7	16:40

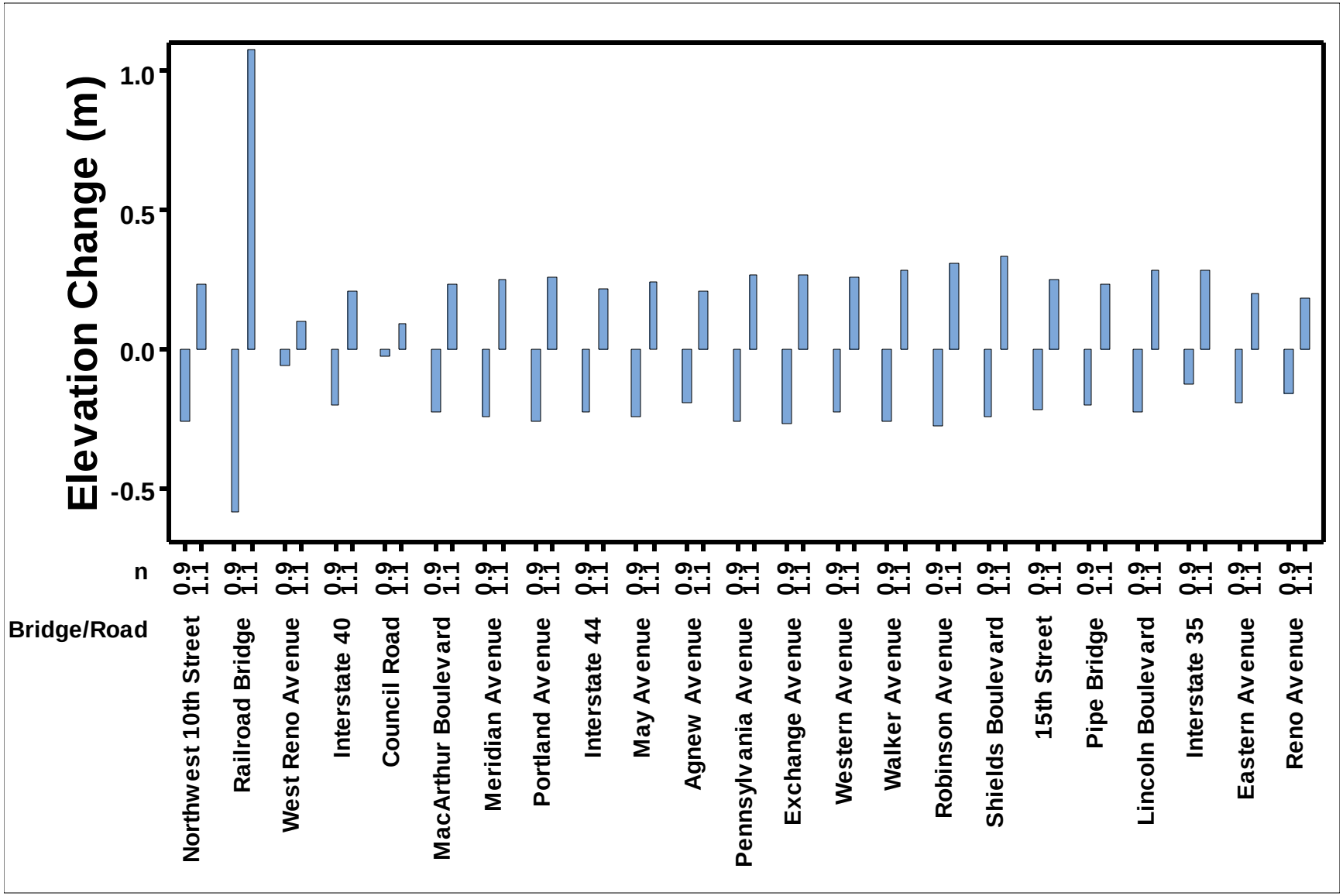

Figure 4.1. Difference in elevation change for Manning's roughness coefficients equal to 0.9 and 1.1 times the calibrated Manning's roughness coefficients for 23 bridges from the Lake Overholser model sensitivity analysis. [m, meters; n, Manning's roughness coefficient]

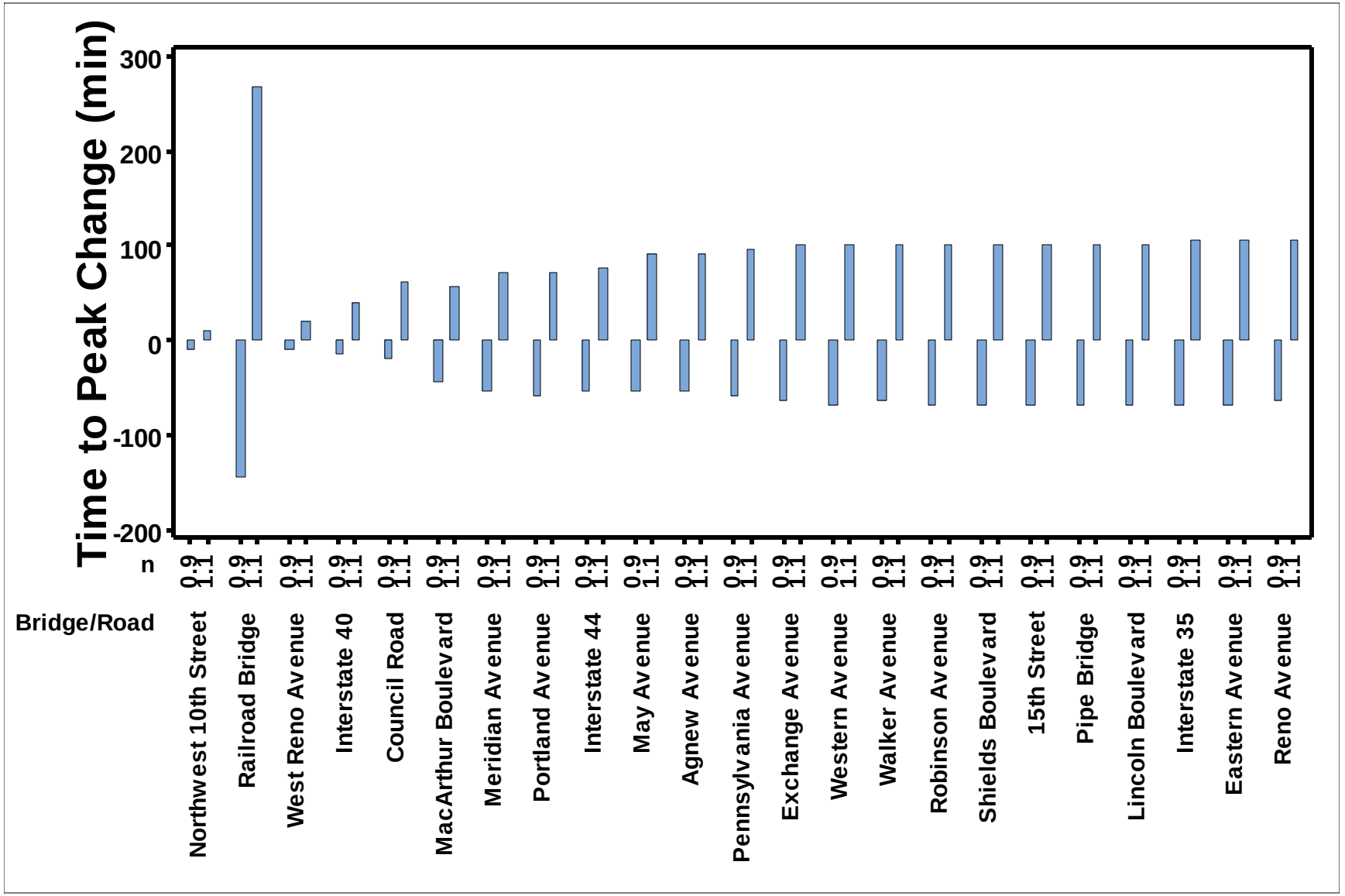

Figure 4.2. Difference in time to peak for Manning's roughness coefficients equal to 0.9 and 1.1 times the calibrated Manning's roughness coefficients for 23 bridges from the Lake Overholser model sensitivity analysis.[min, minutes; n, Manning's roughness coefficient]

The submerged areas and flood wave travel time from the 75% PMF and sunny-day floods for each dam were detailed on the inundation maps after the breach to each bridge intersection. This information is also given in Appendix A. Important points of interest in danger of being inundated were obtained from Google Earth™ and were also labeled on each map, i.e. recreational areas, water and wastewater treatment plants, and other important community locations. Due to the size of the inundation maps, flooded areas were subdivided into map tiles at a 1:16,000 scale for Dolese Youth Park Lake, Dry Creek Detention Reservoir, Lightning Creek Holding Pond A, Lightning Creek Holding Pond C, Northeast (Zoo) Lake, Northwest Oklahoma City Sludge Lagoon, and Will Rogers Park Holding Pond; a 1:24,000 scale for Lake Overholser and Stanley Draper Lake; and a 1:32,000 scale for Atoka Reservoir and Lake Hefner. The resulting flood-inundation maps were produced using HEC-GeoRAS and can be found in Appendix B.

4.2 Uncertainties

HEC-RAS prediction uncertainties were produced at every step of dam-breach modeling. A HEC-RAS uncertainty study was performed on Strouds Creek in North Carolina. The uncertainty analysis concluded that a decrease in water surface elevation of 0.4 m could reduce the inundation extent by 19%, and an increase of water surface elevation of 1.0 m could increase the inundation extent by 34% (Merwade et al., 2008).

The first introduced error was a result of the LiDAR data accuracy used to construct the channel and floodplain cross-sections. Elevation data were obtained from Oklahoma City, OK in 2004 and Norman, OK in 2007, fifteen years and eight years, respectively, earlier than the HEC-RAS models represented. Because of the urban setting of the dams selected for this study, there was a high probability that the topography and land-use classifications changed downstream of the dam between the time the data were collected and the model was completed. If the land use did change, e.g. from cultivated crop land to developed low intensity urban, Manning's roughness coefficients with their associated cross

sections likely changed as well. Horritt and Bates (2002) suggested the use of HEC-RAS over a two-dimensional (2-D) model when friction parameters were limited.

Model input uncertainties, i.e. inflow hydrographs, boundary conditions and Manning's roughness coefficients, are often overlooked as insignificant. However input uncertainties can range from 18 to 25 percent at peak discharges (Pappenberger et al., 2006). Because Manning's roughness coefficient can affect the extent of the inundated area as well as the time to peak, performing a sensitivity analysis on one reservoir and applying the results to the other reservoirs reduces the prediction certainty. Temporal changes in flood-plain hydrology and differences between reservoirs may result in significant changes in Manning's roughness coefficients. As the floodplain hydraulics change over time, the calibrated Manning's roughness coefficient may no longer apply. More accurate inundation maps could be produced if a sensitivity analysis was performed on every reservoir. However, the insignificant change in time to peak and peak flood stage observed on the sensitivity analysis that was performed led to the use of calibrated Manning's roughness coefficients from one reservoir being used for all the reservoirs modeled.

For this study, HEC-RAS was used only to model the movement of water and did not include the transportation of sediment or debris resulting from the breach. Disregarding debris flows can result in lower predicted peak discharges at bridges, which may significantly reduce the predicted inundated areas (Walder & O'Connor, 1997). Peak flood stage predictions in densely urbanized areas contained high uncertainty due to heterogeneous Manning's roughness coefficients and complex flow patterns caused by the large amount of structures (Singh & Snorrason, 1984).

Due to the uncertainties associated with flood modeling, all reported flood areas, wave travel times, and flood wave elevations were estimated and should be treated as such. The inundated areas were heavily based on the type of dam failure, the failure location on the dam, and the preexisting conditions of the reservoir and downstream river reach. Inundated areas were approximate and were contingent upon

the accuracy of the topographical maps. Assumptions made throughout the modeling also affected the precision of the predicted flood wave.

4.3 Assumptions and Limitations

Assuming that all the modeled reservoirs had similar channel and floodplain characteristics introduced ambiguity into the predicted inundation maps. The lack of available stream flow data for the modeled reservoirs prevented developing a calibrated model for each reservoir. However, since the majority of the reservoirs were located inside urban areas, the assumption that the channel and floodplain characteristics were similar was reasonable. Atoka Reservoir was located in more rural southeastern Oklahoma, and thus to develop a more accurate inundation map the HEC-RAS model should be calibrated using stream flow data from USGS stream-gage stations Muddy Boggy Creek near Farris, Oklahoma (07334000) and Muddy Boggy Creek near Unger, Oklahoma (7335300).

Another assumption was a 1-D model, i.e. the water surface elevation was constant across the cross-sections, which created biased predictions for the water stored in the flood plain (Horritt & Bates, 2001). Using the cross-section-points filter to simplify the geography of the channel and floodplain minimally affected the elevation across each cross section. Although it reduced the number of elevation points per cross section to 500, the cross-section-points filter tool conserved the general shape and hydraulic characteristics of the cross section. A study by Omer et al. (2003) calculated that filtering elevation points to four degrees gave an average elevation error of 0.01 m, an error of 0.42 percent in area, and a hydraulic radius error of 0.71 percent. Omer et al. (2003) states that "…filtering results in significant time savings when performing flood inundation studies of digital terrain models." A sample cross section with and without the cross-section-points filter is given in Figure 4.3.

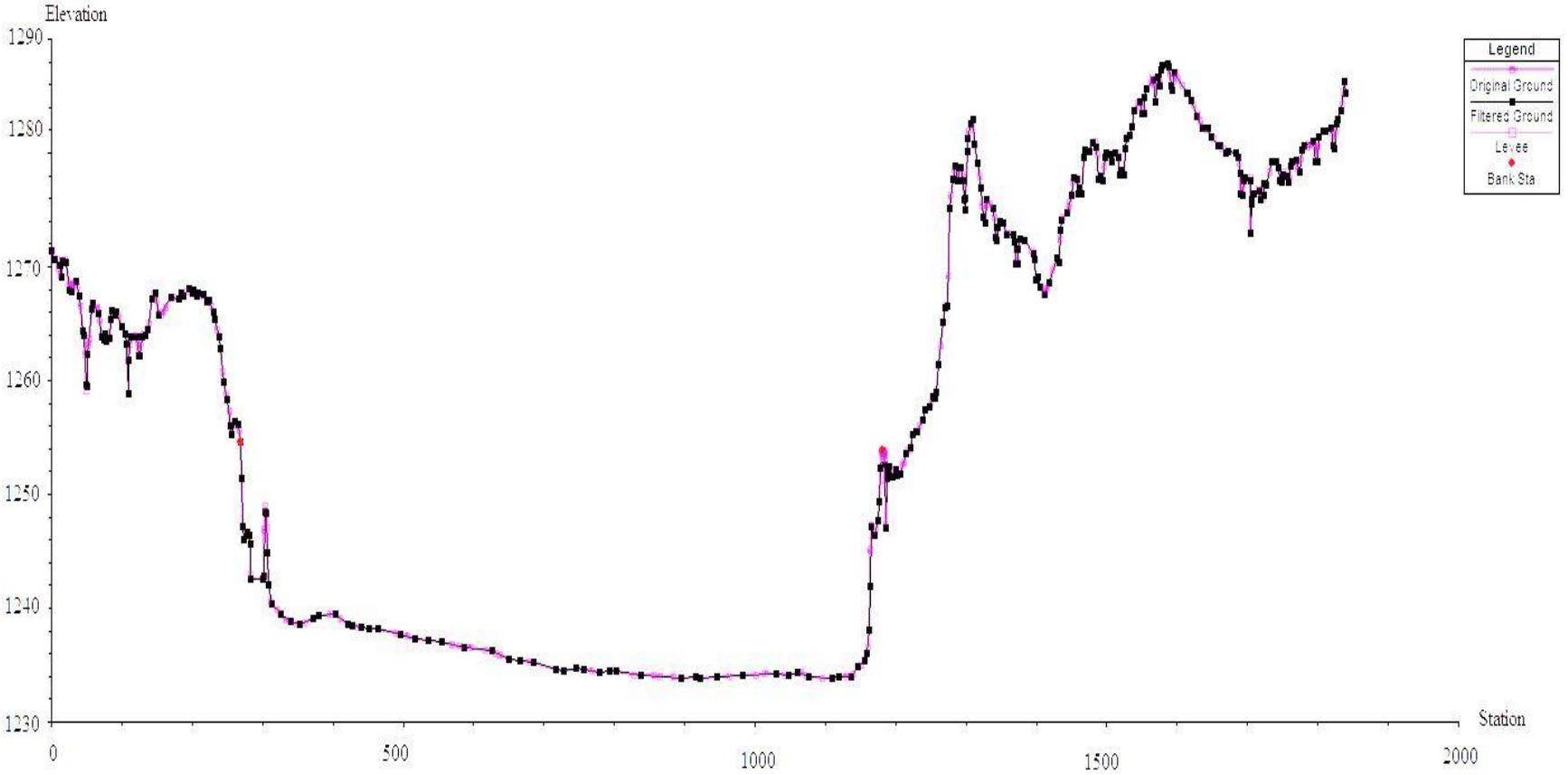

Figure 4.3. Example stream cross section derived using light detection and ranging (LiDAR) elevation data and the cross-section-point filter tool in Hydrologic Engineering Centers River Analysis System (HEC-RAS) (Hydrologic Engineering Center, 2010a) showing the cross section with and without filtered elevation data.[elevation and station are in units of meter]

Several assumptions were made during the user input phase of HEC-RAS. Assumptions associated with the location, type, and characteristics of the dam breach, as previously discussed, affect the extent of the inundated areas. Cross sections at some locations could not be positioned perpendicular to the river centerline due to the meandering of the river. Cross sections can only intersect the stream centerline once. If the river meanders back on itself, there was not enough space for the cross section to intersect perpendicular to the centerline. The option to include interpolated cross sections to assist in model stabilization in areas of the river channel with complex geography was exercised. However, inclusion of interpolated cross sections that do not accurately represent the actual field geography can result in errors and/or discontinuity of the inundation map (Yang et al., 2006).

Lateral losses, such as backwater on an adjoining tributary, channel storage, or flood waters filling adjacent basins along the reach, even if modeled, would also be difficult to estimate; expanding the inundated areas and possibly reducing the peak stage downstream. Liberties were taken during the creation of the inundation maps with the discontinuity at interpolated cross sections and locations along the river reach with complex geography were smoothed and adjusted based on the contour lines to display a more accurate and realistic inundation map.

4.4 May 1993 Flood Comparison

The maximum predicted flow for the HEC-RAS dam breach was 150 m^3/s compared to 430 m^3/s resulting from the May 1993 rain event (Tortorelli, 1996). Tortorelli (1996) compared his findings with a FEMA (1990) report, with the May 1993 flow of 430 m^3/s well above the FEMA 100-year and 500-year floods of 230 and 320 m^3/s, respectively (Tortorelli, 1996). The HEC-RAS predicted flow from a dam breach was only 36 percent of the May 1993 flood-event flow. Based on the hydrograph in the Lightning Creek Phase I report (OWRB, 1979b), if a dam

breach was to ever occur, the flow would not reach the Tortorelli (1996) predictions. Therefore, the Tortorelli (1996) report was not applicable for the dam breach study.

The peak stages for the HEC-RAS 75% PMF dam breach scenario range between 2 to 4 m (6 to 14 feet) lower than those calculated by Tortorelli (1996). This difference can also partly be attributed to the ability of HEC-RAS to compute energy loss, more accurately model bridge openings, and the use of more accurate cross-sectional elevation data (Yang et al., 2006). The Tortorelli (1996) statement, "cross-sectional geometry, Manning's roughness coefficients, and number of cross sections used," agrees with the variations in water surface elevations of the predicted model. Note that all elevations in Table 4.5 were converted to NAVD88 for comparison. HEC-RAS predicted maximum surface water elevation differences above the streambed for Lightning Creek were within 55% of the maximum surface water difference above the streambed estimated by Tortorelli (1996).

Table 4.5. Comparison between current HEC-RAS model predictions of stage and results from Tortorelli (1996) for selected bridges on Lightning Creek. [m, meters; maximum surface water elevation should be considered accurate to 0.1 m based on accuracy of elevation data and modeling uncertainty]

Bridge	**HEC-RAS 75% PMF**	**May 8, 1993 Flood**
	Maximum Surface Water Elevation, m	
51st Street	367.4	369.0
Sage Street	366.8	368.6
44th Street	365.9	367.7
Grand Boulevard	364.2	366.0
29th Street	362.9	365.7
25th Street	360.1	364.3

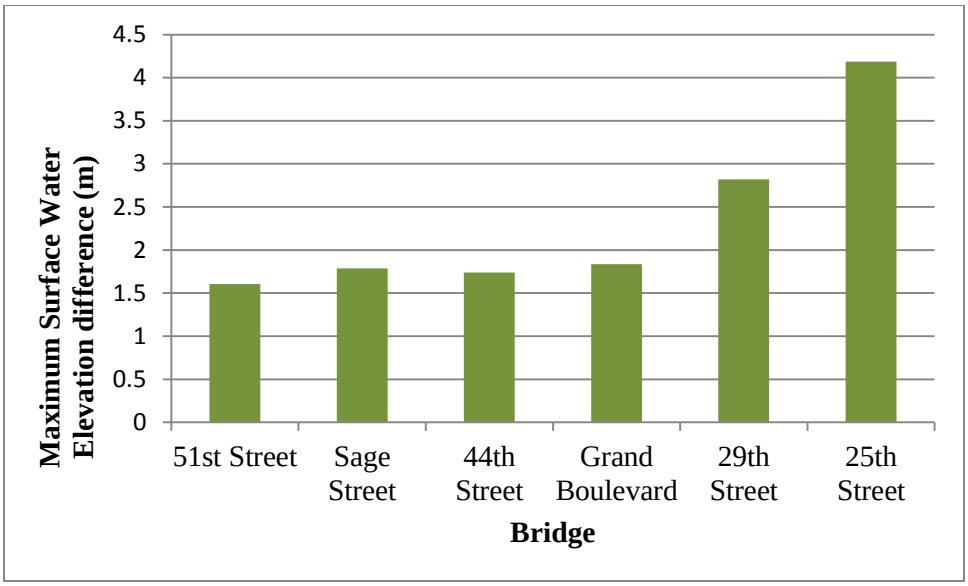

Figure 4.4. Difference in measured maximum water-surface elevation between the 1993 flood (Tortorelli, 1996) and the current Hydrologic Engineering Centers River Analysis System (HEC-RAS) model predictions for six bridges along Lightning Creek, Oklahoma. [m, meters]

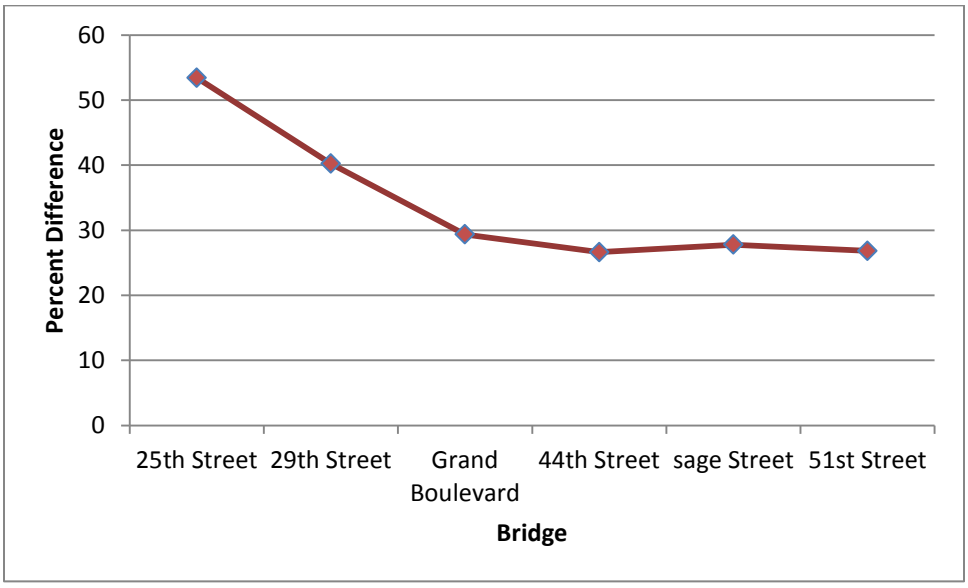

Figure 4.5. Percent difference in measured water-surface elevation between the 1993 flood (Tortorelli, 1996) and the current Hydrologic Engineering Centers River Analysis System (HEC-RAS) model predictions for six bridges along Lightning Creek, Oklahoma.

A study by Yochum et al. (2008) compared high-water mark elevations resulting from the Big Bay Dam failure (2004) and HEC-RAS predicted elevations. On March 4, 2004 the Big Bay Dam failed damaging 104 homes. The fair-weather failure occurred at normal pool elevation releasing approximately 17.5 million m^3 of water into the valley. High-water marks were documented as a reference for the modeled water elevations, and the differences in water-surface estimates between the HEC-RAS predicted elevations and the observed high-water marks ranged from -0.02 to -0.90 m (-0.07 to -3.0 ft.) and 0.01 to 0.60 m (0.03 to 2.0 ft.) (Yochum et al., 2008). This study corroborates the uncertainty associated with the quality of high-water marks as references for flood mapping.

CHAPTER V

SUMMARY AND CONCLUSIONS

The purpose of this study was to model and validate dam-breach scenarios for eleven dams owned and operated by the City of Oklahoma City, located near Oklahoma City, OK and Atoka, OK using HEC-RAS. A dam is a structure that disrupts water flow and provides water storage. All of the dams in this study were selected for their hazard classification or urban location and were therefore required to have dam breach evacuation plans containing inundation maps. All eleven predicted dam breaches were profiled using a 75% PMF scenario and a sunny day scenario. HEC-RAS was used as the hydrologic model to determine the water surface elevations and the time to peak of the flood wave at intersecting bridges along the river reach. Streamflow gage data from USGS streamflow-gaging stations were used to evaluate the sensitivity of the model for the sunny day scenario, which was necessary for the selection of appropriate Manning's roughness coefficients for modeling.

The estimated damage costs for the sensitivity model employed a simple method to estimate the economic effects of a dam failure on a community. The analysis showed the damage costs were dependent upon the inundated area. The heaviest economic burden is often felt by the community directly downstream of the dam failure (Ellingwood et al., 1993). With the majority of the selected dams in this study being located in urban areas, the potential property loss could be devastating to Oklahoma City residents. The cost analysis did not include the damage to business or other non-residential structures. Inundation maps created for this study can be used in a more extensive economic cost analysis to provide more comprehensive and accurate estimates.

This study, along with other studies like the Big Bay Dam failure (Yochum et al., 2008), help justify the use of the 1-D HEC-RAS model for predictive flood modeling. HEC-RAS results when compared to the 2-D model were marginally better in 67% of the cases tested (Horritt & Bates, 2002). The difference in maximum water elevations between Tortorelli (1996) and the HEC-RAS predicted elevations was acceptable. However, this comparison was necessary because the May 1993 flood study was the only one performed on a corresponding reach selected for this study. HEC-RAS predicted elevations and flows for Lightning Creek were appropriate since the dam breach was modeled with the reservoir at full capacity and at 75% PMF.

Several insights were developed during the course of this study. The most important of which was modeling was heavily dependent upon user interpretation. Multiple people can model the same dam breach and obtain multiple outcomes depending on their selection of breach location and parameters, Manning's roughness coefficients, and model stability practices. In addition, fully justifying and documenting the modeling process was required to defend my model predictions. Regardless of the errors and uncertainties associated with modeling, the flood inundation maps will be extremely useful in emergency situations and can even be deemed "lifesaving".

Walder and O'Connor (1997) stated that "few dam failures have been observed in any detail" and very little information was available on how breached dams react over time. Although their study was done almost 20 years ago, their statement still holds true; unfortunately for scientists and engineers, in order to collect observed data a dam must actually breach, possibly resulting in the loss of life and property. Predictive flood modeling, such as the type prepared through this study, was essential for the safety of residents located downstream of a dam structure.

Future major advances in the HEC-RAS program include software tools that allow 2-D flow modeling, which reduces the supercritical flow areas and model instability. Sediment and debris flow software is currently being developed and will be helpful in determining their effect on flow patterns as the flood wave proliferates downstream. Future projects using HEC-RAS predictive flood modeling could include: hurricane and tsunami inundation mapping, comparison between HEC-RAS predicted 100-year floodplain maps and those used by insurance companies, economic studies based on the inundation maps to determine evacuation costs, structural damage, and the rebuilding cost in the event of a dam breach, and a study determining the environmental impacts of flooding.

Time and the implementation of progressive computational methods will allow for a better understanding of dam breach formation and lead to a better system for modeling breaches. Most important of all, with the continuation of gained knowledge of dam breaches and the propagation of the resulting flood wave, future dam and bridge structures will have improved designs and the use of inundation maps for emergency flood warning systems will result in a significant reduction in the death toll associated with dam failures.

REFERENCES

Arcement, G. J., & Schneider, V. R. (1989). Guide for selecting Manning's roughness coefficients for natural channels and flood plains.

Bales, J. D., & Wagner, C. R. (2009). Sources of uncertainty in flood inundation maps. *Journal of Flood Risk Management*, *2*(2), 139-147.

Barlow, R. A., Nardi, M. R., & Reyes, B. (2008). *Use of Light Detection and Ranging (LiDAR) to Obtain High-Resolution Elevation Data for Sussex County, Delaware*. US Department of the Interior, US Geological Survey.

Barnes, H. H. (1967). *Roughness characteristics of natural channels* (No. 1849). US Govt. Print. Off.

City of Oklahoma City, 2004, Lidar-derived bare-earth digital elevation model — Sanborn Colorado LLC: Prepared for the city of Oklahoma City, Oklahoma.

City of Oklahoma City, 2014, Parks and Recreation, accessed December, 18, 2014, at *https://www.okc.gov/index.html*.

City of Norman, 2007, Lidar-derived bare-earth digital elevation model and accuracy report — Merrick & Company: Prepared for the city of Norman, Oklahoma.

Coon, W. F. (1998). *Estimation of roughness coefficients for natural stream channels with vegetated banks* (Vol. 2441). US Geological Survey.

Cost of Flooding | Measure Flood Damage | Flood Tool | FloodSmart. (n.d.). Retrieved April 30, 2016, from https://www.floodsmart.gov/floodsmart/pages/flooding_flood_risks/the_cost_of_flooding

Davies, W. E., Bailey, J. F., & Kelly, D. B. (1972). *West Virginia's Buffalo Creek flood; a study of the hydrology and engineering geology* (No. 667). [US Geological Survey].

Ellingwood, B., Corotis, R. B., Boland, J., & Jones, N. P. (1993). Assessing cost of dam failure. *Journal of Water Resources Planning and Management*, *119*(1), 64-82.

Environmental Systems Research Institute, 2011, ArcGIS Help: Redlands, Calif., accessed April 1, 2011, at http://webhelp.esri.com/arcgiSDEsktop/9.3/index.cfm?TopicName=welcome.

Environmental Systems Research Institute, 2015, ArcGIS resource center—Topo to raster (spatial analyst): ArcGIS 10.1, accessed January 26, 2015, at *http://resources.arcgis.com/en/help/main/10.1/index.html#//009z0000006s000000*.

Federal Emergency Management Agency, 1990, Flood Insurance Study, City of Oklahoma City, Oklahoma, Community Number 405378,178 p.

Federal Emergency Management Agency, 2004, Federal Guidelines for Dam Safety: U.S. Department of Homeland Security Federal Emergency Management Agency [variously paged].

Federal Emergency Management Agency, 2013, Federal Guidelines for Inundation Mapping of Flood Risks Associated with Dam incidents and Failures: U.S. Department of Homeland Security Federal Emergency Management Agency [variously paged].

Fread, D. L. (1977, October). The development and testing of a dam-break flood forecasting model. In *Proc. of Dam-Break Flood Modeling Workshop, US Water Resources Council, Washington, DC* (pp. 164-197).

Froehlich, D. C. (2008). Embankment dam breach parameters and their uncertainties. *Journal of Hydraulic Engineering*, *134*(12), 1708-1721.

Gesch, D. B., Oimoen, M. J., & Evans, G. A. (2014). *Accuracy assessment of the US Geological Survey National Elevation Dataset, and comparison with other large-area elevation datasets: SRTM and ASTER* (No. 2014-1008). US Geological Survey.

Hicks, F. E., & Peacock, T. (2005). Suitability of HEC-RAS for flood forecasting. *Canadian Water Resources Journal*, *30*(2), 159-174.

Hoogestraat, G. K. (2011). *Flood hydrology and dam-breach hydraulic analyses of four reservoirs in the Black Hills, South Dakota*.

Horizon Systems Corporation, 2008, National Hydrography Dataset Plus Version 1 (NHDPlus): accessed November 13, 2008, at http://www.horizon-systems.com/nhdplus/.

Horritt, M. S., & Bates, P. D. (2001). Effects of spatial resolution on a raster based model of flood flow. *Journal of Hydrology*, *253*(1), 239-249.

Horritt, M. S., & Bates, P. D. (2002). Evaluation of 1D and 2D numerical models for predicting river flood inundation. *Journal of Hydrology*, *268*(1), 87-99.

Hu, Y. (2001). Analysis and Processing of Airborne LIDAR Data.

Hydrologic Engineering Center, CEIWR-HEC Suite of Software factsheet, accessed January 20, *2016 at* http://www.hec.usace.army.mil/FactSheets/Software/HEC_FactSheet_Software.pdf [variously paged].

Hydrologic Engineering Center, 1991, HEC-2 Water Surface Profiles user's manual: Davis, Calif., accessed January 20, 2016, at *http://www.hec.usace.army.mil/publications/ComputerProgramDocumentation/HEC-2_UsersManual_(CPD-2a).pdf* [variously paged].

Hydrologic Engineering Center, 2010a, HEC-RAS River Analysis System user's manual, version 4.1: Davis, Calif., accessed April 1, 2011, at ftp://ftp.usace.army.mil/pub/iwr-hec-web/software/ras/documentation/HEC-RAS_4.1_Users_Manual.pdf [variously paged].

Hydrologic Engineering Center, 2010b, HEC-RAS River Analysis System hydraulic reference manual, version 4.1: Davis, Calif., accessed April 1, 2011, at http://www.hec.usace.army.mil/software/hec-ras/documents/HEC-RAS_4.1_Reference_Manual.pdf [variously paged].

Hydrologic Engineering Center, 2011, HEC-GeoRAS GIS tools for support of HEC-RAS using ArcGIS, version 4.3.93: Davis, Calif., accessed April 1, 2011, at http://www.hec.usace.army.mil/software/hec-ras/documents/HEC-GeoRAS_43_Users_Manual.pdf [variously paged].

Intermap Technologies, 2014, NEXTMap 5-meter digital terrain model of Atoka and Choctaw Counties, Oklahoma, accessed June 20, 2014, at http://www.intermap.com/en-us/databases/nextmap.aspx

Merwade, V., Olivera, F., Arabi, M., & Edleman, S. (2008). Uncertainty in flood inundation mapping: current issues and future directions. *Journal of Hydrologic Engineering*, *13*(7), 608-620.

Steel Tape Line Accuracy. (n.d.). Retrieved April 30, 2016, from http://www.mid-continents.com/steel-tape-line-accuracy

Multi-Resolution Land Characteristics Consortium, 2011, 2006 National Land Cover Database (NLCD), accessed April 1, 2013, at *http://www.mrlc.gov/nlcd2006.php.*

National Agriculture Imagery Program, 2013, NAIP imagery, accessed June 1, 2011 at http://www.fsa.usda.gov/FSA/apfoapp?area=home&subject=prog&topic=nai.

National Geodetic Survey, 2011, Continuously Operating Reference Station (CORS): National Geodetic Survey, accessed April 1, 2011, at http://www.ngs.noaa.gov/CORS/.

National Oceanic and Atmospheric Administration, 2015, Vertcon, accessed January 5, 2015, at *http://www.ngs.noaa.gov/cgi-bin/VERTCON/vert_con.prl.*

Oklahoma City, 2012, DMA 2000 Hazard Mitigation Plan-Oklahoma City, Oklahoma, accessed April 21, 2016, at https://www.oklahomacounty.org/emergencymanagement/documents/PDF/Section%205_3_1.pdf

Oklahoma City, Oklahoma. (n.d.). Retrieved April 30, 2016, from http://www.city-data.com/city/Oklahoma-City-Oklahoma.html

Oklahoma Department of Transportation, 2014, ArcView SHP files – Oklahoma Highway System, accessed December 15, 2014, at http://www.okladot.state.ok.us/maps/shp/index.htm.

Oklahoma Water Resources Board, 1978a, Phase I Inspection Report Dry Creek Detention Dam and Spillway: National Dam Safety Report, Inventory No. OK 11061, 164 p.

Oklahoma Water Resources Board, 1978b, Phase I Inspection Report Northeast Lake Dam and Spillway: National Dam Safety Report, Inventory No. OK 02424, 112 p.

Oklahoma Water Resources Board, 1978c, Phase I Inspection Report NW Oklahoma City Sludge Lagoon Dam No. 1: National Dam Safety Report, Inventory No. OK 11051, 58 p.

Oklahoma Water Resources Board, 1979a, Phase I Inspection Report Overholser Lake Dam and Spillway: National Dam Safety Report, Inventory No. OK 02537, 166 p.

Oklahoma Water Resources Board, 1979b, Phase I Inspection Report Lightning Creek Holding Pond A: National Dam Safety Report, Inventory No. OK 11070, 132 p.

Oklahoma Water Resources Board, 1979c, Phase I Inspection Report Stanley Draper Lake: National Dam Safety Report, Inventory No. OK 02580, 85 p.

Oklahoma Water Resources Board, 1979d, Phase I Inspection Report Will Rogers Park Dam: National Dam Safety Report, Inventory No. OK 11069, 121 p.

Oklahoma Water Resources Board, 2011, Hydrologic and hydraulic guidelines for dams in Oklahoma: Oklahoma Water Resources Board, p. 12–20.

Oklahoma Water Resources Board, 2013, Title 785. Chapter 25. Dams and Reservoirs, accessed April 21, 2016, at http://www.owrb.ok.gov/util/rules/pdf_rul/current/Ch25.pdf

Oklahoma Water Resources Board, 2014, Bathymetric Lake Studies, accessed August 19, 2014, at http://www.owrb.ok.gov/maps/pmg/owrbdata_Bathy.html.

Oklahoma Water Resources Board, 2014, Bathymetric Lake Studies, accessed August 19, 2014, at http://www.owrb.ok.gov/maps/pmg/owrbdata_Bathy.html.

Omer, C. R., Nelson, E. J., & Zundel, A. K. (2003). Impact of varied data resolution on hydraulic modeling and floodplain delineation1. *Journal of American Water Resources Association*, *02120*, 467-475.

Pappenberger, F., et al., (2006). Influence of uncertain boundary conditions and model structure on flood inundation predictions. Advances in Water Resources, 29(10), 1430-1449.

Ponce, V. M., Taher-shamsi, A., & Shetty, A. V. (2003). Dam-breach flood wave propagation using dimensionless parameters. *Journal of Hydraulic Engineering*, *129*(10), 777-782.

Quick Facts: Oklahoma City, Oklahoma, 2010-2014. (n.d.). Retrieved April 30, 2016, from http://www.census.gov/quickfacts/table/HSD310214/4055000,00)

Rendon, S. H., Ashworth, C. E., & Smith, S. J. (2012). *Dam-breach analysis and flood-inundation mapping for Lakes Ellsworth and Lawtonka near Lawton, Oklahoma* (No. 2012-5026). US Geological Survey.

Rydlund, P. H. (2006). *Peak Discharge, Flood Profile, Flood Inundation, and Debris Movement Accompanying the Failure of the Upper Reservoir at the Taum Sauk Pump Storage Facility near Lesterville, Missouri* (No. 2006-5284). US Geological Survey

Samuels, P. G. (1989). Backwater lengths in rivers. *Proceedings of the Institution of Civil Engineers*, *87*(4), 571-582.

Seed, H.B. & Duncan, J.M. (1981). The Teton dam failure a retrospective review. In Proc. of 10th Inter. Conf. SMFE. Stockholm (Vol. 3).

Shivers, M. J. et al. (2015). Dam-breach analysis and flood-inundation mapping for selected dams in Oklahoma City, Oklahoma, and near Atoka, Oklahoma. US Department of Interior, US Geological Survey.

Singh, K. P., & Snorrason, A. (1984). Sensitivity of outflow peaks and flood stages to the selection of dam breach parameters and simulation models. *Journal of hydrology*, *68*(1-4), 295-310.

Stevens, M. R., & Hoogestraat, G. K. (2013). *Flood hydrology and dam-breach hydraulic analyses of five reservoirs in Colorado* (No. 2012-5097). US Geological Survey.

Tate, E. C., & Maidment, D. R. (1999). *Floodplain mapping using HEC-RAS and ArcView GIS* (Master's thesis, University of Texas at Austin).

Timbadiya, P. V., Patel, P. L., & Porey, P. D. (2011). Calibration of HEC-RAS model on prediction of flood for lower Tapi River, India. *Journal of Water Resource and Protection*, *3*(11), 805.

Tortorelli, R. L. (1996). *Estimated Flood Peak Discharges on Twin, Brock, and Lightning Creeks, Southwest Oklahoma City, Oklahoma, May 8, 1993*. US Department of the Interior, US Geological Survey.

Tortorelli, R. L., & McCabe, L. P. (2001). *Flood frequency estimates and documented and potential extreme peak discharges in Oklahoma*. US Department of the Interior, US Geological Survey.

Trimble Navigation Limited, 2003, Trimble R7/R8 GPS receiver user guide, version 1.00, revision A: Sunnyvale, Calif., Trimble Navigation Limited, 216 p.

Trimble Navigation Limited, 2005, Trimble Geomatics Office, version 1.63, build 10: Sunnyvale, Calif., Trimble Navigation Limited [variously paged].

U.S. Board on Geographic Names, 2014, Geographic Names Information System (GNIS), accessed December 15, 2014, at *http://geonames.usgs.gov/domestic/*.

U.S. Census Bureau, 2014, TIGER/Line Shapefiles and TIGER/Line Files, accessed December 15, 2014, at *http://www.census.gov/geo/maps-data/data/tiger-line.html*

U.S. Geological Survey, 2013, USGS water data for the Nation: National Water Information System (NWISWeb), accessed June 18, 2014, at http://waterdata.usgs.gov/nwis/.

U.S. Geological Survey, 2014, National Elevation Dataset: U.S. Geological Survey, accessed on December 15, 2014 at http://ned.usgs.gov/.

U.S. Geological Survey, 2016, Floods: Recurrence intervals and 100-year floods, accessed on April 22, 2016, at http://water.usgs.gov/edu/100yearflood.html

Von Thun, J. L., & Gillette, D. R. (1990). *Guidance on breach parameters*. US Department of the Interior, Bureau of Reclamation.

Wahl, T. L. (1998). Prediction of embankment dam breach parameters: a literature review and needs assessment.

Wahl, T. L. (2004). Uncertainty of predictions of embankment dam breach parameters. *Journal of hydraulic engineering*, *130*(5), 389-397.

Walder, J. S., & O'Connor, J. E. (1997). Methods for predicting peak discharge of floods caused by failure of natural and constructed earthen dams. *Water Resources Research*, *33*(10), 2337-2348.

Yang, J., Townsend, R. D., & Daneshfar, B. (2006). Applying the HEC-RAS model and GIS techniques in river network floodplain delineation. *Canadian Journal of Civil Engineering*, *33*(1), 19-28.

Yochum, S. E., Goertz, L. A., & Jones, P. H. (2008). Case study of the big bay dam failure: accuracy and comparison of breach predictions. Journal of Hydraulic Engineering, 134(9), 1285-1293.

Zhou, R. D., Judge, D. G., & Donnelly, C. R. (2005, October). Comparison of HEC-RAS with FLDWAV and DAMBRK models for dam break analysis. In *CDA Annual Conference* (pp. 1-12).

APPENDIX A

SURFACE WATER ELEVATION TABLES

Table A.1. Maximum surface water elevation and time to peak for 75% Probable Maximum Flood (PMF) and sunny day breach scenarios for identified bridges for eleven dams in Oklahoma City, Oklahoma and near Atoka, Oklahoma. [m, meters; hh:mm, hours and minutes of time to peak after dam breach time; due to the uncertainty of elevation data, maximum water surface elevation for Atoka Reservoir is accurate within 3 m. elevations were displayed to .01 for consistency.]

Bridge/Road Name	Atoka Reservoir			
	75% PMF		Sunny Day	
	Maximum Surface Water Elevation			
	(m)	(hh:mm)	(m)	(hh:mm)
US Highway 69	176.2	02:00	164.8	04:20
Railroad Bridge	173.5	02:05	164.7	04:25
Tellico Road	171.1	03:05	164.3	04:35
Half Bank Road	160.7	22:40	153.4	29:25
McGee Creek Road	155.6	26:40	147.6	46:45
Private Bridge	150.8	29:35	52.30	62:30
State Highway 3	148.9	30:05	143.0	68:00
Unnamed Road	137.0	61:40	134.9	96:00[1]
Dolese Youth Park Lake				
Meridian Avenue	387.9	03:06	386.0	00:30
Meridian Avenue	387.9	03:06	379.6	00:30
60th Street	378.7	03:06	378.1	00:35
Northwest Expressway	369.6	04:31	369.1	00:40
Dry Creek Detention Reservoir				
Quail Creek Road	348.8	00:25	348.3	00:35
122nd Street	346.6	02:30	345.8	01:00
Fairway Culvert	345.5	00:35	345.3	01:25
Quail Creek Golf Course Bridge	342.8	00:40	341.2	01:25
Twisted Oak Road	342.8	00:40	340.9	01:30
Quail Creek Golf Course Bridge	343.1	00:50	340.5	01:30
Quail Creek Golf Course Bridge	339.4	00:55	338.1	01:35
Quail Creek Golf Course Bridge	336.7	01:05	335.4	01:40
Quail Creek Golf Course Bridge	336.5	01:05	335.1	01:40
Lake Hefner Parkway	333.6	01:05	332.3	01:40
John Kilpatrick Turnpike Ramp	332.5	01:10	331.3	01:40
150th Street	325.1	01:50	322.8	03:35
164th Street	321.8	03:20	320.6	05:05

[1]Time to peak stage was not yet reached at the maximum allowable simulation time of 96 hours

Table A.2. Maximum surface water elevation and time to peak for 75% Probable Maximum Flood (PMF) and sunny day breach scenarios for identified bridges for eleven dams in Oklahoma City, Oklahoma and near Atoka, Oklahoma. [m, meters; hh:mm, hours and minutes of time to peak after dam breach time; due to uncertainty of elevation data bridges located outside of Oklahoma City limits are accurate within 2 m. elevations displayed to 0.1 m for consistency.]

Bridge/Road Name	Lake Hefner			
	75% PMF		Sunny Day	
	Maximum Surface Water Elevation			
	(m)	(hh:mm)	(m)	(hh:mm)
122nd Street	343.8	01:55	343.0	01:45
Val Verde Drive	340.5	02:00	339.8	01:55
John Kilpatrick Turnpike	338.0	02:00	337.6	01:55
Gaillardia Golf Course Bridge	335.0	02:10	334.3	02:05
150th Street	332.2	02:15	331.6	02:10
164th Street	328.4	02:30	327.8	02:25
178th Street	323.5	02:50	322.9	02:40
Covell Road	320.9	04:40	319.6	04:50
Portland Avenue	320.9	04:40	319.5	04:55
Sorghum Mill Road	320.9	04:40	319.5	04:55
Waterloo Road	316.4	04:50[1]	315.3[2]	05:05
Charter Oak Road	314.7	05:10	313.8	05:30
Pennsylvania Avenue	312.5	05:20[1]	310.7[3]	06:20
Western Avenue	312.2	05:35	310.2	06:30
Seward Avenue	306.8	06:10	304.8	07:05
Eastern Road	304.3	06:30	302.3	08:10
Phillips/Academy Road	302.8	06:40	300.7	08:25
Industrial Road	296.7	06:55	295.2	08:45
5th Street	293.6	07:55[1]	292.6	10:35
State Highway 33	296.0	08:20	293.3	11:40
College Avenue	295.8	08:20	293.0	11:40
Railroad Bridge	295.4	08:20	292.5	11:45
Sooner Road	295.4	08:20	292.4	11:45
Lake Overholser				
Northwest 10th Street	378.8	02:40	372.0	04:00
Railroad Bridge	377.0	03:00	370.7	04:40
West Reno Avenue	377.0	03:00	370.2	04:50
Interstate 40	376.2	03:20	370.3	04:50
Council Road	374.0	03:30	368.6	05:40
MacArthur Boulevard	372.0	05:20	365.2	08:00
Meridian Avenue	370.8	06:00	361.9	08:30
Portland Avenue	369.9	06:40	360.9	08:40
Interstate 44	369.3	06:50	360.1	08:40
May Avenue	368.5	07:10	358.6	09:10
Agnew Avenue	367.5	07:40	358.3	09:20

[1]Time was interpolated from times at upstream and downstream bridges. Model instability resulted in calculated time to peak.

[2]Stage was interpolated from stage at upstream and downstream bridges. Model instability resulted in calculated time to peak.

Table A.3. Maximum surface water elevation and time to peak for 75% Probable Maximum Flood (PMF) and sunny day breach scenarios for identified bridges for eleven dams in Oklahoma City, Oklahoma and near Atoka, Oklahoma. [m, meters; hh:mm, hours and minutes of time to peak after dam breach time; due to uncertainty of elevation data bridges located outside of Oklahoma City limits are accurate within 2 m. elevations displayed to 0.1 m for consistency.]

Bridge/Road Name	Lake Overholser (Cont.)			
	75% PMF		Sunny Day	
	Maximum Surface Water Elevation			
	(m)	(hh:mm)	(m)	(hh:mm)
Pennsylvania Avenue	366.7	08:10	358.1	09:20
Exchange Avenue	365.7	08:40	357.6	09:30
Railroad Bridge	365.4	08:50	357.4	09:30
Western Avenue	365.1	09:00	357.1	10:20
Walker Avenue	364.7	09:00	355.8	10:40
Robinson Avenue	364.3	09:10	355.6	10:50
Shields Boulevard	364.0	09:10	355.6	10:50
15th Street	363.0	09:20	355.5	11:00
Pipe Bridge	362.9	09:20	355.4	11:00
Railroad Bridge	362.1	09:30	355.2	11:00
Lincoln Boulevard	361.8	09:40	355.2	11:00
Interstate 35	361.3	09:40	354.8	11:30
Eastern Avenue	360.7	09:50	354.6	11:30
Reno Avenue	359.7	09:50	354.0	11:40
Interstate 40 Eastbound	358.7	09:50	353.6	11:40
Interstate 40 Westbound	358.6	09:50	353.5	11:40
Railroad Bridge	357.5	11:00	353.0	11:50
4th Street	357.3	11:00	352.8	12:00
10th Street	356.7	11:20	352.0	12:20
23rd Street	355.9	11:30	350.9	15:20
36th Street	354.6	12:20	350.6	16:50
Midwest Boulevard	352.0	12:50	348.5	21:20
63rd Street	350.4	13:20	346.5	24:50
Britton Road	349.2	13:30	344.0	27:30
Hefner Road	346.7	14:10	342.5	29:40
122nd Street	344.7	14:50	340.8	30:20
Hiwassee Road	343.2	15:10	337.9	33:20
Britton Road	338.5	16:10	334.7	34:50
Lightning Creek Holding Pond A				
Broadway Avenue	390.9	00:45	390.2	01:05
Walker Avenue	386.8	01:00	386.2	01:15
Trafalgar Drive	386.0	01:05	385.6	01:20
Shartel Avenue	385.0	01:10	384.7	01:25
89th Street	382.2	01:25	381.9	01:35
Western Avenue	367.4	01:30	380.6	01:45
84th Street	379.8	01:30	379.0	01:55
Western Avenue	377.3	01:40	375.4	02:00
Interstate 240 Service Road	376.1	02:00	373.6	02:15
67th Street	373.6	02:10	370.7	02:20
59th Street	369.1	02:20	367.1	02:25
Walker Avenue	368.2	02:20	366.1	02:30

Table A.4. Maximum surface water elevation and time to peak for 75% Probable Maximum Flood (PMF) and sunny day breach scenarios for identified bridges for eleven dams in Oklahoma City, Oklahoma and near Atoka, Oklahoma. [m, meters; hh:mm, hours and minutes of time to peak after dam breach time; elevations displayed to 0.1 m for consistency]

Bridge/Road Name	Lightning Creek Holding Pond A (Cont.)			
	75% PMF		Sunny Day	
	Maximum Surface Water Elevation			
	(m)	(hh:mm)	(m)	(hh:mm)
51st Street	367.4	02:25	365.3	02:35
Sage Avenue	366.8	02:25	364.5	02:40
Unnamed Road	366.4	02:25	364.4	02:40
44th Street	365.9	02:30	364.1	02:40
Santa Fe Avenue	365.6	02:30	363.8	02:40
Draper Park Bridge	364.9	02:35	363.0	02:45
Santa Fe Avenue	364.6	02:35	362.3	02:50
Grand Boulevard	364.2	02:35	361.8	02:55
29th Street	362.8	02:45	360.9	03:00
28th Street	362.5	02:45	360.6	03:00
27th Street	362.1	02:45	360.2	03:00
25th Street	360.1	02:50	359.5	03:00
23rd Street	361.3	02:50	358.8	03:05
18th Street	358.2	02:55	356.6	03:05
15th Street	356.0	02:55	354.4	03:05
Foot Bridge	355.5	02:55	353.7	03:10
Lightning Creek Holding Pond C				
81st Street				
81st Street	381.2	00:35	380.8	00:35
Western Avenue	378.4	00:45	377.9	00:45
Interstate 240 Service	377.3	00:45	376.1	00:45
Road	376.0	00:55	373.8	00:50
67th Street	373.6	01:05	370.9	00:55
59th Street	369.0	01:15	367.2	01:00
Walker Avenue	368.2	01:20	366.2	01:10
51st Street	367.4	01:20	365.4	01:10
Sage Avenue	366.8	01:20	364.6	01:15
Unnamed Road	366.4	01:25	364.5	01:15
44th Street	365.9	01:25	364.2	01:20
Santa Fe Avenue	365.6	01:25	363.9	01:20
Draper Park Bridge	364.9	01:30	363.0	01:20
Santa Fe Avenue	364.6	01:30	362.3	01:25
Grand Boulevard	364.2	01:35	361.8	01:30
29th Street	362.8	01:40	360.9	01:35
28th Street	362.5	01:40	360.6	01:35
27th Street	362.1	01:40	360.2	01:35
25th Street	361.9	01:40	359.5	01:40
23rd Street	361.3	01:40	358.7	01:40
18th Street	358.2	01:45	356.5	01:45
15th Street	356.0	01:45	354.4	01:45
Foot Bridge	355.5	01:45	353.7	01:45

Table A.5. Maximum surface water elevation and time to peak for 75% Probable Maximum Flood (PMF) and sunny day breach scenarios for identified bridges for eleven dams in Oklahoma City, Oklahoma and near Atoka, Oklahoma. [m, meters; hh:mm, hours and minutes of time to peak after dam breach time, elevations displayed to 0.1 m for consistency]

Bridge/Road Name	Northeast (Zoo) Lake			
	75% PMF		Sunny Day	
	Maximum Surface Water Elevation			
	(m)	(hh:mm)	(m)	(hh:mm)
Remington Place	332.6	00:30	329.5	00:35
Interstate 35	326.9	01:00	321.8	00:45
Bryant Avenue	325.1	01:05	320.5	00:50
63rd Street	324.2	01:10	319.3	00:55
Wilshire Boulevard	322.2	01:45	316.4	01:30
Britton Road	317.3	02:25	312.5	02:00
Hefner Road	314.4	03:15	309.9	02:55
Sooner Road	313.3	03:35	309.3	03:20
122nd Street	312.7	04:25	309.1	03:45
Interstate 44	312.2	04:35	308.3	04:25
Memorial Road	310.4	05:30	307.7	05:45
Northwest Oklahoma City Sludge Lagoon				
Pony Road				
122nd Street	347.0	00:25	346.4	00:20
Val Verde Drive	339.2	00:25	338.9	00:25
John Kilpatrick Turnpike	333.3	00:40	332.4	00:40
Gaillardia Golf Course	327.7	00:50	327.1	00:45
Bridge	326.2	00:55	325.7	00:55
150th Street	323.2	01:20	322.9	01:05
164th Street	320.8	01:40	320.6	01:40
Stanley Draper Lake				
149th Street	343.3	01:40	342.3	01:35
164th Street	339.0	01:50	337.6	01:50
179th Street	337.1	01:55	335.7	01:55
Franklin Road	331.6	02:10	330.6	02:25
Alameda Street	324.9	03:10	323.9	03:10
Will Rogers Park Holding Pond				
Unnamed Road	365.4	01:30	360.2	01:00
Drexel Boulevard	365.3	01:30	359.3	01:00
May Avenue	365.3	01:30	358.4	01:05
Venice Boulevard	363.2	02:05	355.7	01:05
36th Street	357.7	02:25	354.1	01:05
Interstate 44	354.9	02:50	351.9	01:10
Youngs Boulevard	354.0	04:30	349.2	01:10
Pennsylvania Avenue	349.7	04:35	347.5	01:15
Interstate 44	348.1	04:35	346.5	01:20
Hemingway Drive	347.3	06:10	346.0	01:25
Interstate 44 Ramp	347.5	06:10	345.8	01:25
Northwest Expressway	347.7	06:10	345.9	01:25

Table A.6. Maximum surface water elevation and time to peak for 75% Probable Maximum Flood (PMF) and sunny day breach scenarios for identified bridges for eleven dams in Oklahoma City, Oklahoma and near Atoka, Oklahoma. [m, meters; hh:mm, hours and minutes of time to peak after dam breach time, elevations displayed to 0.1 m for consistency]

Bridge/Road Name	Will Rogers Park Holding Pond			
	75% PMF		Sunny Day	
	Maximum Surface Water Elevation			
	(m)	(hh:mm)	(m)	(hh:mm)
Belle Isle Boulevard	348.8	06:15	345.7	01:25
Classen Boulevard	347.9	06:20	343.5	01:35
Western Avenue	342.6	06:25	338.5	01:35
Interstate 44	338.7	06:30	337.1	01:40
Interstate 44 Ramp	338.6	06:35	332.1	02:05
Interstate 235	338.6	06:35	332.0	02:05
Lincoln Boulevard Southbound	336.8	07:20	329.6	02:25
Lincoln Boulevard Northbound	330.2	08:45	327.6	02:25
Unnamed Road	329.9	08:45	325.8	02:35
Kelly Avenue	329.9	08:45	325.3	02:45
Grand Boulevard	329.9	08:45	324.3	02:55
Martin Luther King Avenue	323.2	08:45	321.7	03:05
Interstate 35	321.6	09:00	318.9	03:25
Bryant Avenue	324.7	09:05	319.5	03:25
63rd Street	318.5	09:10	317.2	03:30
Wilshire Boulevard	316.2	09:30	314.0	03:50

APPENDIX B

INUNDATION AREA MAPS

B1 Atoka Reservoir

A link to higher resolution pdf versions of the inundation maps was included below. Inundation map pdfs are provided by the US Geological Survey.

http://pubs.usgs.gov/sir/2015/5052/downloads/sir2015-5052_Appendix02.pdf

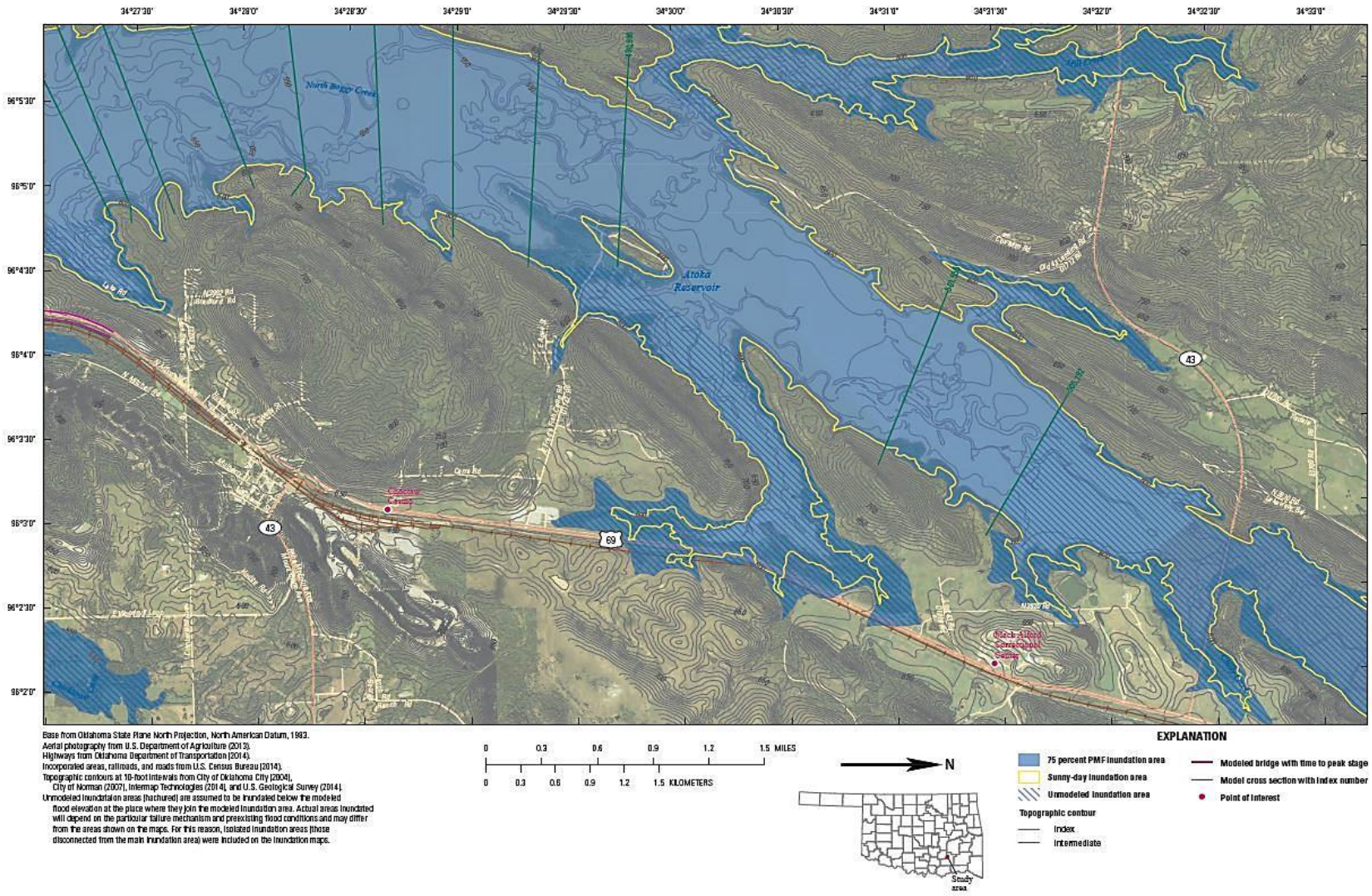

Figure B.1.1. Inundated area for Atoka Reservoir. Map of the inundated areas for both 75% PMF and sunny day dam breach scenarios for Atoka Reservoir. Times to peak stage for 75% PMF breach scenario at modeled bridges, as well as points of interest are shown. Figure courtesy of U.S. Geological Survey.

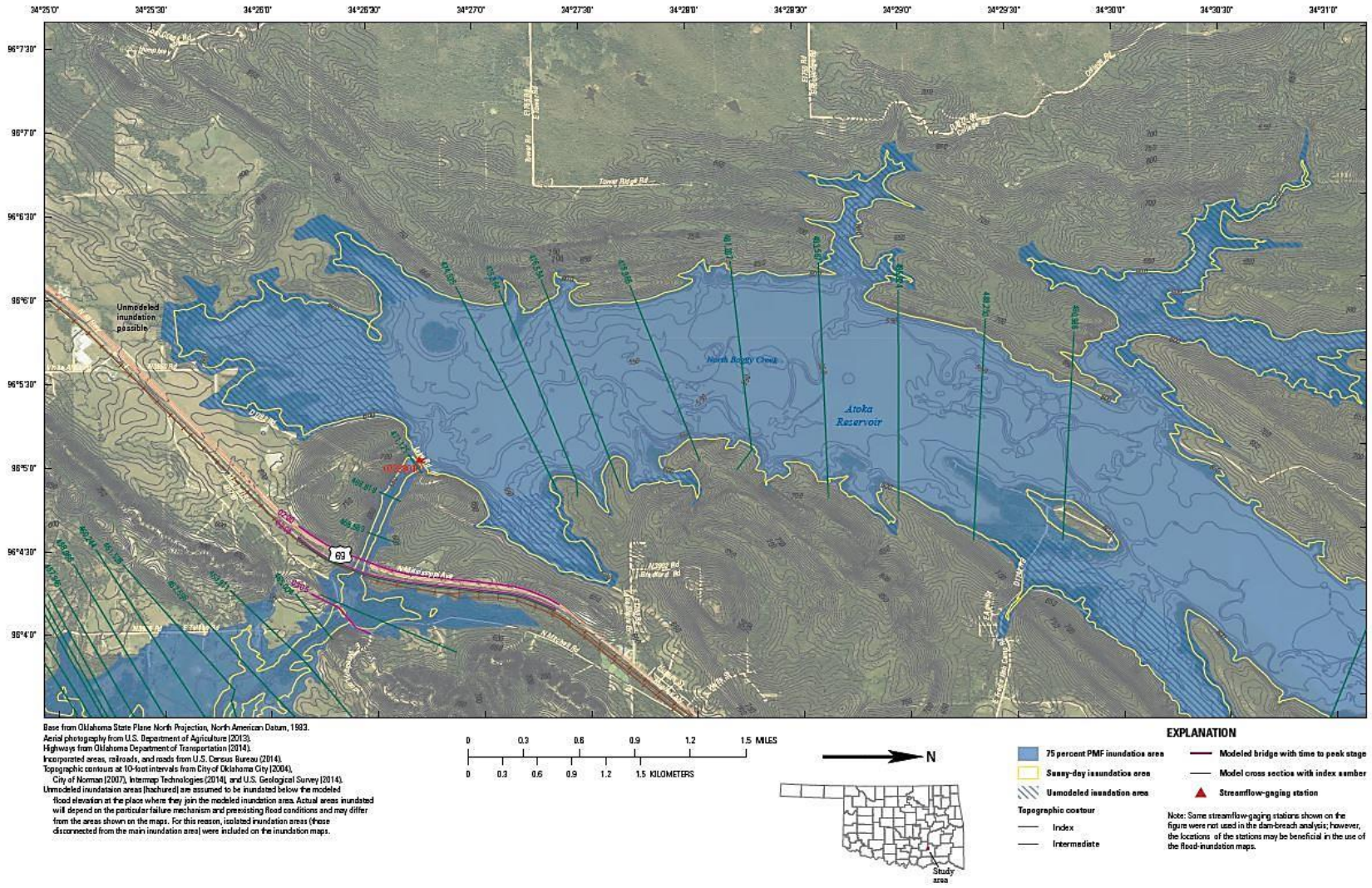

Figure B.1.2. Inundated area for Atoka Reservoir. Map of the inundated areas for both 75% PMF and sunny day dam breach scenarios for Atoka Reservoir. Times to peak stage for 75% PMF breach scenario at modeled bridges, as well as points of interest are shown. Figure courtesy of U.S. Geological Survey.

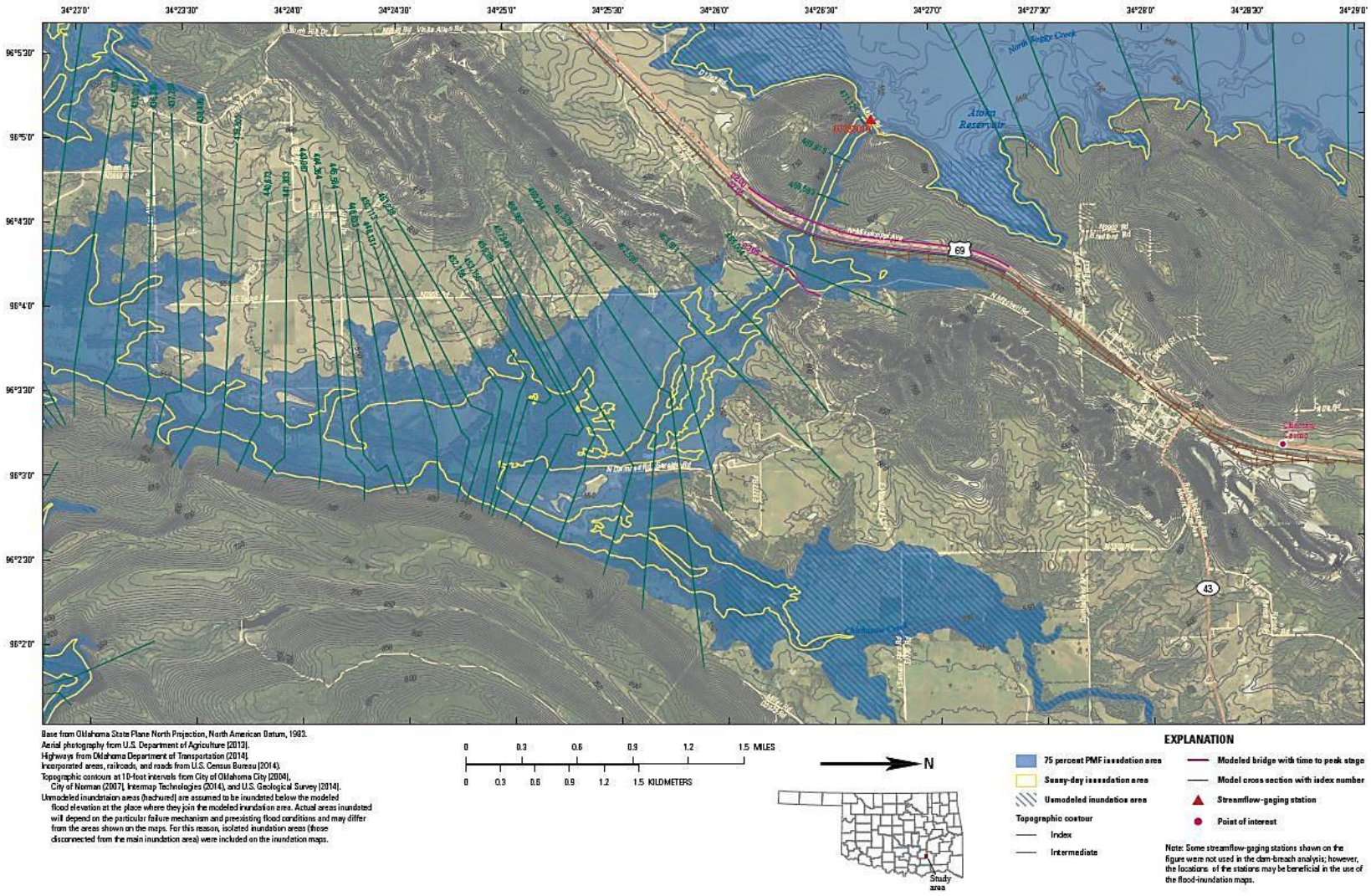

Figure B.1.3. Inundated area for Atoka Reservoir. Map of the inundated areas for both 75% PMF and sunny day dam breach scenarios for Atoka Reservoir. Times to peak stage for 75% PMF breach scenario at modeled bridges, as well as points of interest are shown. Figure courtesy of U.S. Geological Survey.

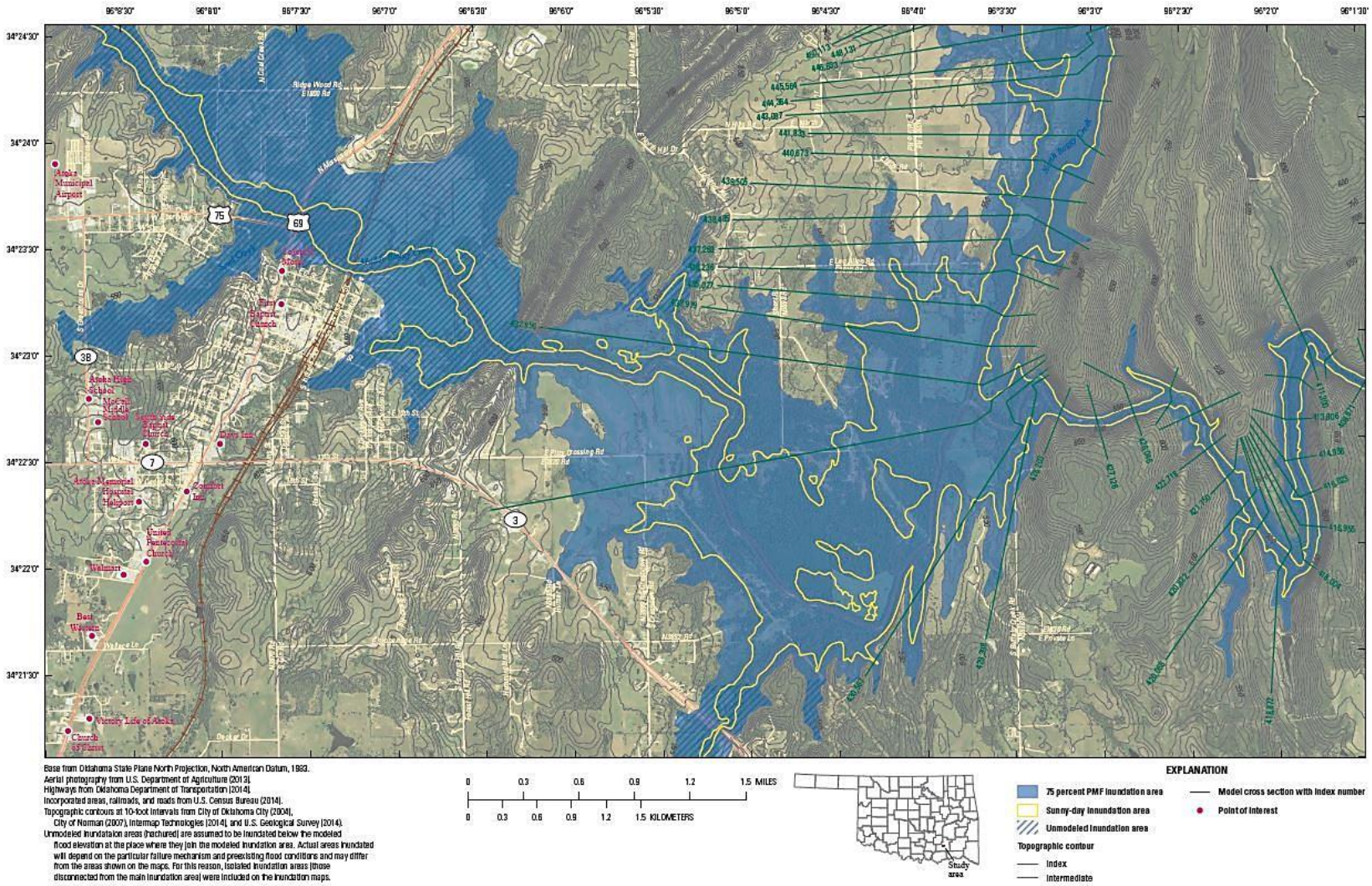

Figure B.1.4. Inundated area for Atoka Reservoir. Map of the inundated areas for both 75% PMF and sunny day dam breach scenarios for Atoka Reservoir. Times to peak stage for 75% PMF breach scenario at modeled bridges, as well as points of interest are shown. Figure courtesy of U.S. Geological Survey.

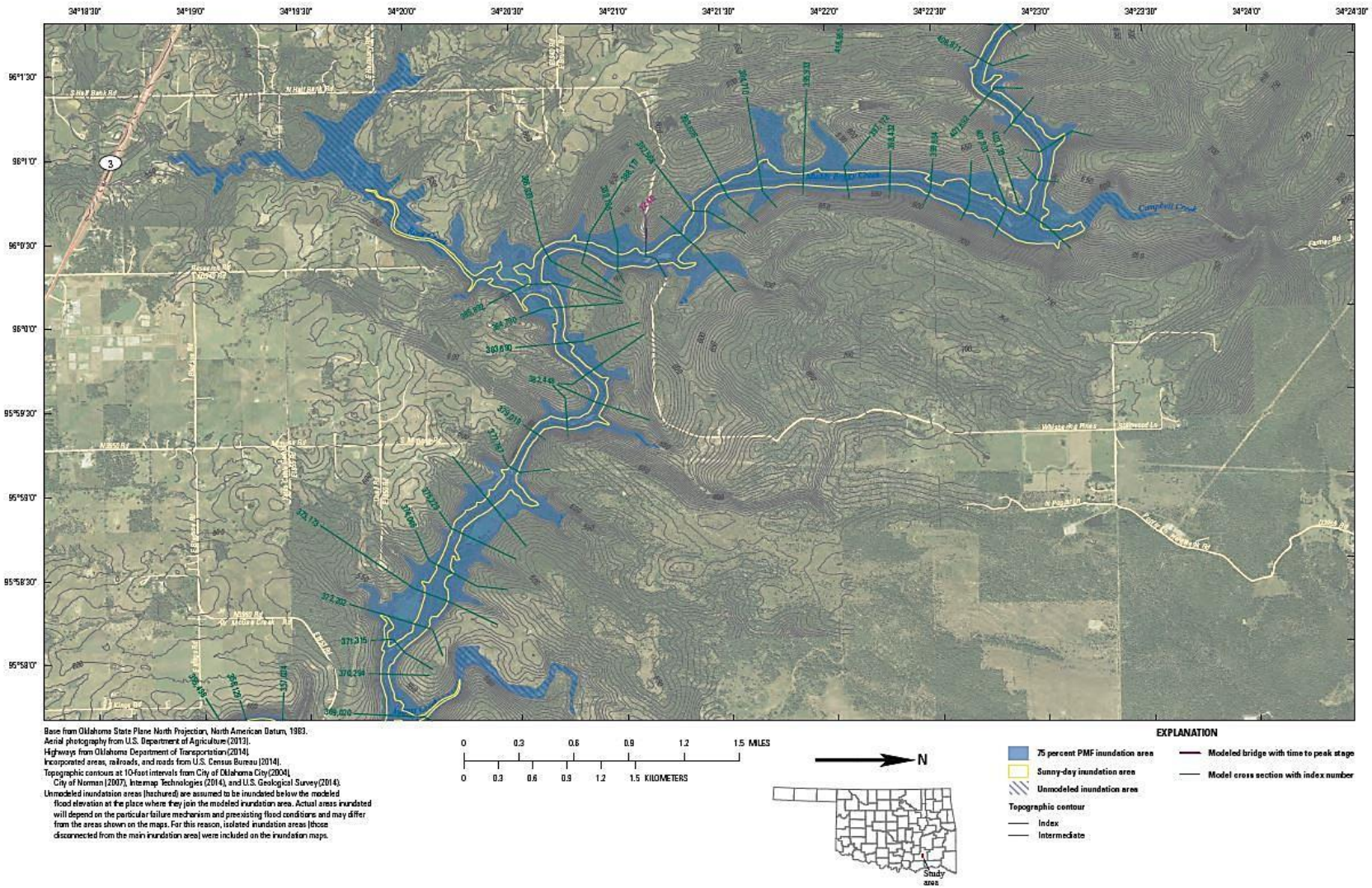

Figure B.1.5. Inundated area for Atoka Reservoir. Map of the inundated areas for both 75% PMF and sunny day dam breach scenarios for Atoka Reservoir. Times to peak stage for 75% PMF breach scenario at modeled bridges, as well as points of interest are shown. Figure courtesy of U.S. Geological Survey.

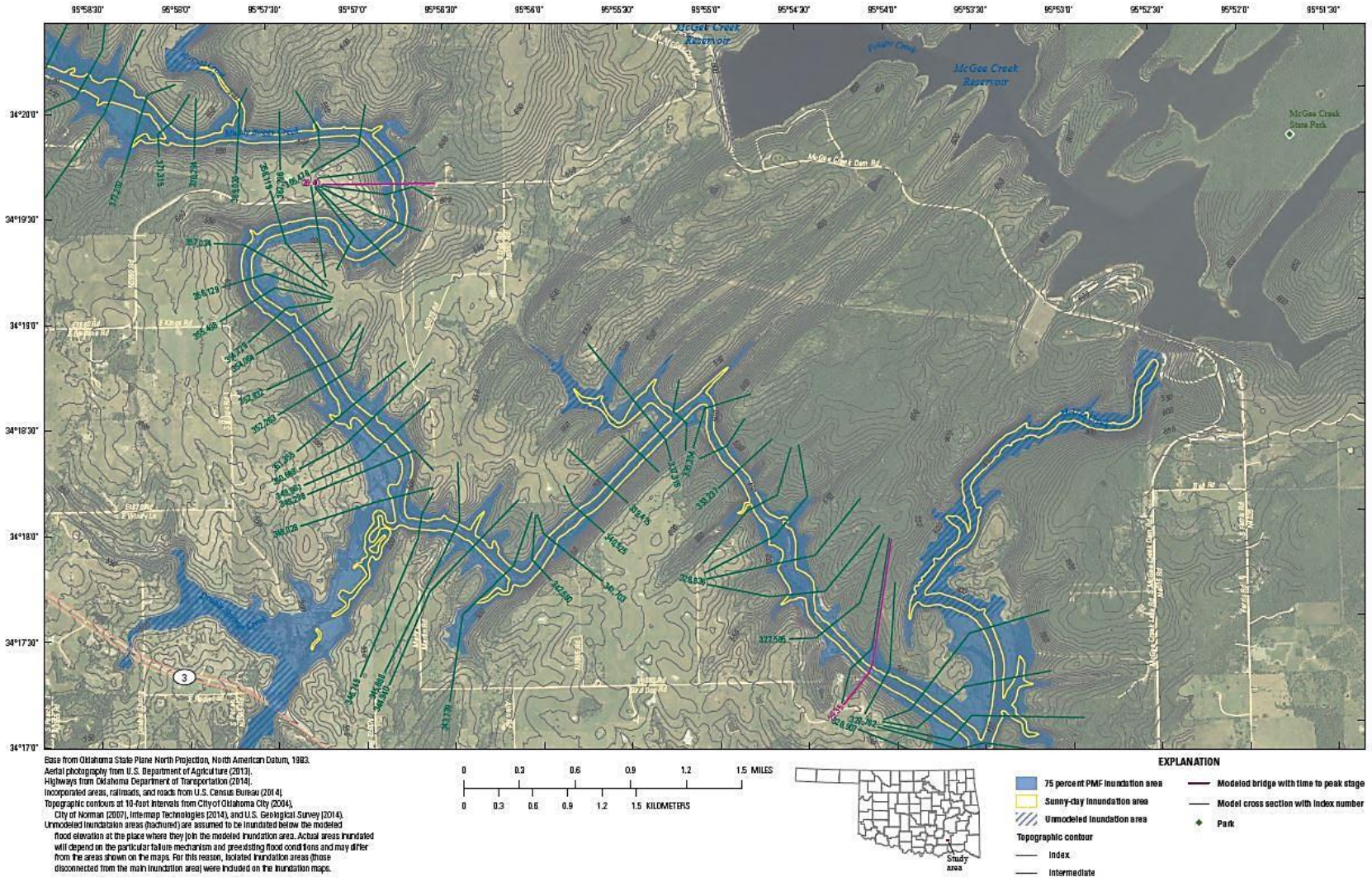

Figure B.1.6. Inundated area for Atoka Reservoir. Map of the inundated areas for both 75% PMF and sunny day dam breach scenarios for Atoka Reservoir. Times to peak stage for 75% PMF breach scenario at modeled bridges, as well as points of interest are shown. Figure courtesy of U.S. Geological Survey.

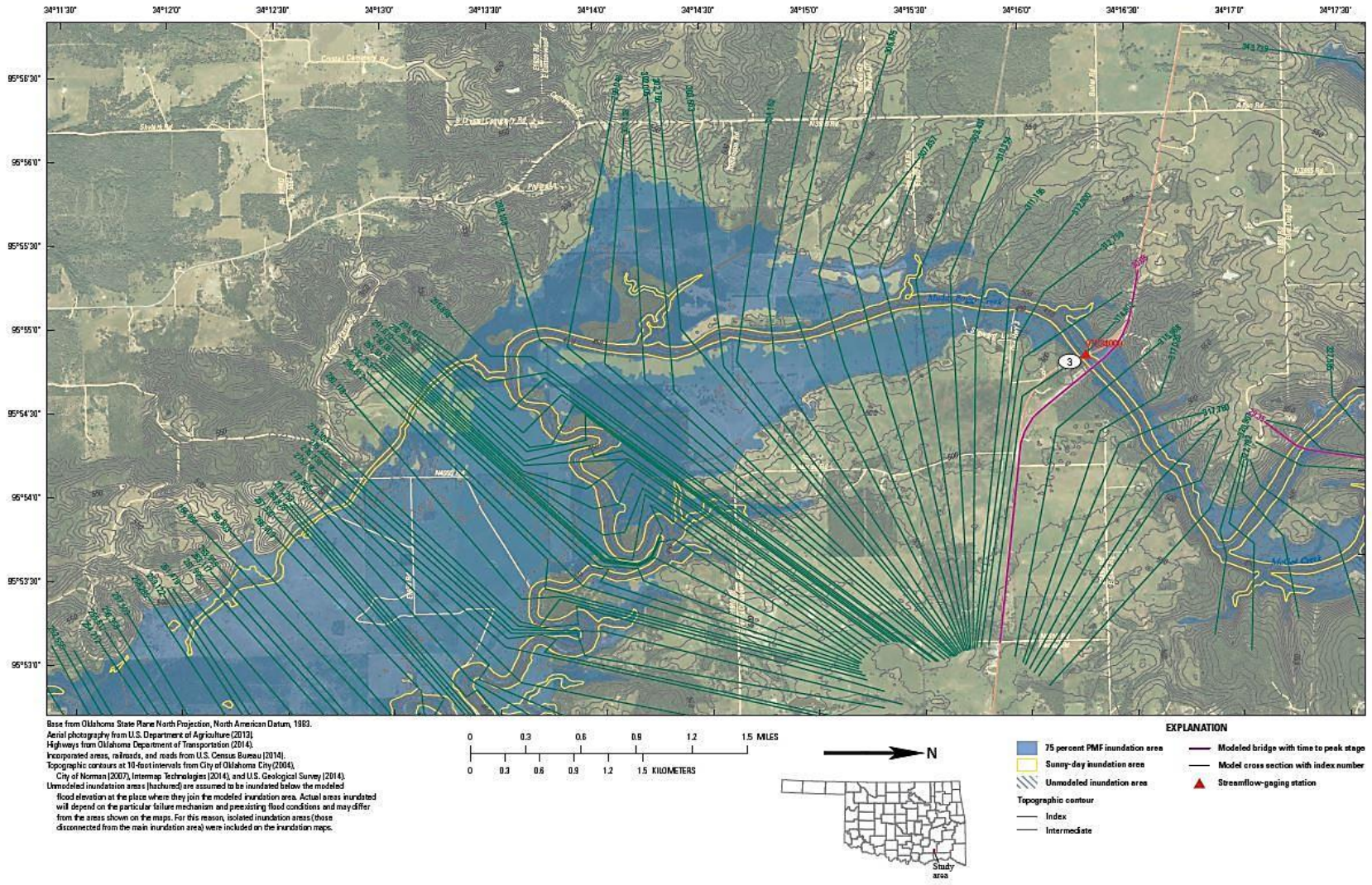

Figure B.1.7. Inundated area for Atoka Reservoir. Map of the inundated areas for both 75% PMF and sunny day dam breach scenarios for Atoka Reservoir. Times to peak stage for 75% PMF breach scenario at modeled bridges, as well as points of interest are shown. Figure courtesy of U.S. Geological Survey.

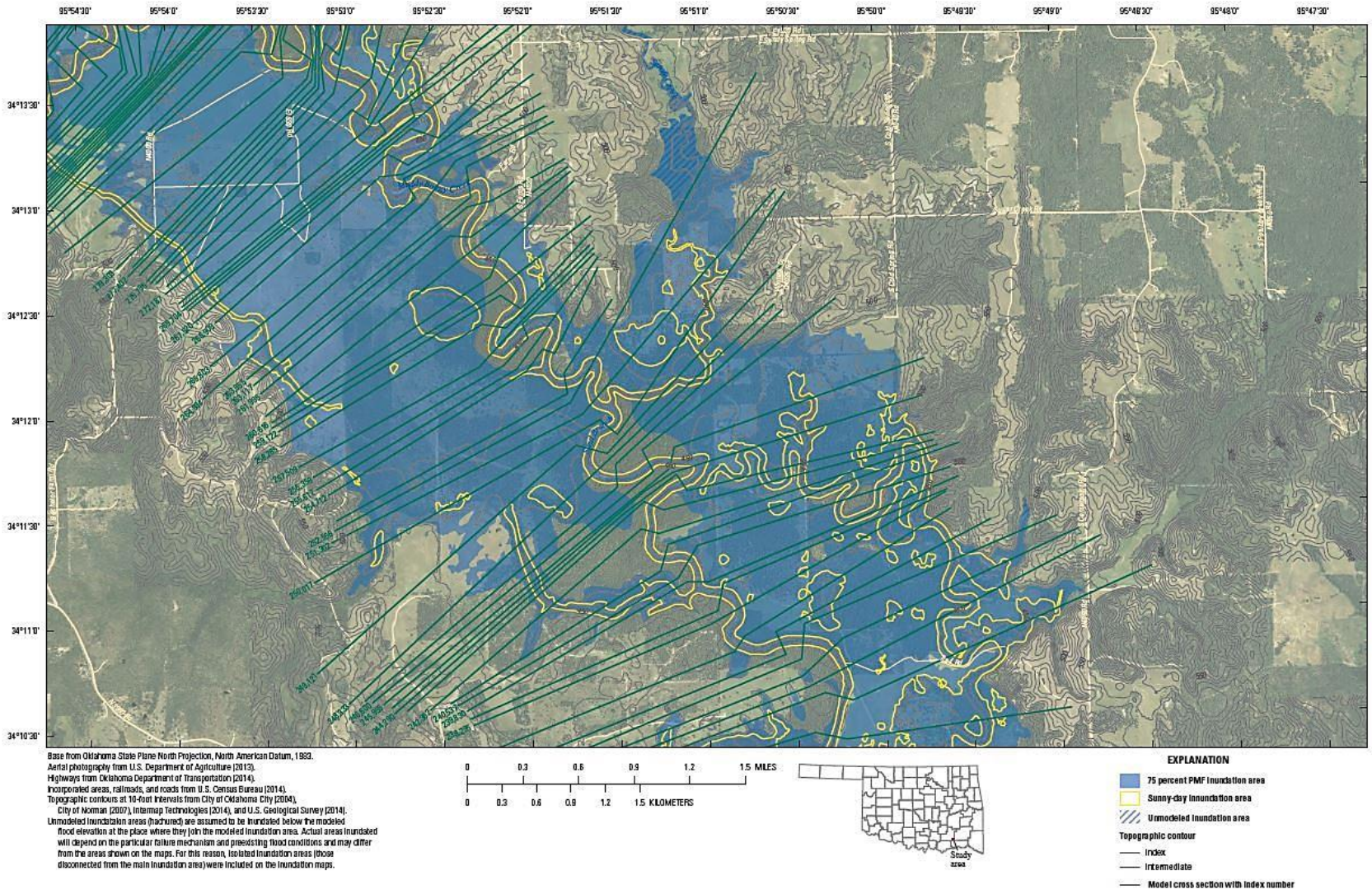

Figure B.1.8. Inundated area for Atoka Reservoir. Map of the inundated areas for both 75% PMF and sunny day dam breach scenarios for Atoka Reservoir. Times to peak stage for 75% PMF breach scenario at modeled bridges, as well as points of interest are shown. Figure courtesy of U.S. Geological Survey.

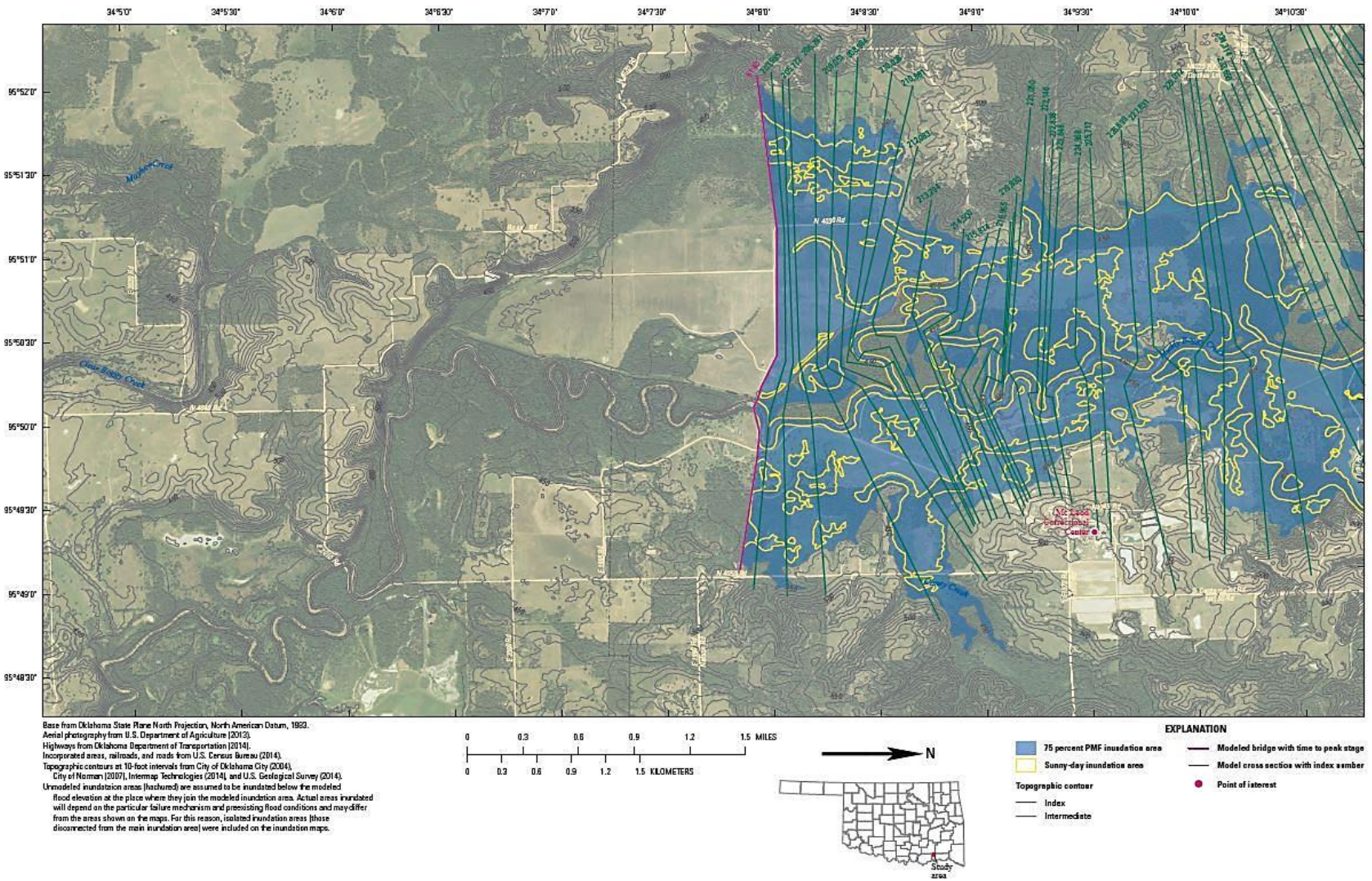

Figure B.1.9. Inundated area for Atoka Reservoir. Map of the inundated areas for both 75% PMF and sunny day dam breach scenarios for Atoka Reservoir. Times to peak stage for 75% PMF breach scenario at modeled bridges, as well as points of interest are shown. Figure courtesy of U.S. Geological Survey.

B2 Dolese Youth Park Lake

A link to higher resolution pdf versions of the inundation maps was included below. Inundation map pdfs are provided by the US Geological Survey.

http://pubs.usgs.gov/sir/2015/5052/downloads/sir2015-5052_Appendix03.pdf

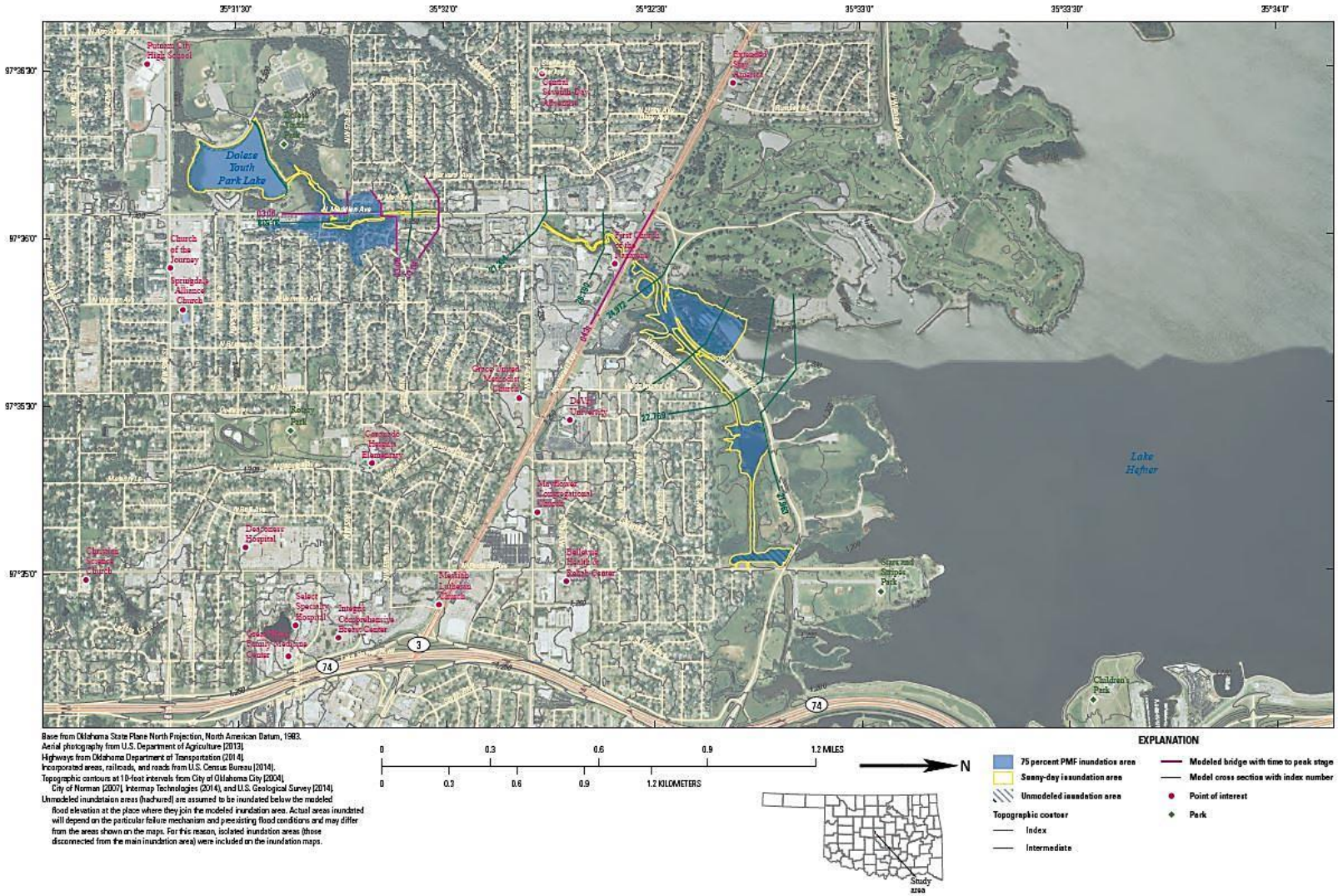

Figure B.2. Inundated area for Dolese Youth Park Lake. Map of the inundated areas for both 75% PMF and sunny day dam breach scenarios for Dolese Youth Park Lake. Times to peak stage for 75% PMF breach scenario at modeled bridges, as well as points of interest are shown. Figure courtesy of U.S. Geological Survey.

B3 Dry Creek Detention Reservoir

A link to higher resolution pdf versions of the inundation maps was included below. Inundation map pdfs are provided by the US Geological Survey.

http://pubs.usgs.gov/sir/2015/5052/downloads/sir2015-5052_Appendix04.pdf

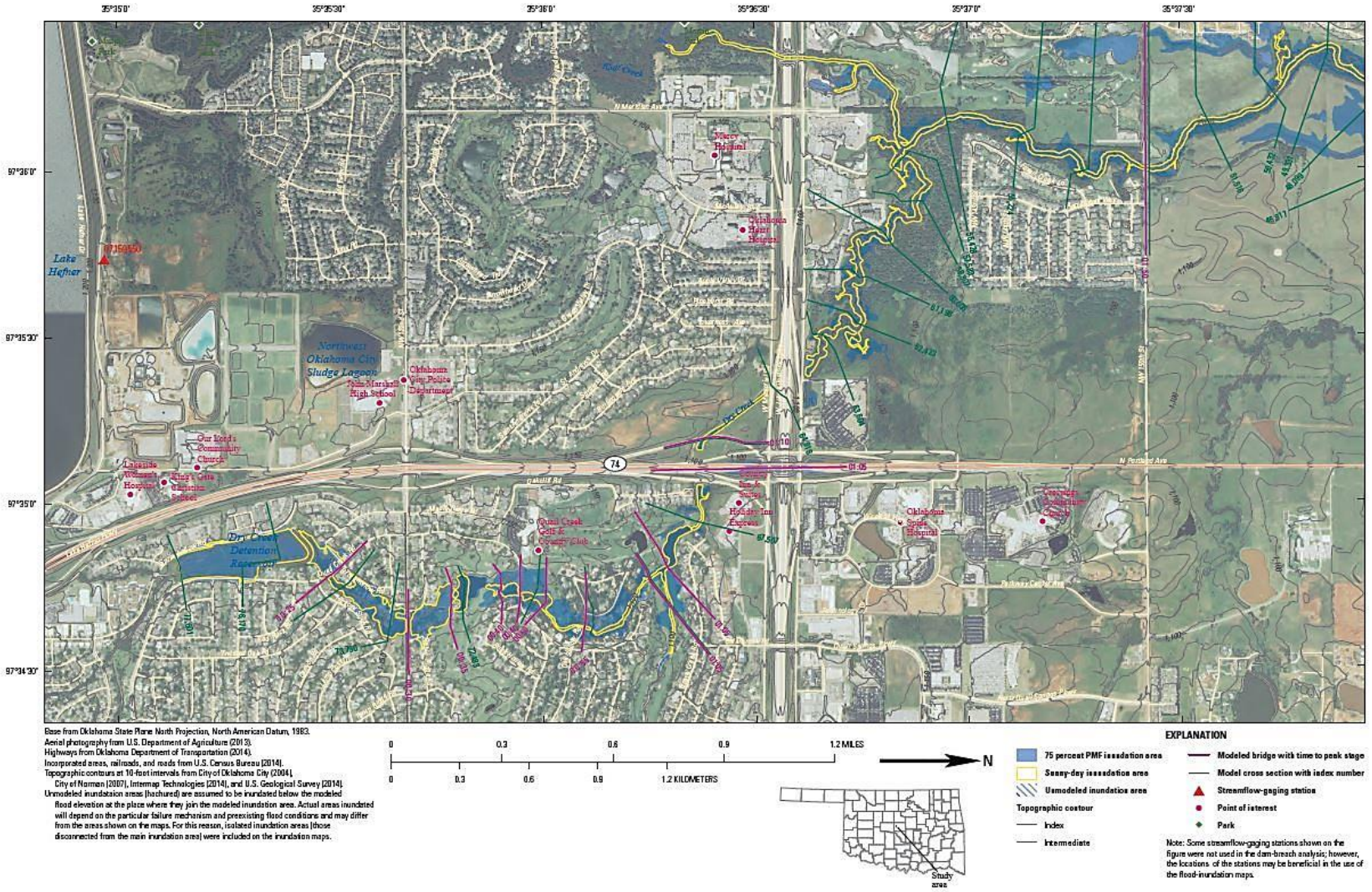

Figure B.3.1. Inundated area for Dry Creek Detention Reservoir. Map of the inundated areas for both 75% PMF and sunny day dam breach scenarios for Dry Creek Detention Reservoir. Times to peak stage for 75% PMF breach scenario at modeled bridges, as well as points of interest are shown. Figure courtesy of U.S. Geological Survey.

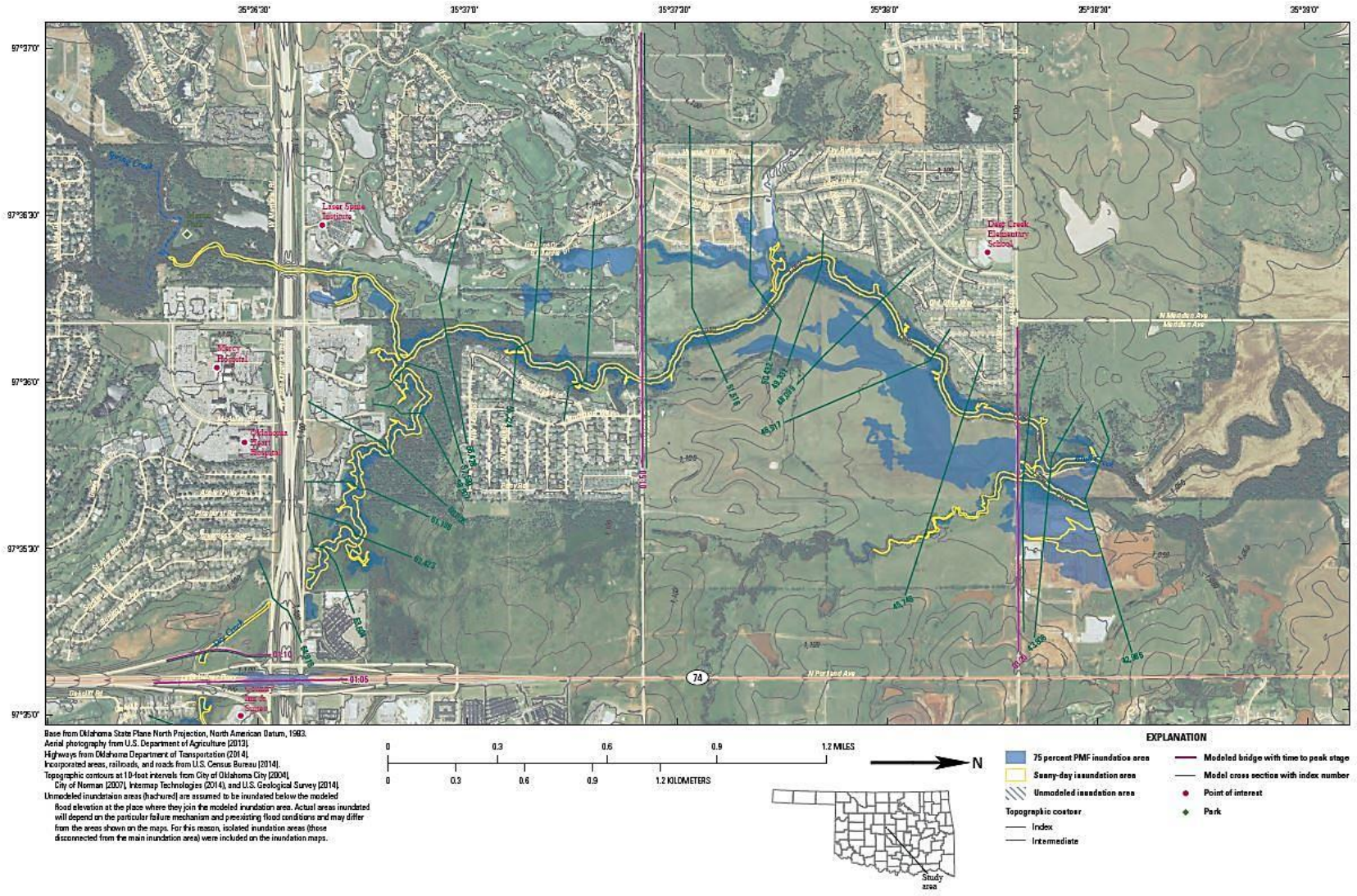

Figure B.3.2. Inundated area for Dry Creek Detention Reservoir. Map of the inundated areas for both 75% PMF and sunny day dam breach scenarios for Dry Creek Detention Reservoir. Times to peak stage for 75% PMF breach scenario at modeled bridges, as well as points of interest are shown. Figure courtesy of U.S. Geological Survey.

B4 Lake Hefner

A link to higher resolution pdf versions of the inundation maps was included below. Inundation map pdfs are provided by the US Geological Survey.

http://pubs.usgs.gov/sir/2015/5052/downloads/sir2015-5052_Appendix05.pdf

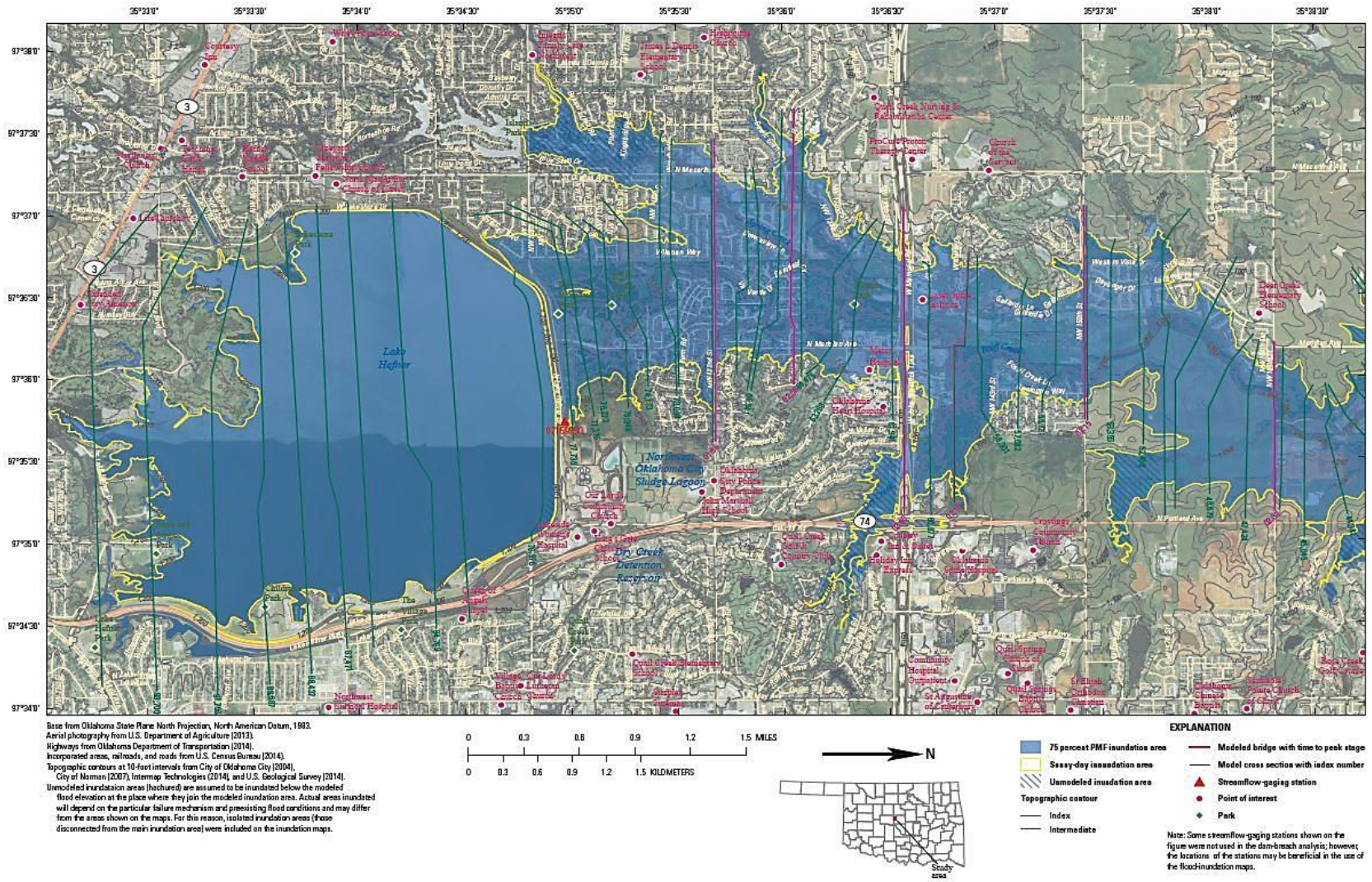

Figure B.4.1. Inundated area for Lake Hefner. Map of the inundated areas for both 75% PMF and sunny day dam breach scenarios for Lake Hefner. Times to peak stage for 75% PMF breach scenario at modeled bridges, as well as points of interest are shown. Figure courtesy of U.S. Geological Survey.

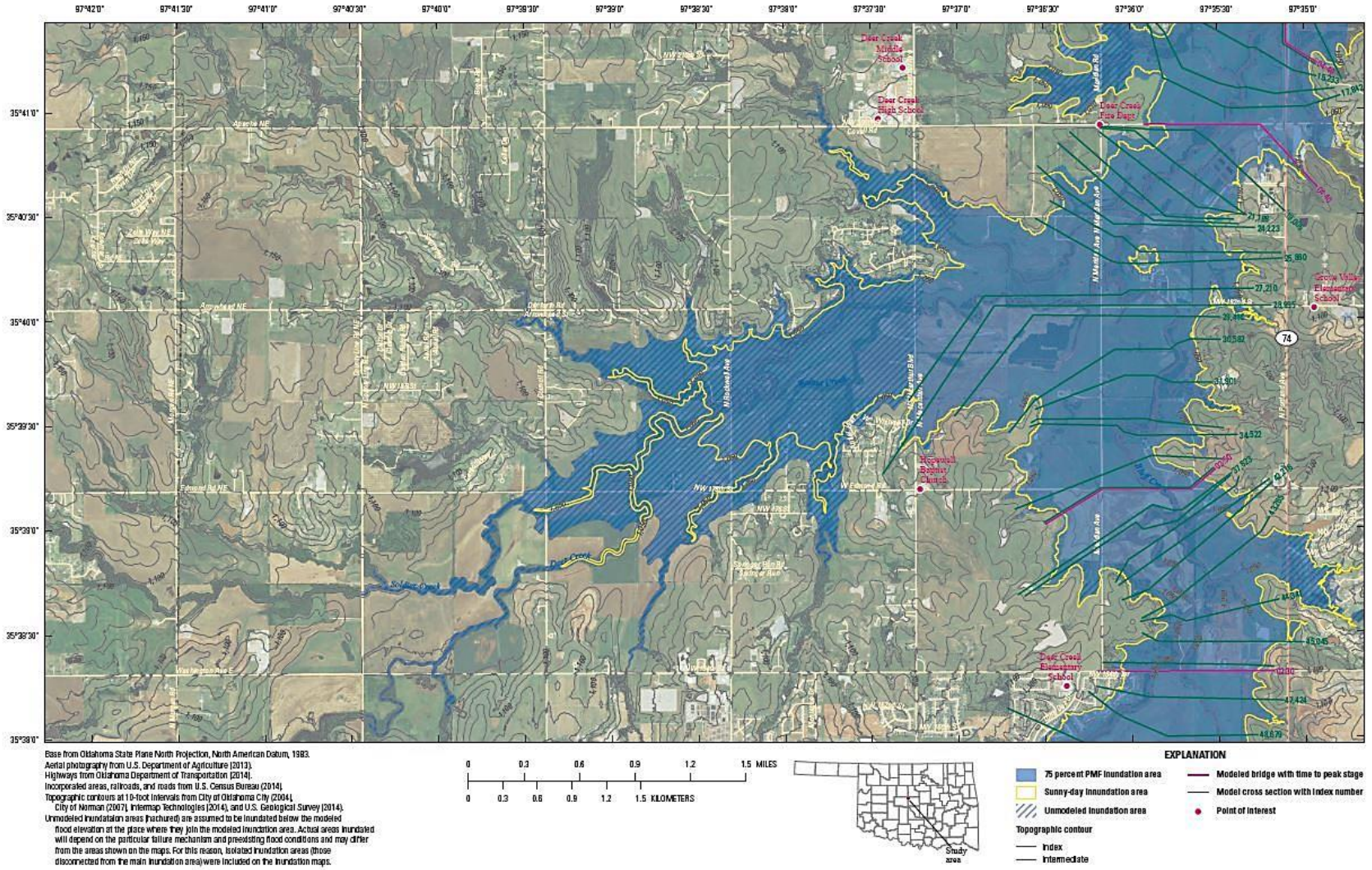

Figure B.4.2. Inundated area for Lake Hefner. Map of the inundated areas for both 75% PMF and sunny day dam breach scenarios for Lake Hefner. Times to peak stage for 75% PMF breach scenario at modeled bridges, as well as points of interest are shown. Figure courtesy of U.S. Geological Survey.

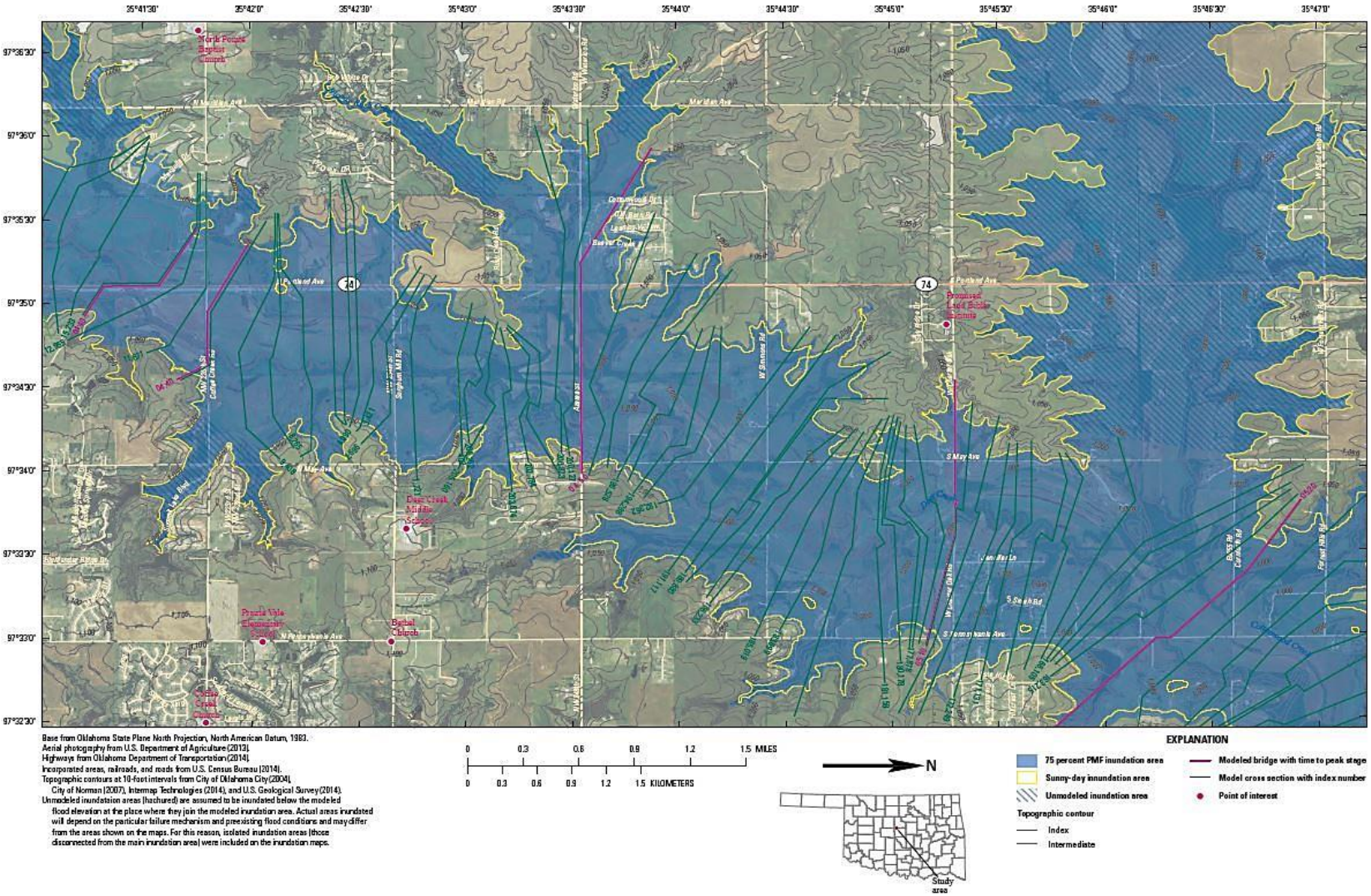

Fiugure B.4.3. Inundated area for Lake Hefner. Map of the inundated areas for both 75% PMF and sunny day dam breach scenarios for Lake Hefner. Times to peak stage for 75% PMF breach scenario at modeled bridges, as well as points of interest are shown. Figure courtesy of U.S. Geological Survey.

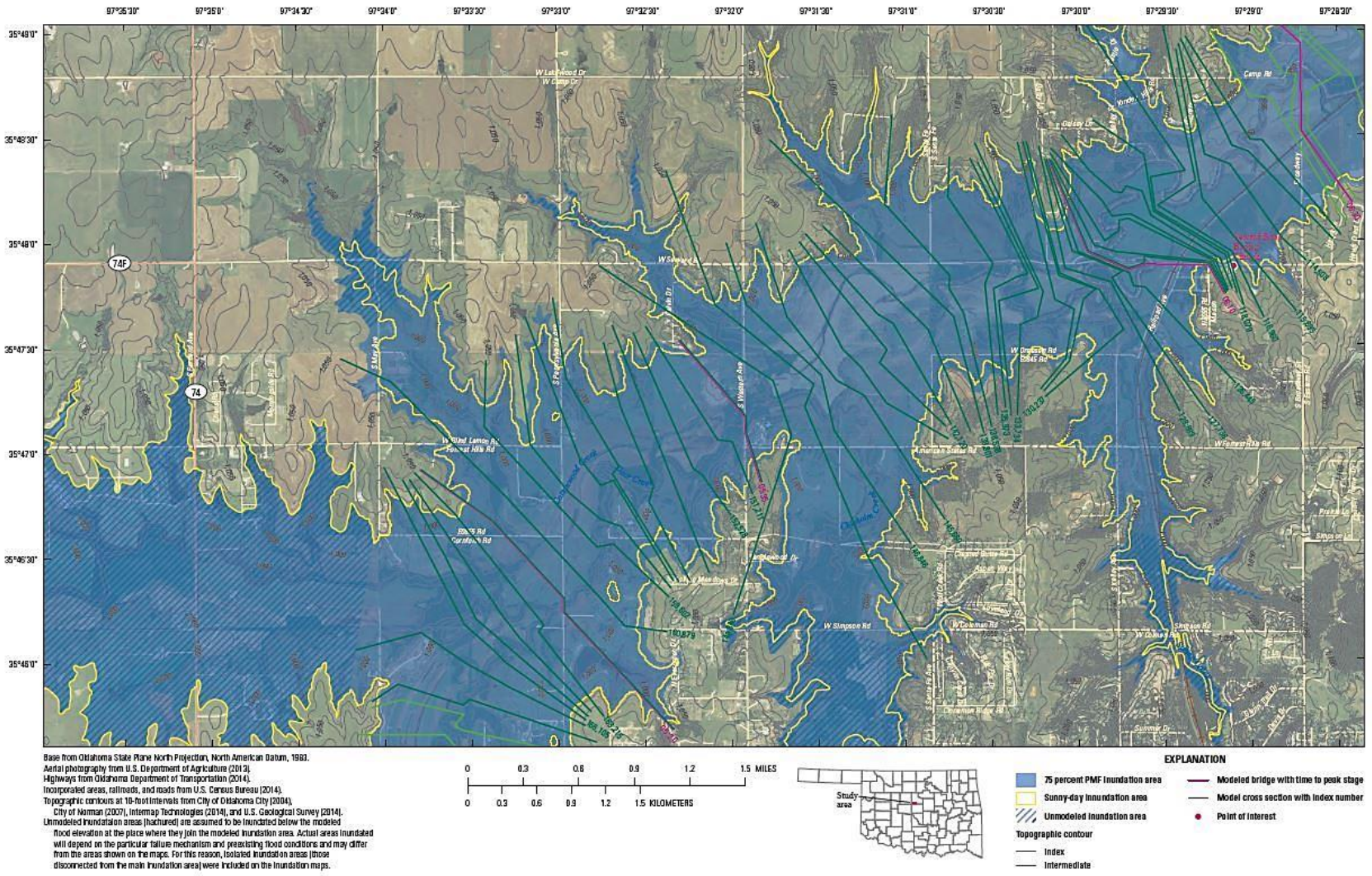

Figure B.4.4. Inundated area for Lake Hefner. Map of the inundated areas for both 75% PMF and sunny day dam breach scenarios for Lake Hefner. Times to peak stage for 75% PMF breach scenario at modeled bridges, as well as points of interest are shown. Figure courtesy of U.S. Geological Survey.

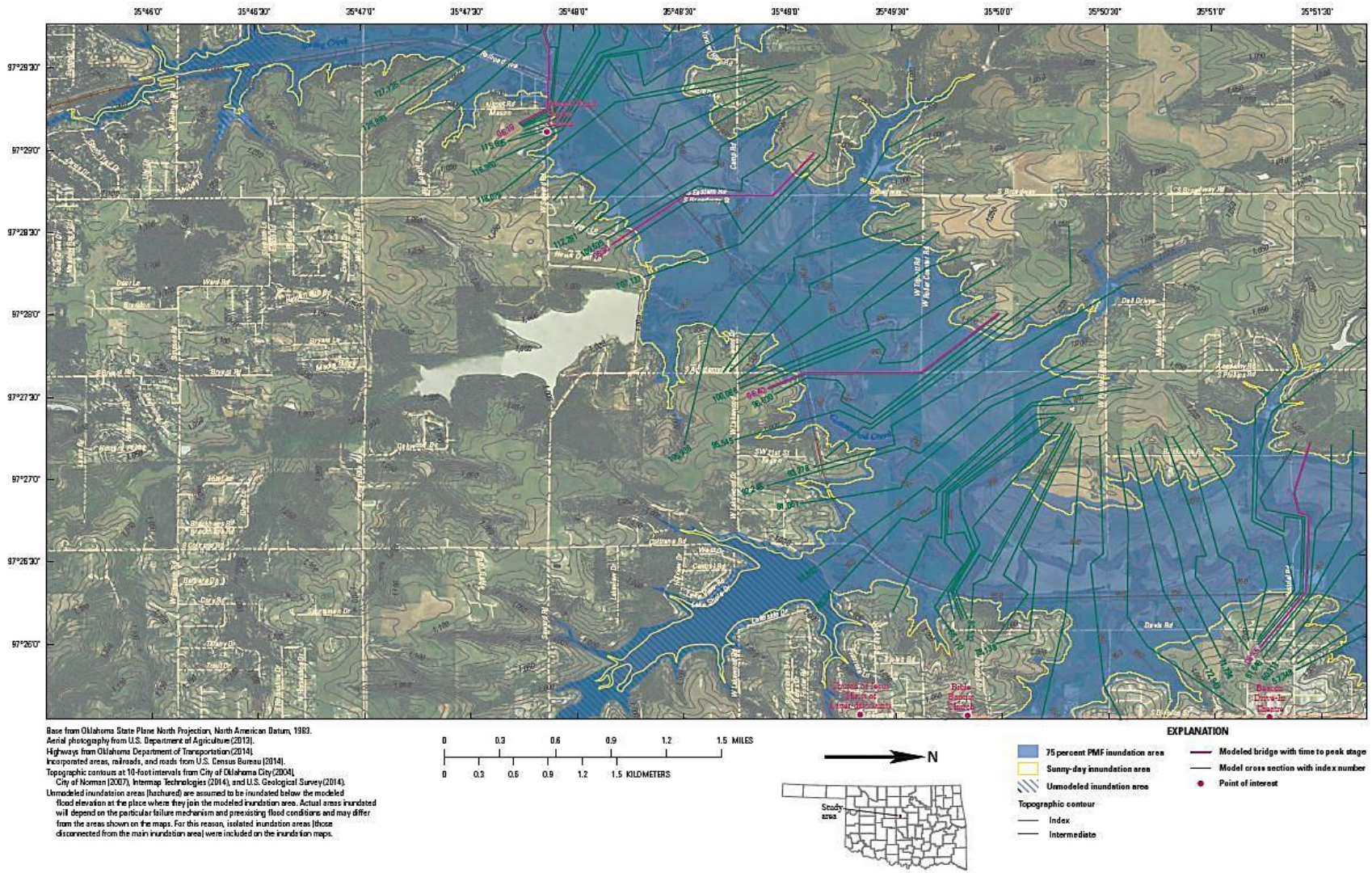

Figure B.4.5. Inundated area for Lake Hefner. Map of the inundated areas for both 75% PMF and sunny day dam breach scenarios for Lake Hefner. Times to peak stage for 75% PMF breach scenario at modeled bridges, as well as points of interest are shown. Figure courtesy of U.S. Geological Survey.

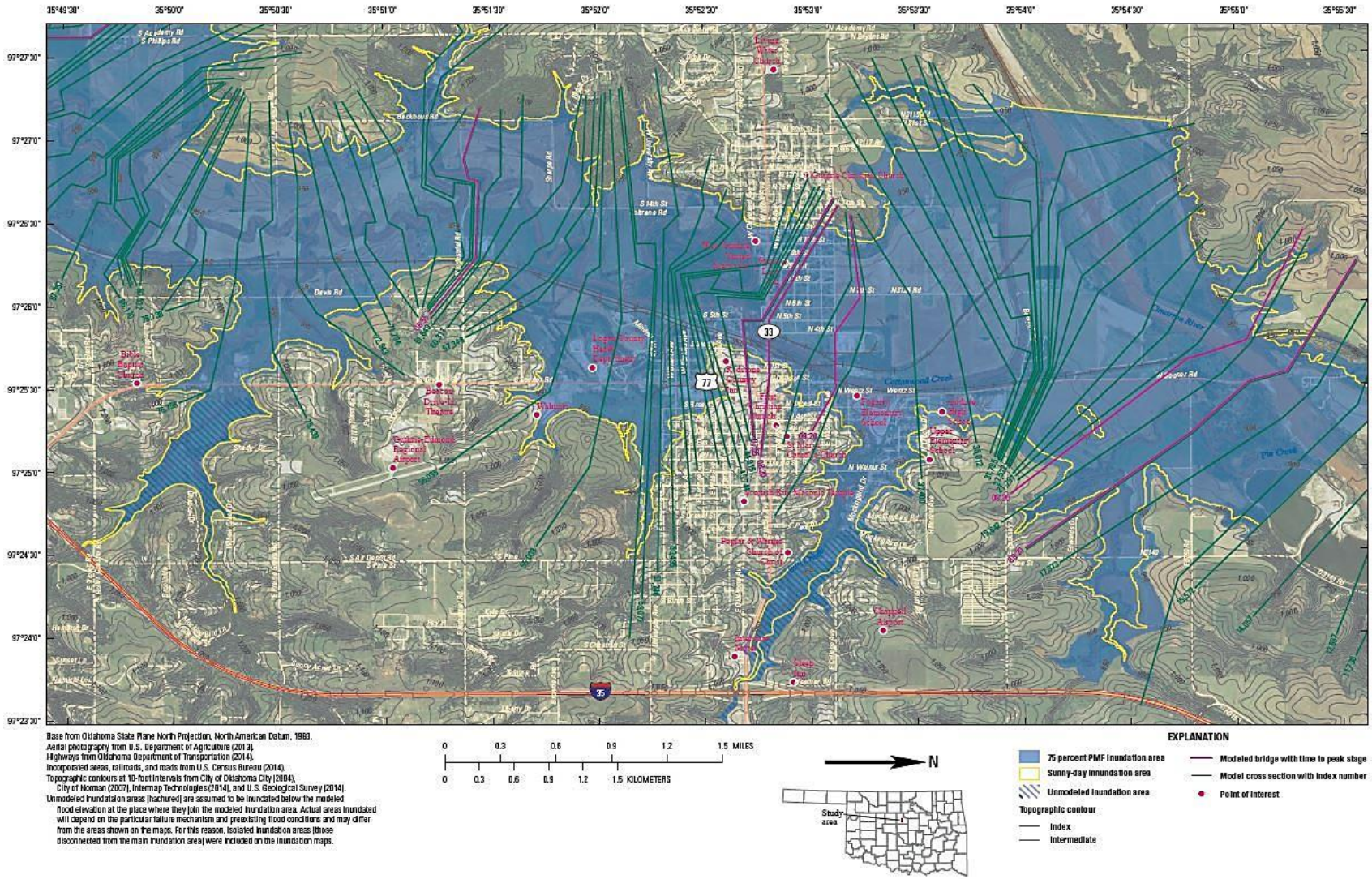

Figure B.4.6. Inundated area for Lake Hefner. Map of the inundated areas for both 75% PMF and sunny day dam breach scenarios for Lake Hefner. Times to peak stage for 75% PMF breach scenario at modeled bridges, as well as points of interest are shown. Figure courtesy of U.S. Geological Survey.

B5 for Lake Overholser

A link to higher resolution pdf versions of the inundation maps was included below. Inundation map pdfs are provided by the US Geological Survey.

http://pubs.usgs.gov/sir/2015/5052/downloads/sir2015-5052_Appendix06.pdf

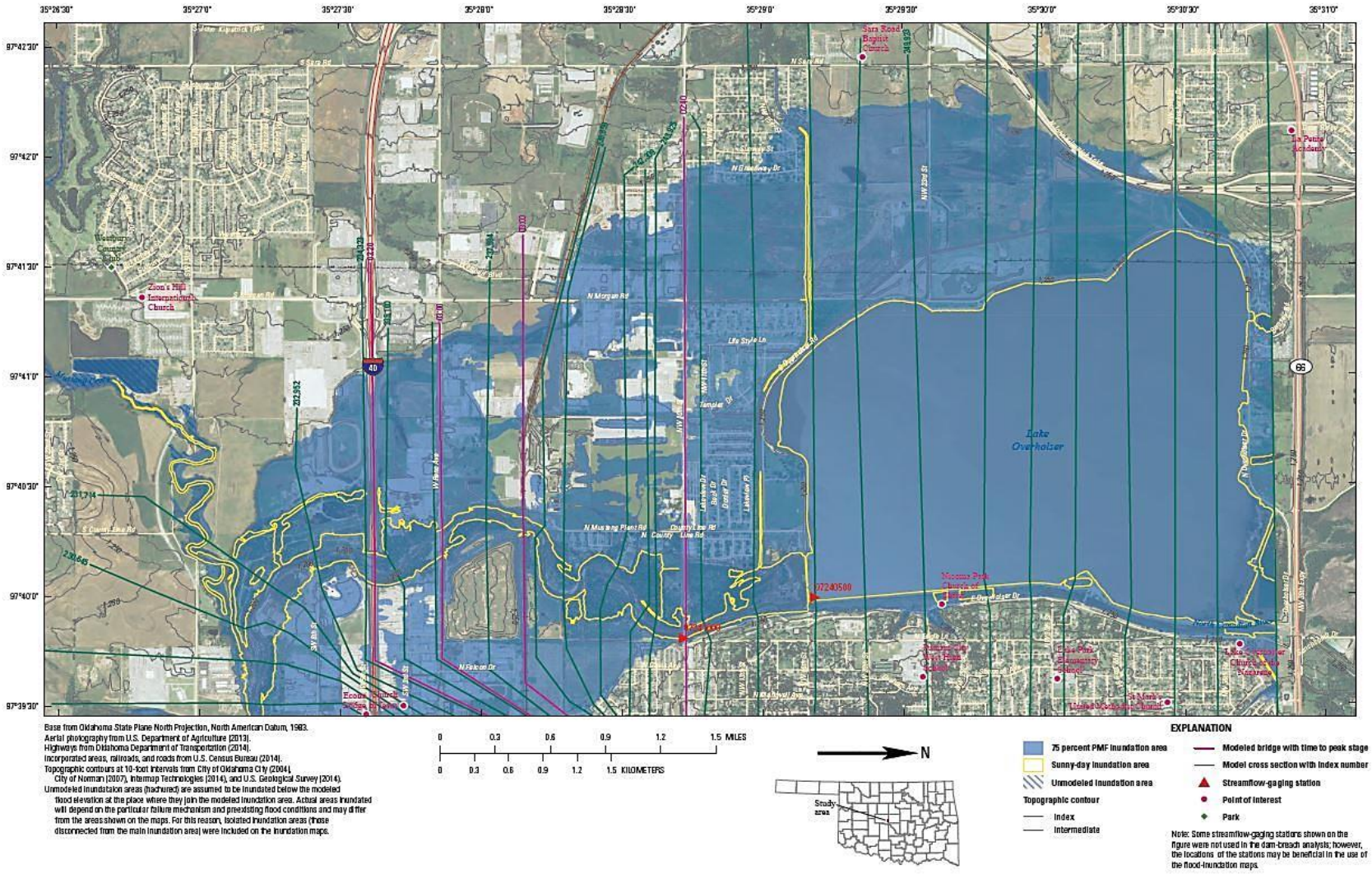

Figure B.5.1. Inundated area for Lake Overholser. Map of the inundated areas for both 75% PMF and sunny day dam breach scenarios for Lake Overholser. Times to peak stage for 75% PMF breach scenario at modeled bridges, as well as points of interest are shown. Figure courtesy of U.S. Geological Survey.

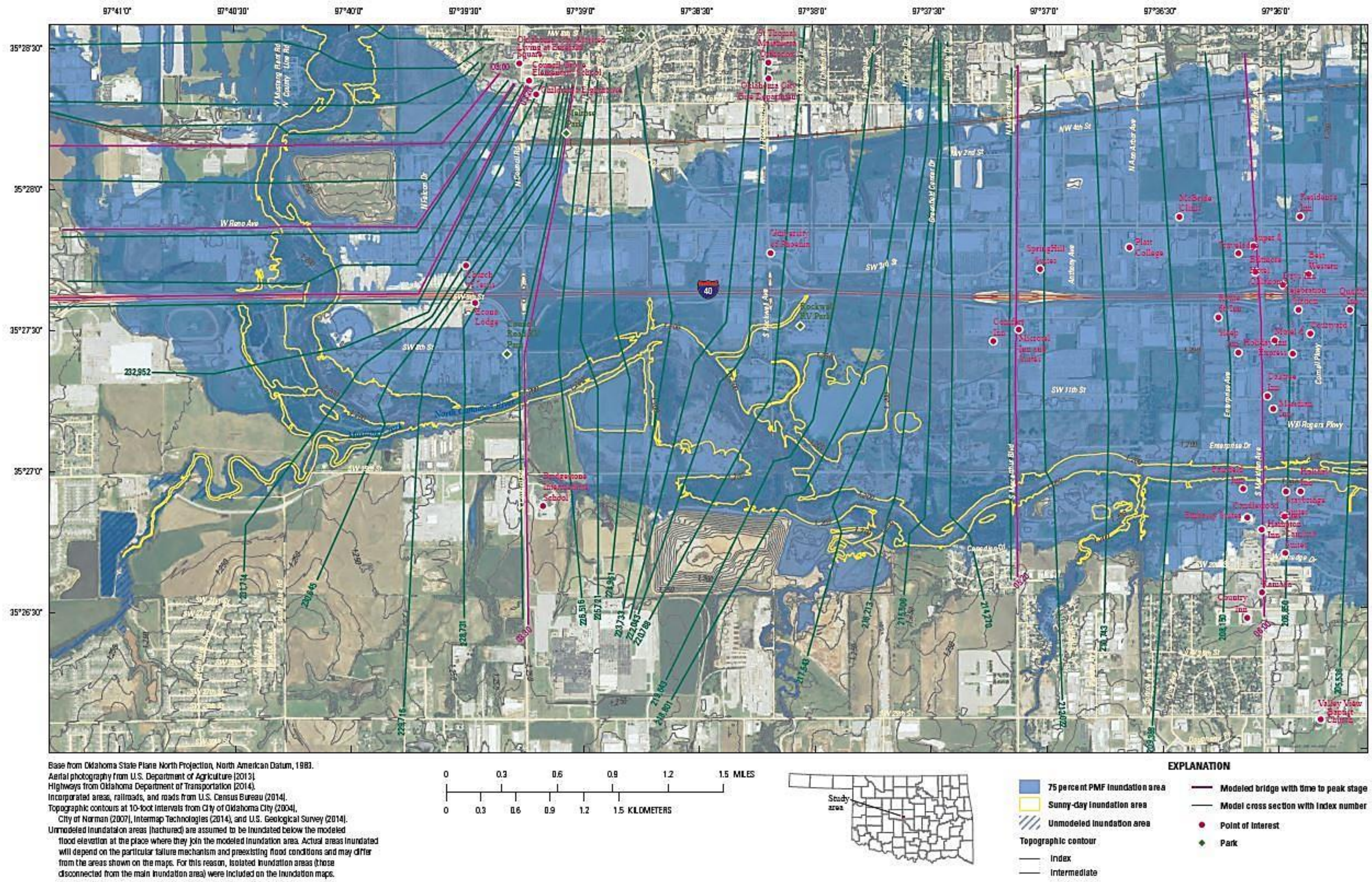

Figure B.5.2. Inundated area for Lake Overholser. Map of the inundated areas for both 75% PMF and sunny day dam breach scenarios for Lake Overholser. Times to peak stage for 75% PMF breach scenario at modeled bridges, as well as points of interest are shown. Figure courtesy of U.S. Geological Survey.

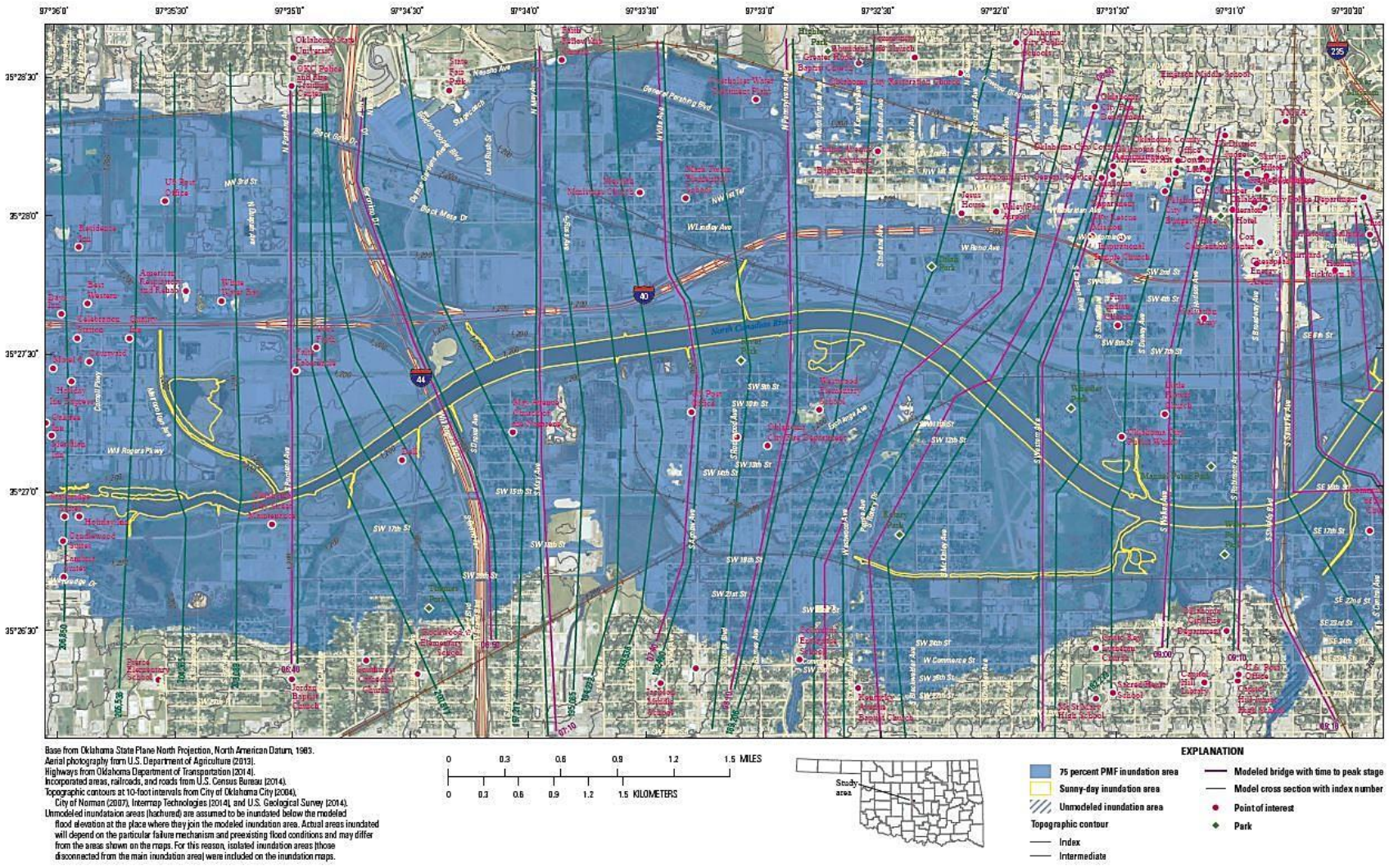

Figure B.5.3. Inundated area for Lake Overholser. Map of the inundated areas for both 75% PMF and sunny day dam breach scenarios for Lake Overholser. Times to peak stage for 75% PMF breach scenario at modeled bridges, as well as points of interest are shown. Figure courtesy of U.S. Geological Survey.

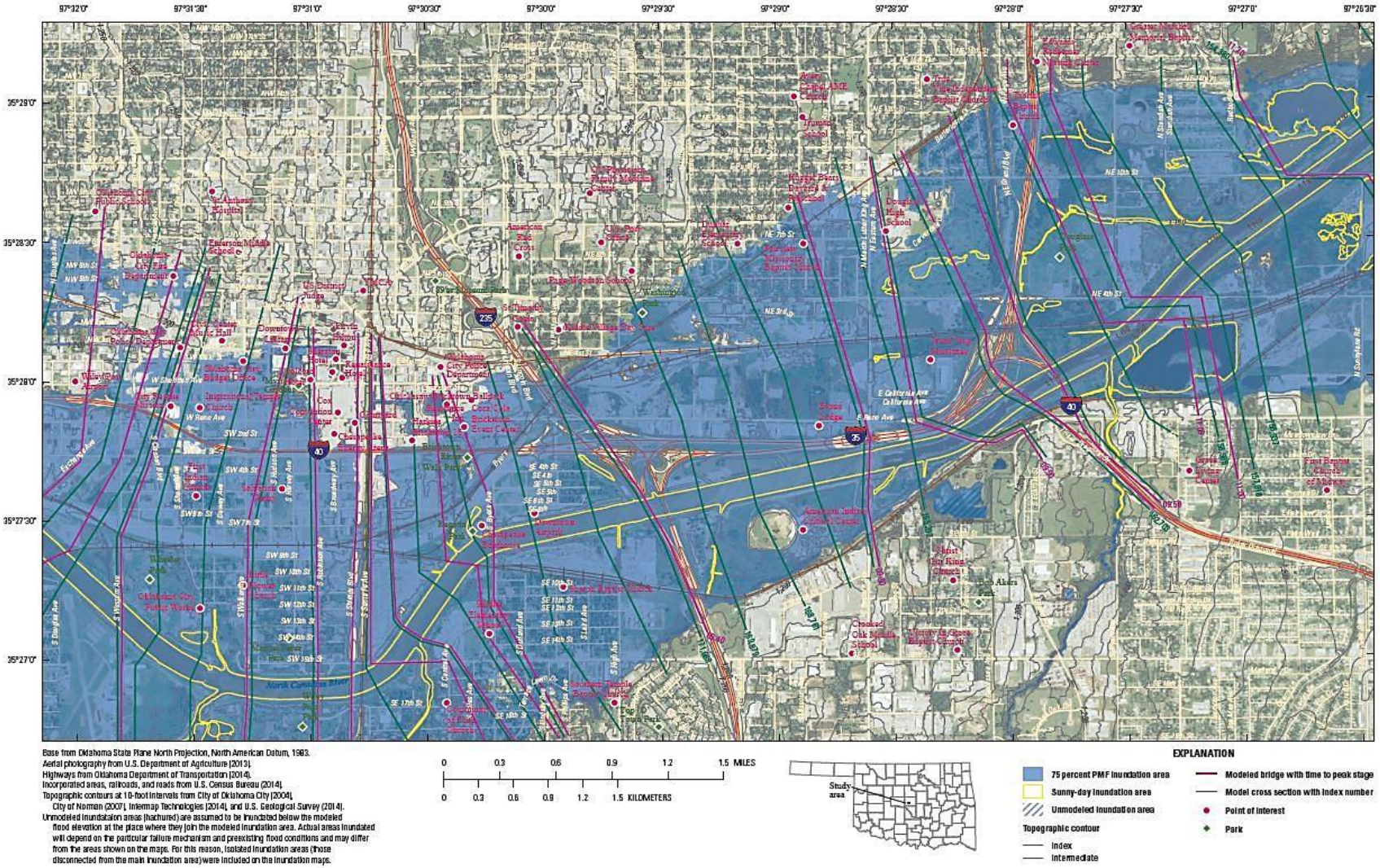

Figure B.5.4. Inundated area for Lake Overholser. Map of the inundated areas for both 75% PMF and sunny day dam breach scenarios for Lake Overholser. Times to peak stage for 75% PMF breach scenario at modeled bridges, as well as points of interest are shown. Figure courtesy of U.S. Geological Survey.

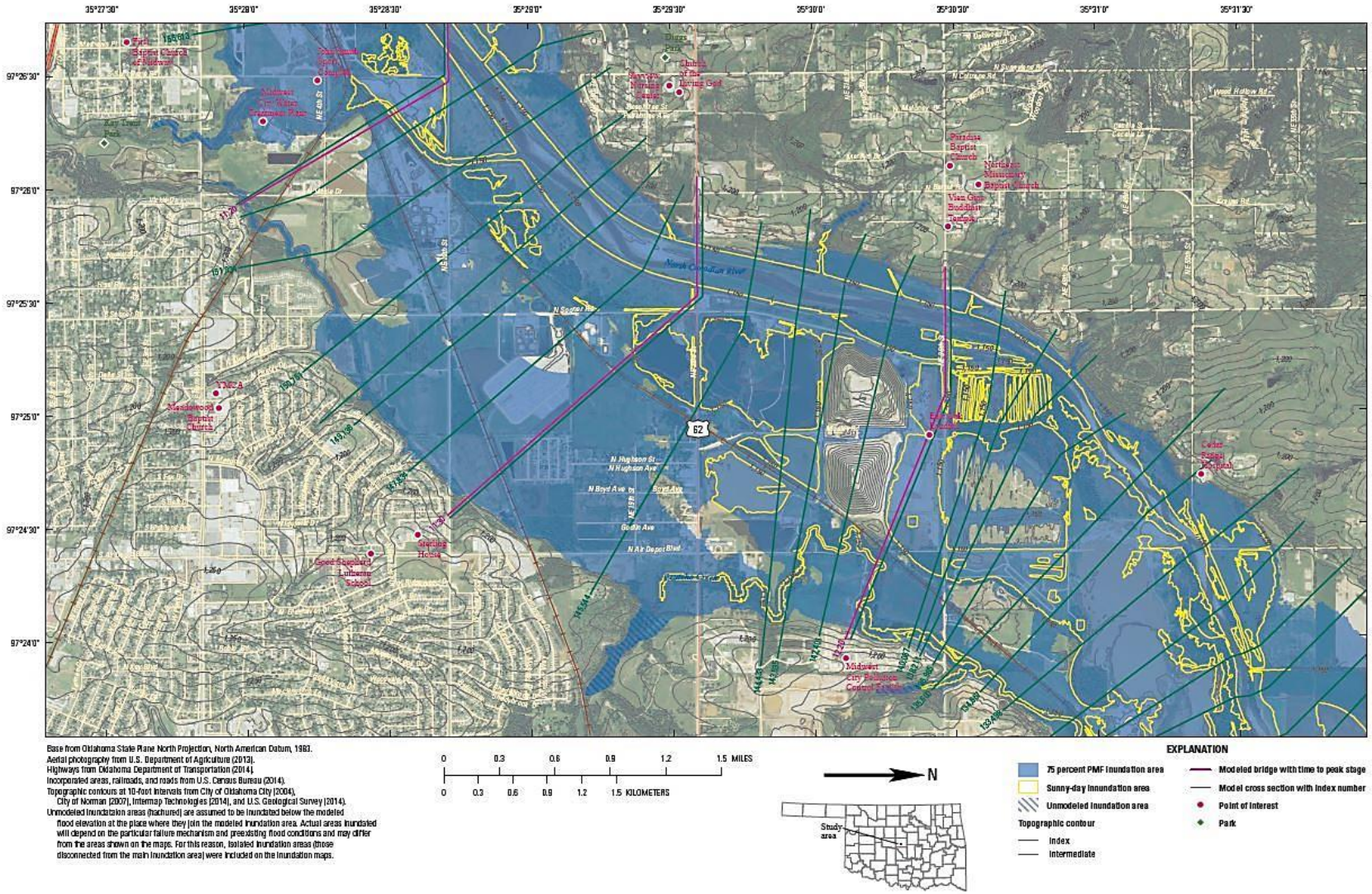

Figure B.5.5. Inundated area for Lake Overholser. Map of the inundated areas for both 75% PMF and sunny day dam breach scenarios for Lake Overholser. Times to peak stage for 75% PMF breach scenario at modeled bridges, as well as points of interest are shown. Figure courtesy of U.S. Geological Survey.

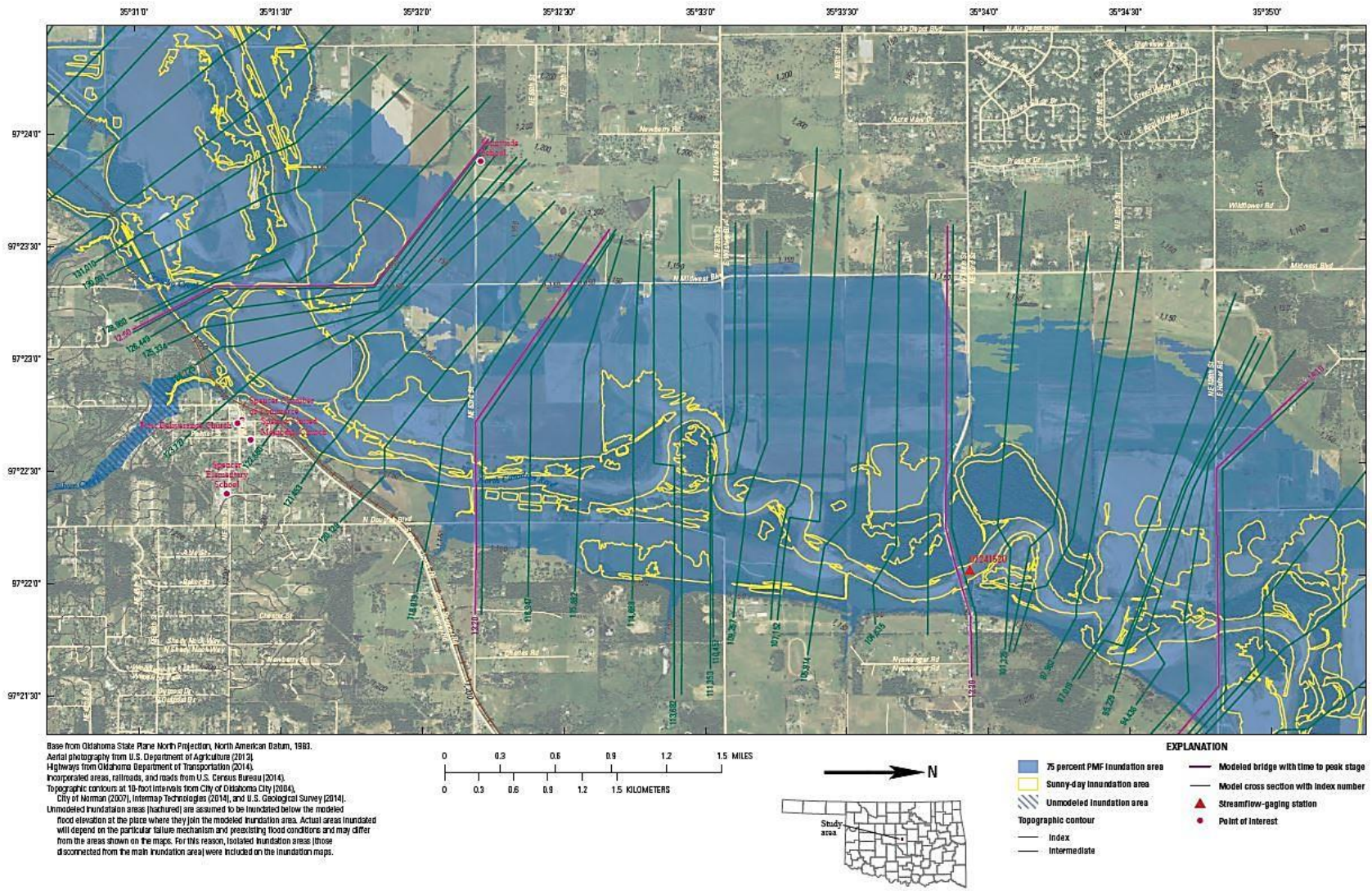

Figure B.5.6. Inundated area for Lake Overholser. Map of the inundated areas for both 75% PMF and sunny day dam breach scenarios for Lake Overholser. Times to peak stage for 75% PMF breach scenario at modeled bridges, as well as points of interest are shown. Figure courtesy of U.S. Geological Survey.

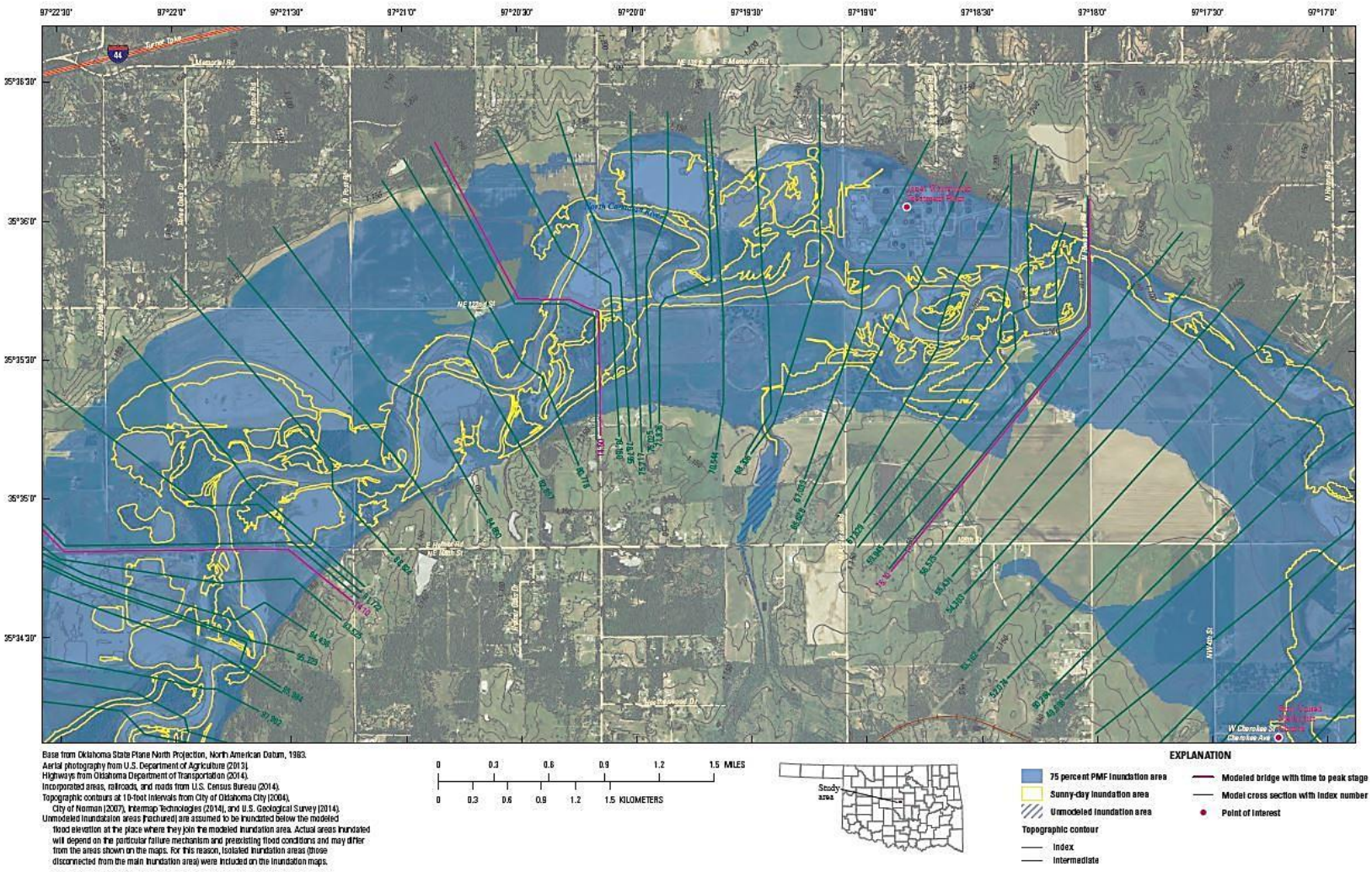

Figure B.5.7. Inundated area for Lake Overholser. Map of the inundated areas for both 75% PMF and sunny day dam breach scenarios for Lake Overholser. Times to peak stage for 75% PMF breach scenario at modeled bridges, as well as points of interest are shown. Figure courtesy of U.S. Geological Survey.

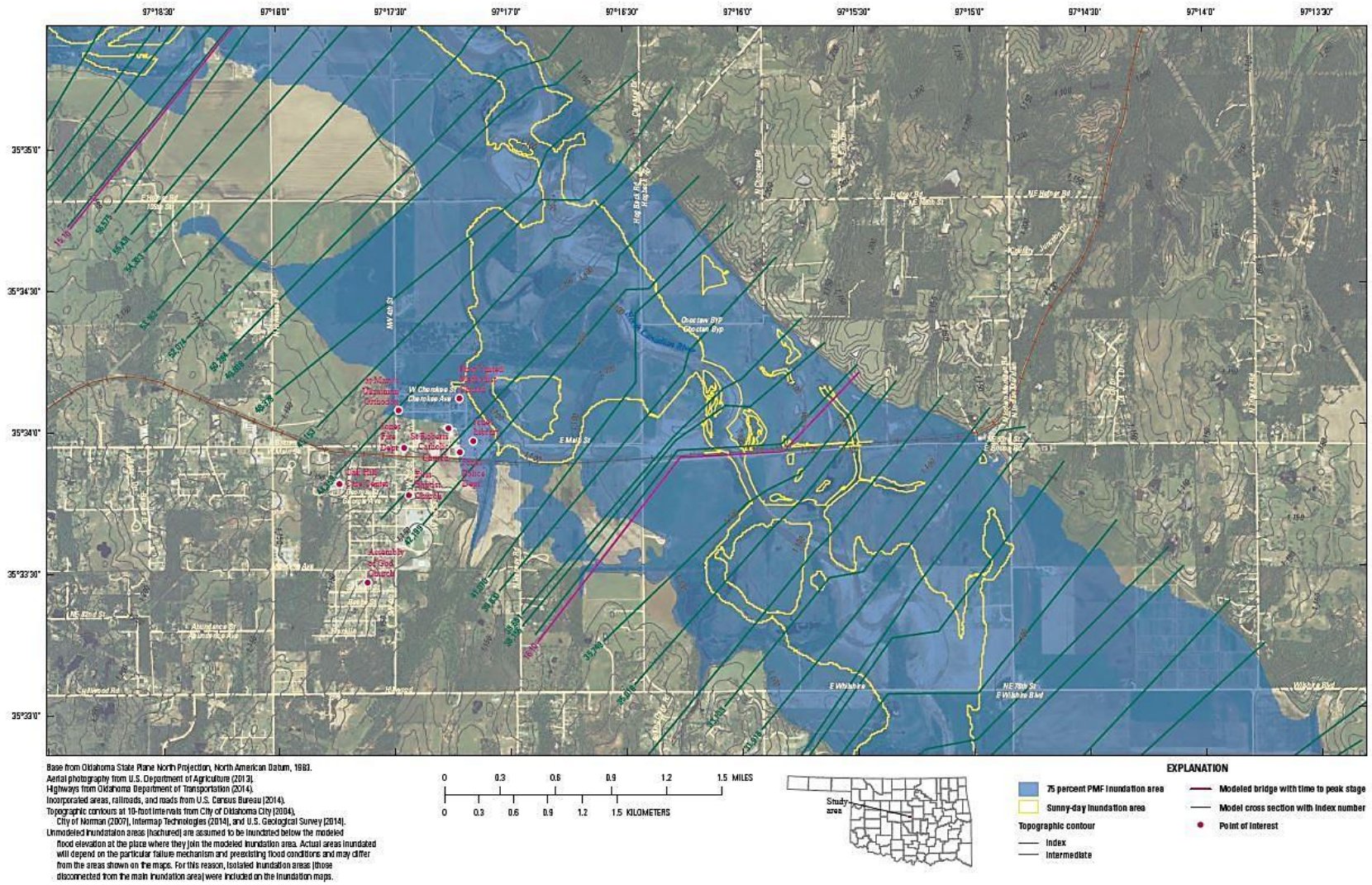

Figure B.5.8. Inundated area for Lake Overholser. Map of the inundated areas for both 75% PMF and sunny day dam breach scenarios for Lake Overholser. Times to peak stage for 75% PMF breach scenario at modeled bridges, as well as points of interest are shown. Figure courtesy of U.S. Geological Survey.

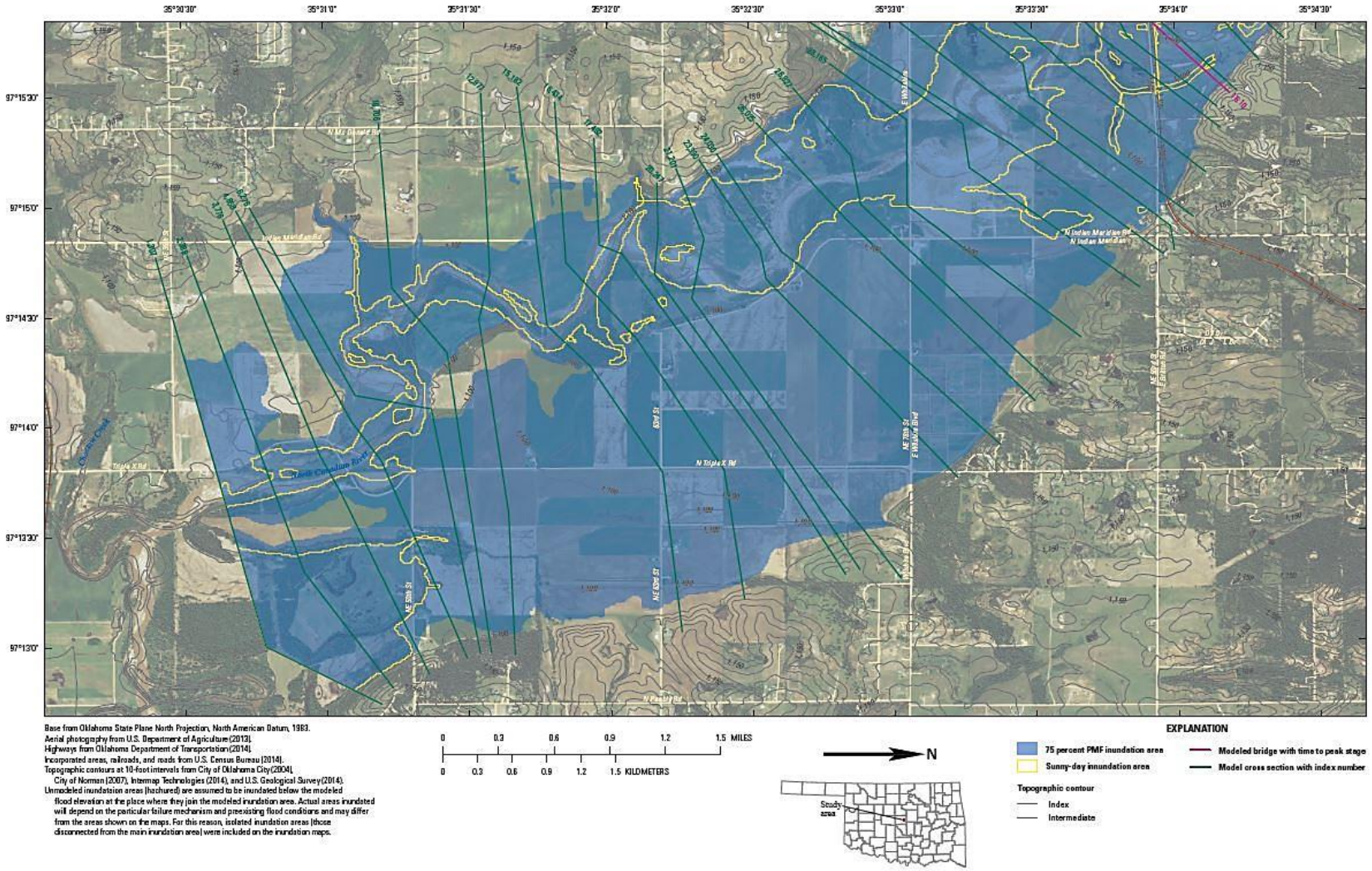

Figure B.5.9. Inundated area for Lake Overholser. Map of the inundated areas for both 75% PMF and sunny day dam breach scenarios for Lake Overholser. Times to peak stage for 75% PMF breach scenario at modeled bridges, as well as points of interest are shown. Figure courtesy of U.S. Geological Survey.

B6 for Lightning Creek Holding Pond A

A link to higher resolution pdf versions of the inundation maps was included below. Inundation map pdfs are provided by the US Geological Survey.

http://pubs.usgs.gov/sir/2015/5052/downloads/sir2015-5052_Appendix07.pdf

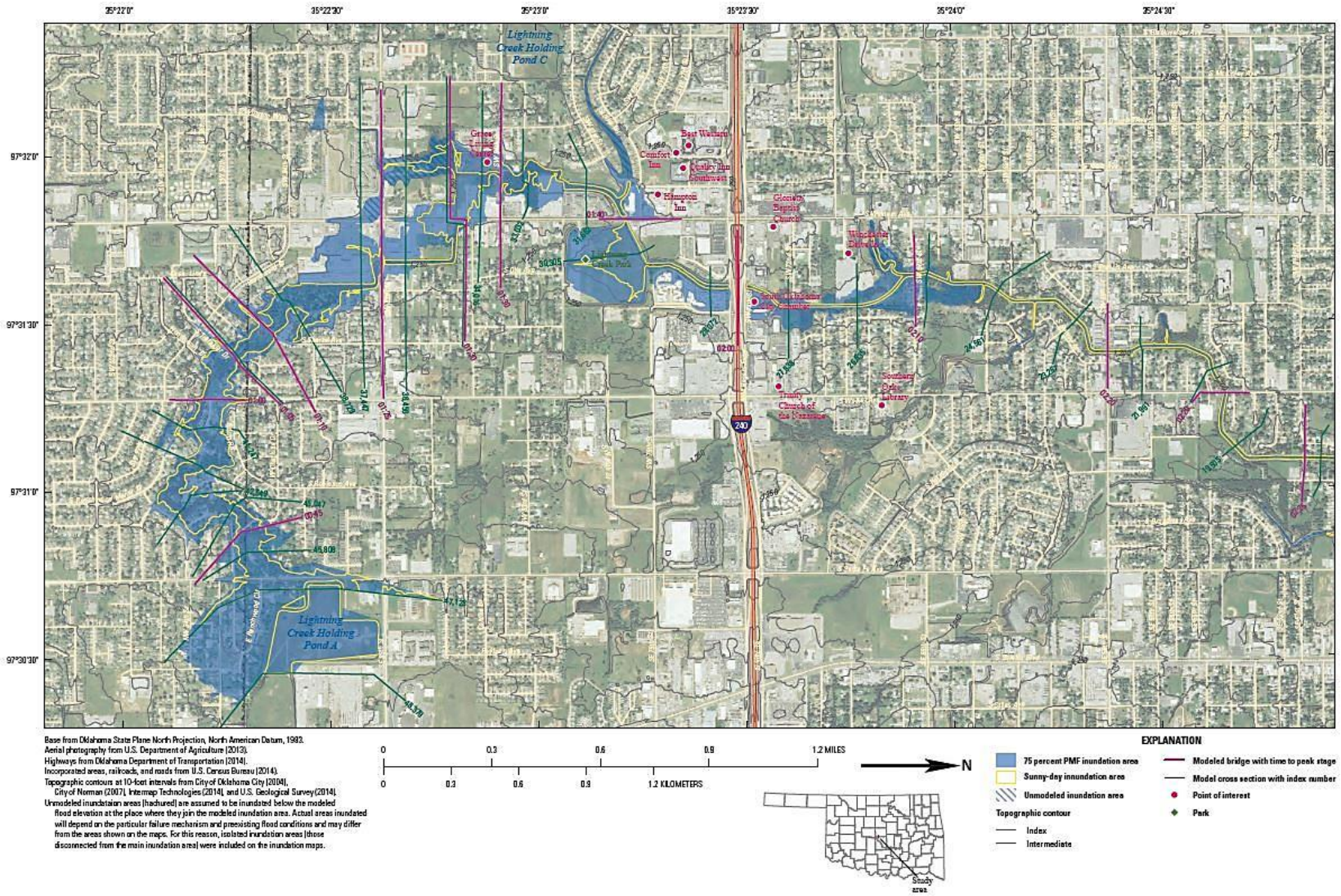

Figure B.6.1. Inundated area for Lightning Creek Holding Pond A. Map of the inundated areas for both 75% PMF and sunny day dam breach scenarios for Lightning Creek Holding Pond A. Times to peak stage for 75% PMF breach scenario at modeled bridges, as well as points of interest are shown. Figure courtesy of U.S. Geological Survey.

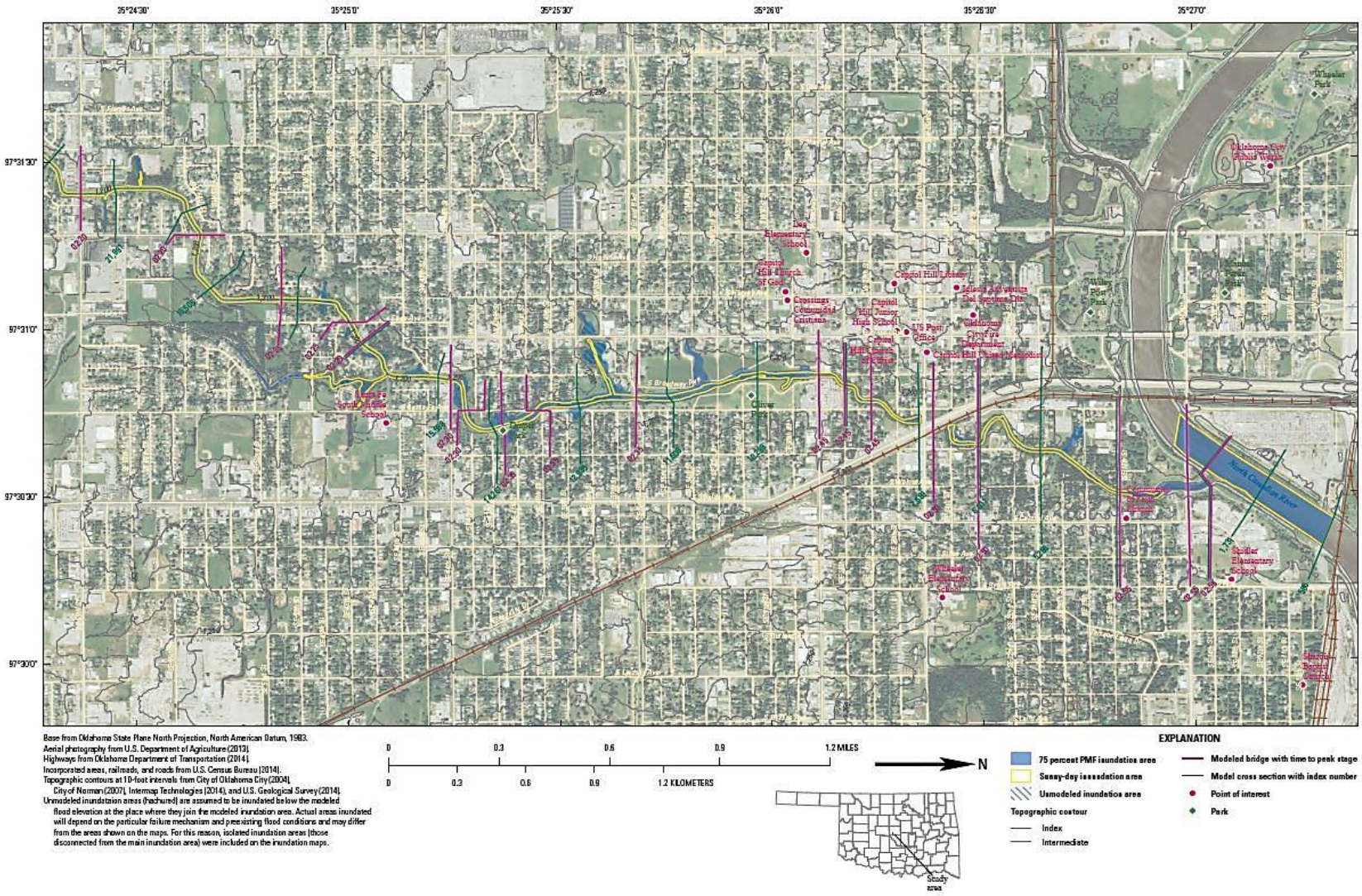

Figure B.6.2. Inundated area for Lightning Creek Holding Pond A. Map of the inundated areas for both 75% PMF and sunny day dam breach scenarios for Lightning Creek Holding Pond A. Times to peak stage for 75% PMF breach scenario at modeled bridges, as well as points of interest are shown. Figure courtesy of U.S. Geological Survey.

B7 for Lightning Creek Holding Pond C

A link to higher resolution pdf versions of the inundation maps was included below. Inundation map pdfs are provided by the US Geological Survey.

http://pubs.usgs.gov/sir/2015/5052/downloads/sir2015-5052_Appendix08.pdf

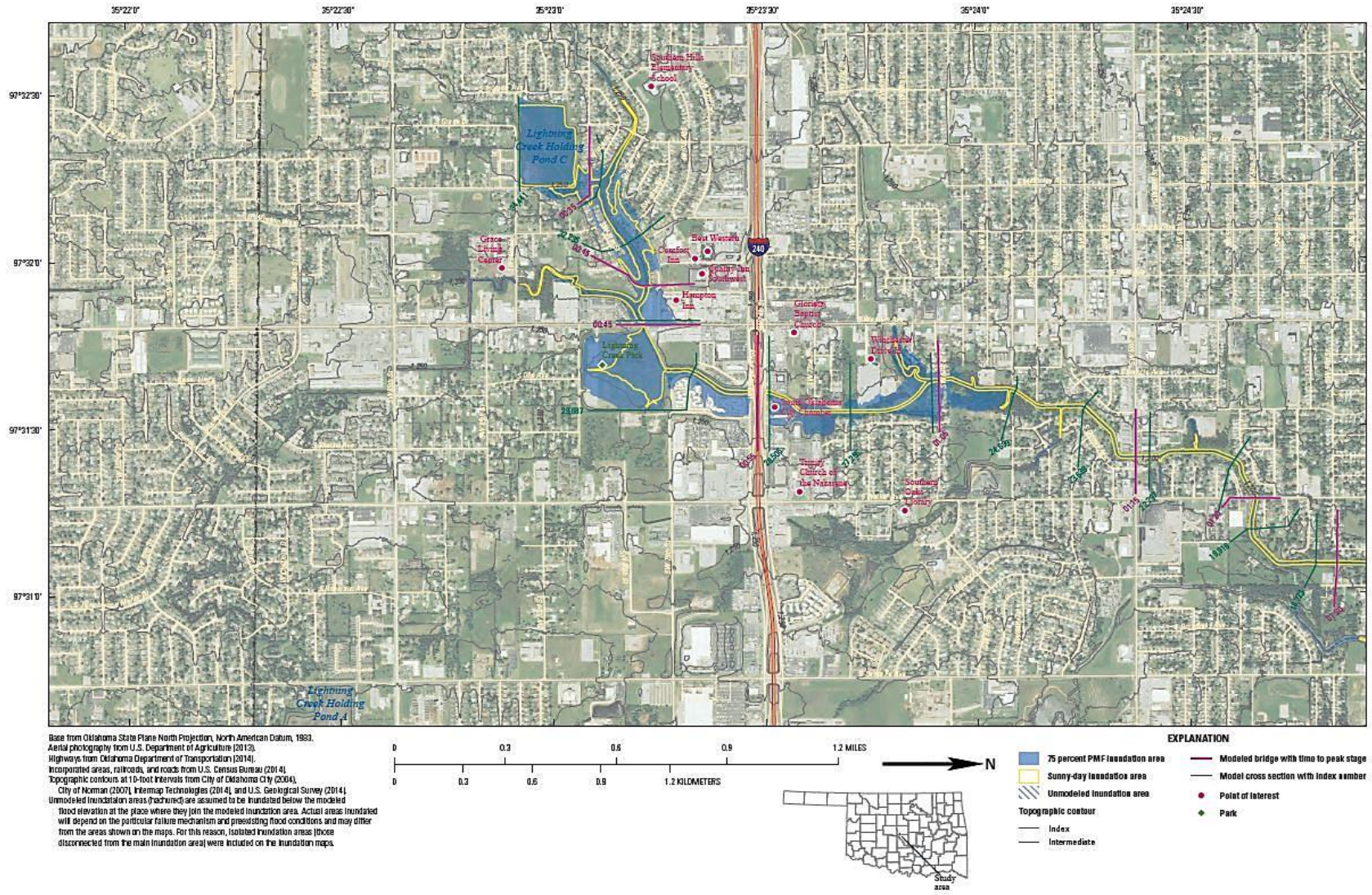

Figure B.7.1. Inundated area for Lightning Creek Holding Pond C. Map of the inundated areas for both 75% PMF and sunny day dam breach scenarios for Lightning Creek Holding Pond C. Times to peak stage for 75% PMF breach scenario at modeled bridges, as well as points of interest are shown. Figure courtesy of U.S. Geological Survey.

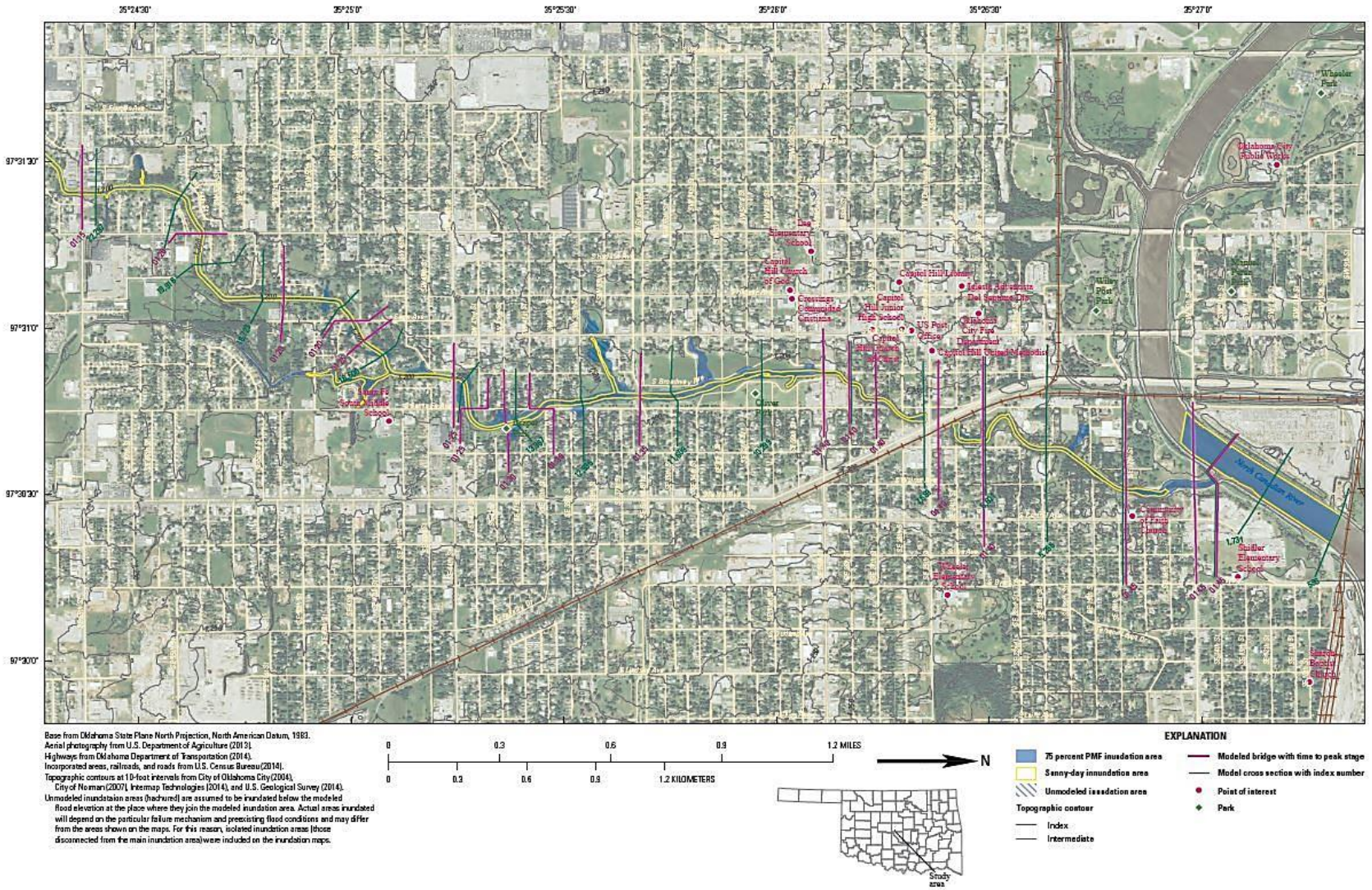

Figure B.7.2. Inundated area for Lightning Creek Holding Pond C. Map of the inundated areas for both 75% PMF and sunny day dam breach scenarios for Lightning Creek Holding Pond C. Times to peak stage for 75% PMF breach scenario at modeled bridges, as well as points of interest are shown. Figure courtesy of U.S. Geological Survey.

B8 Northeast (Zoo) Lake

A link to higher resolution pdf versions of the inundation maps was included below. Inundation map pdfs are provided by the US Geological Survey.

http://pubs.usgs.gov/sir/2015/5052/downloads/sir2015-5052_Appendix09.pdf

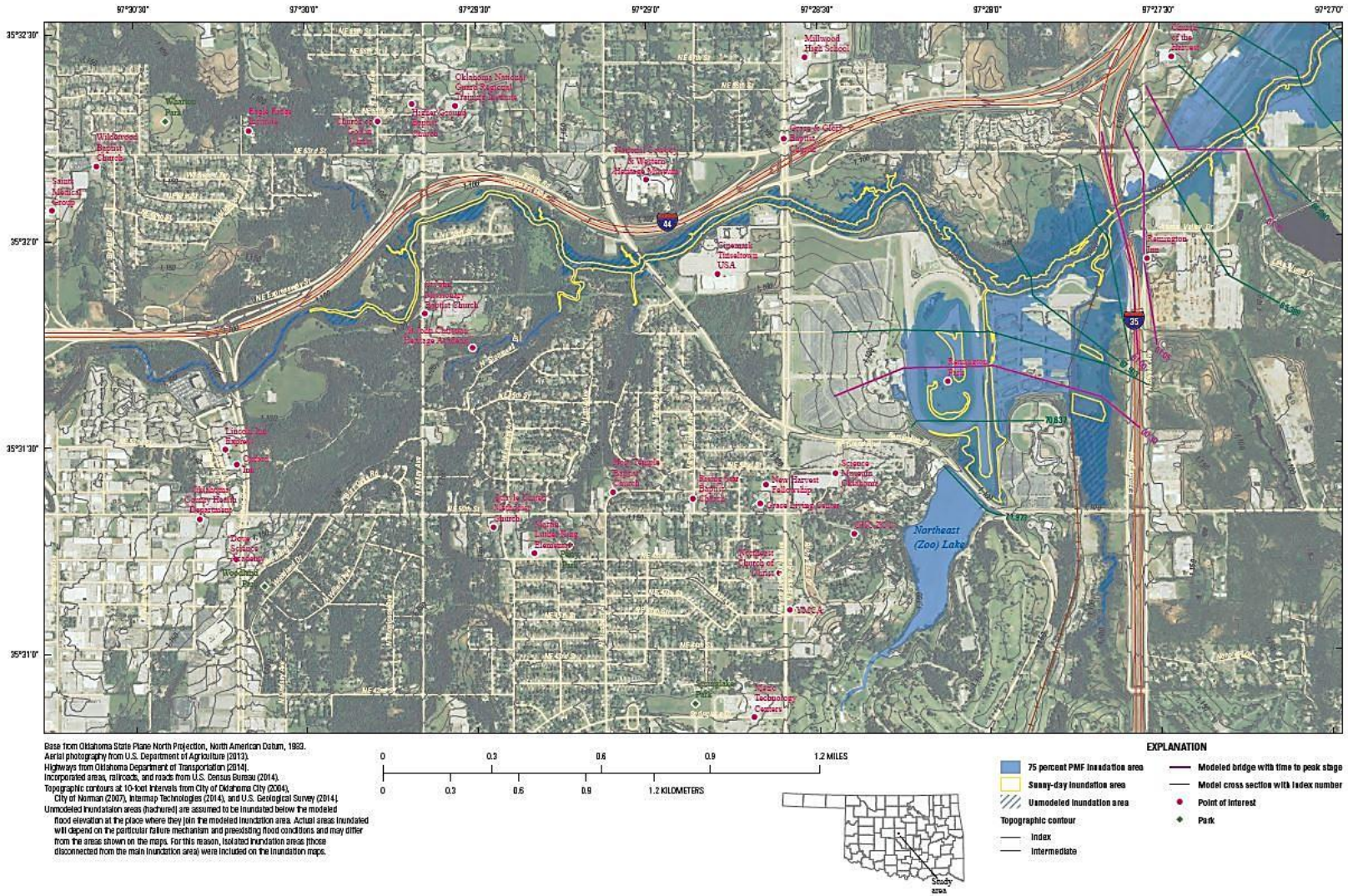

Figure B.8.1. Inundated area for Northeast (Zoo) Lake. Map of the inundated areas for both 75% PMF and sunny day dam breach scenarios for Northeast (Zoo) Lake. Times to peak stage for 75% PMF breach scenario at modeled bridges, as well as points of interest are shown. Figure courtesy of U.S. Geological Survey.

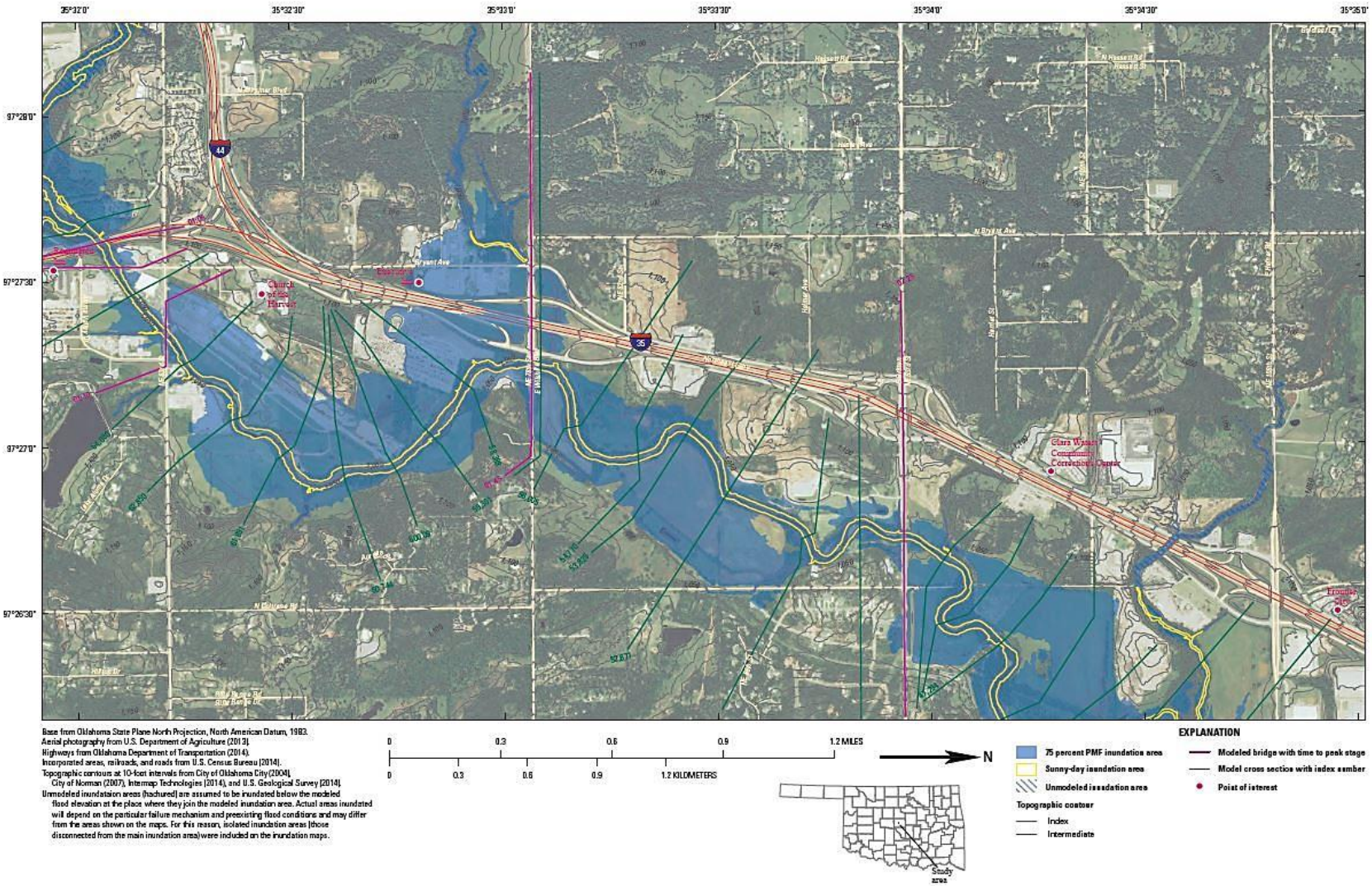

Figure B.8.2. Inundated area for Northeast (Zoo) Lake. Map of the inundated areas for both 75% PMF and sunny day dam breach scenarios for Northeast (Zoo) Lake. Times to peak stage for 75% PMF breach scenario at modeled bridges, as well as points of interest are shown. Figure courtesy of U.S. Geological Survey.

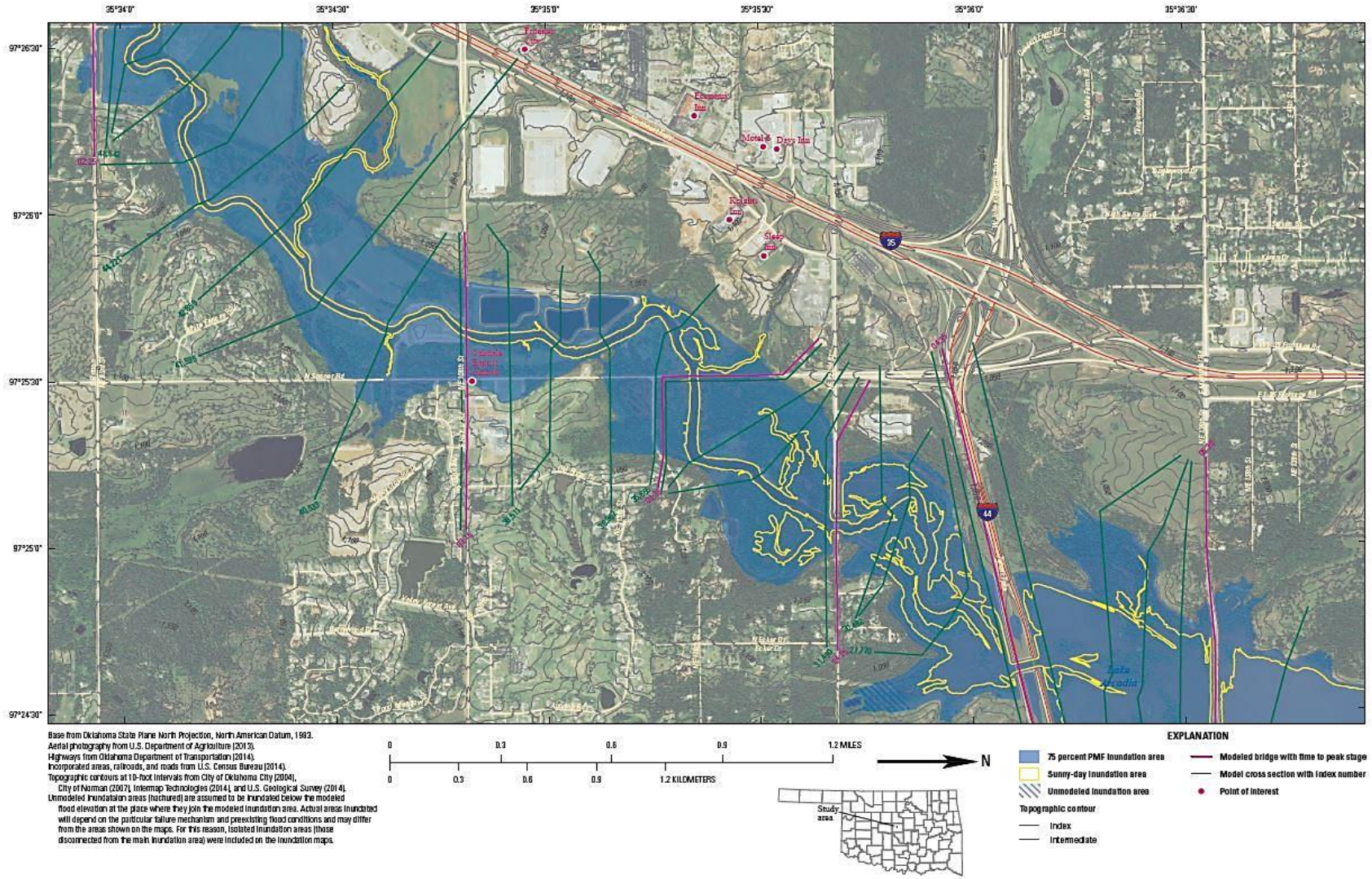

Figure B.8.3. Inundated area for Northeast (Zoo) Lake. Map of the inundated areas for both 75% PMF and sunny day dam breach scenarios for Northeast (Zoo) Lake. Times to peak stage for 75% PMF breach scenario at modeled bridges, as well as points of interest are shown. Figure courtesy of U.S. Geological Survey.

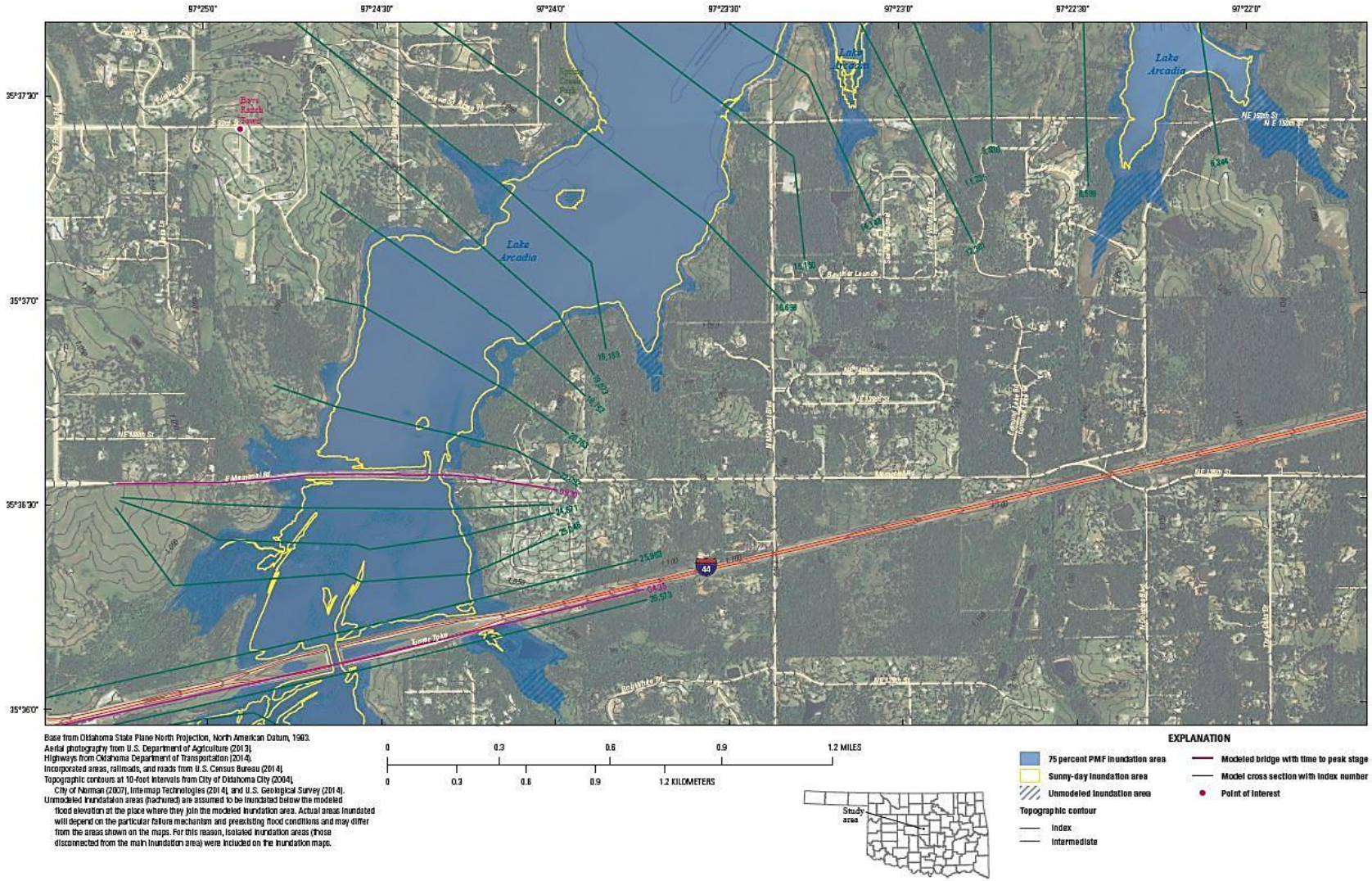

Figure B.8.4. Inundated area for Northeast (Zoo) Lake. Map of the inundated areas for both 75% PMF and sunny day dam breach scenarios for Northeast (Zoo) Lake. Times to peak stage for 75% PMF breach scenario at modeled bridges, as well as points of interest are shown. Figure courtesy of U.S. Geological Survey.

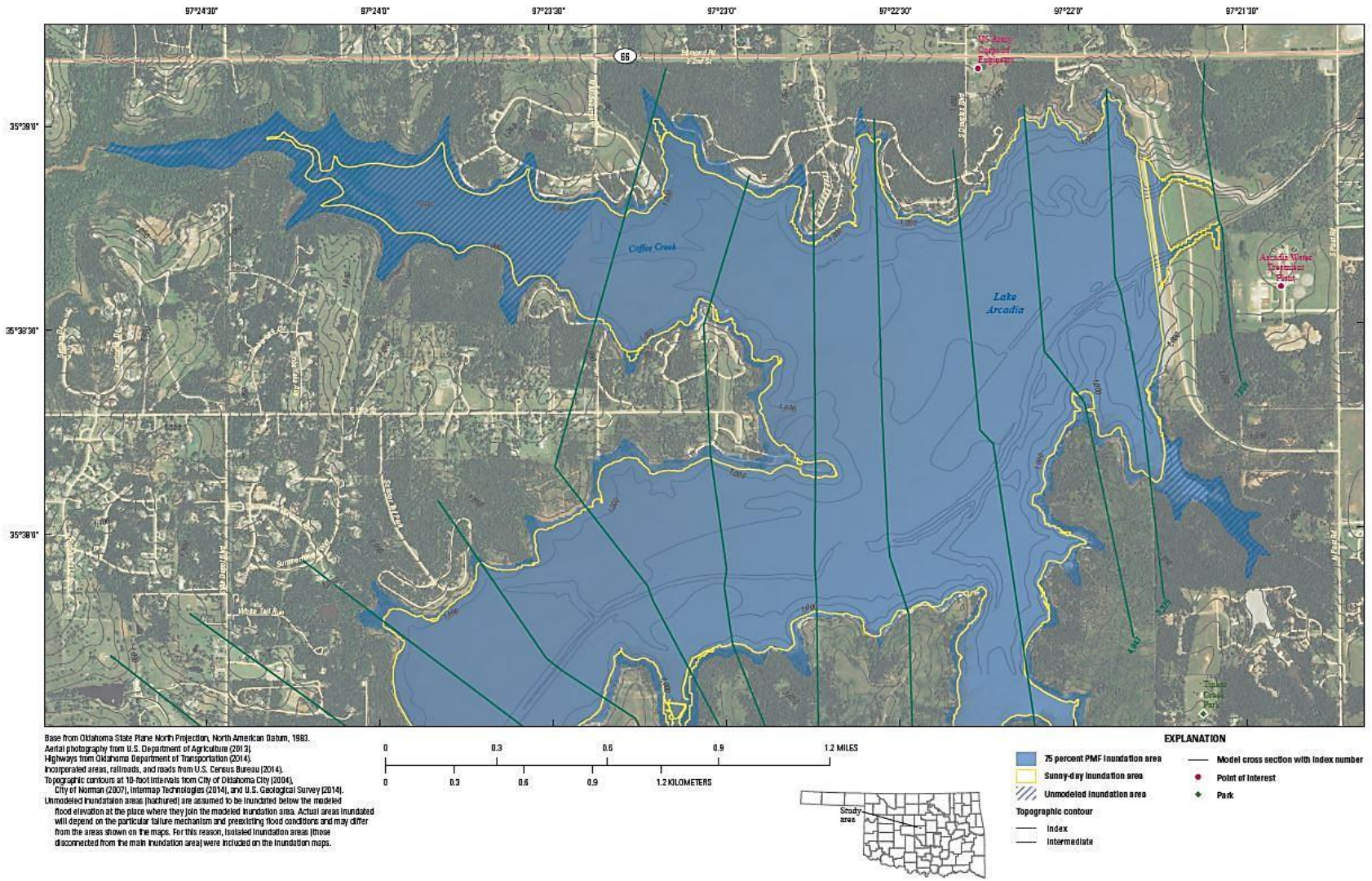

Figure B.8.5. Inundated area for Northeast (Zoo) Lake. Map of the inundated areas for both 75% PMF and sunny day dam breach scenarios for Northeast (Zoo) Lake. Times to peak stage for 75% PMF breach scenario at modeled bridges, as well as points of interest are shown. Figure courtesy of U.S. Geological Survey.

B9 Northwest OKC Sludge Lagoon

A link to higher resolution pdf versions of the inundation maps was included below. Inundation map pdfs are provided by the US Geological Survey.

http://pubs.usgs.gov/sir/2015/5052/downloads/sir2015-5052_Appendix10.pdf

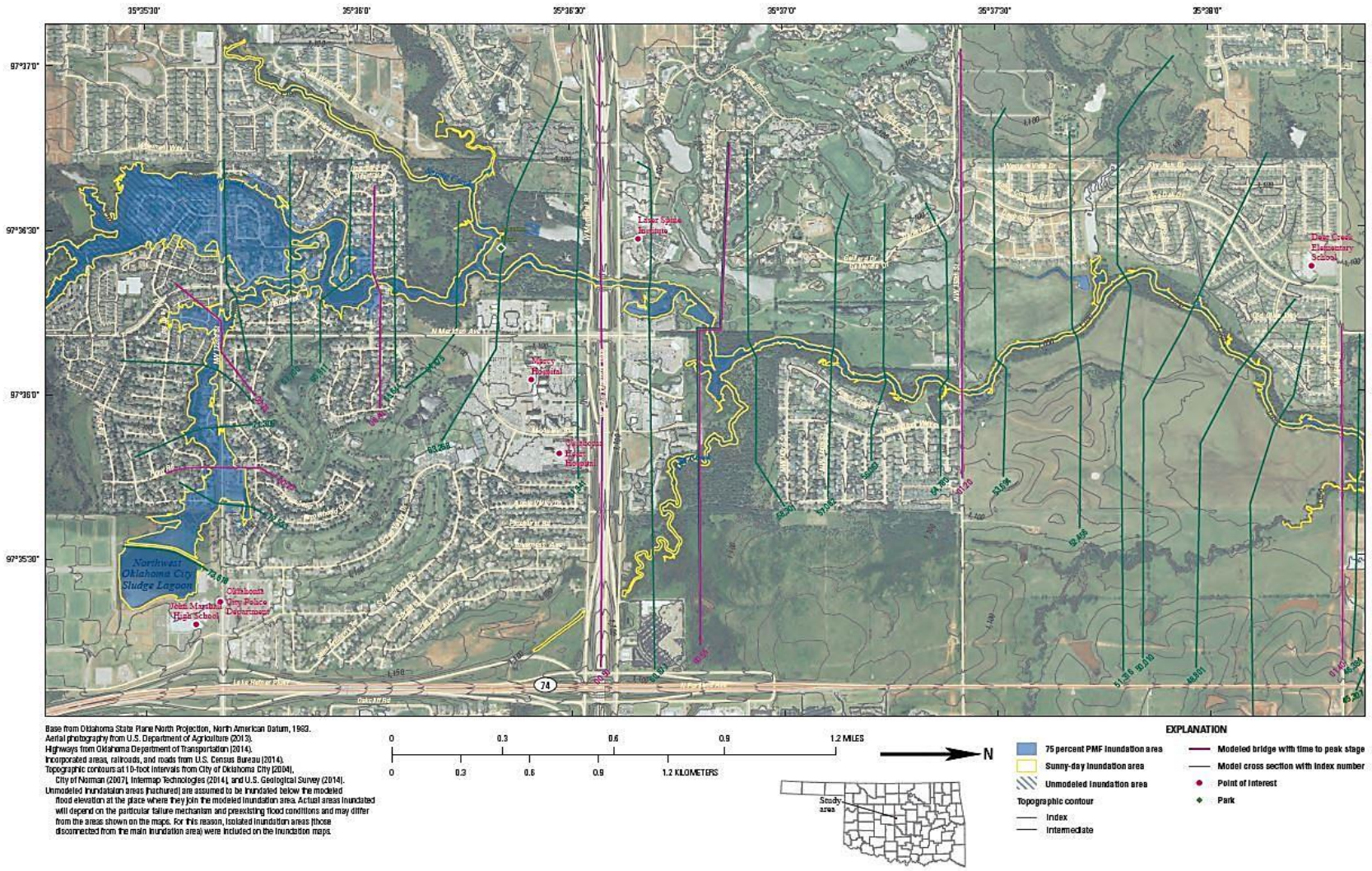

Figure B.9. Inundated area for Northwest OKC Sludge Lagoon. Map of the inundated areas for both 75% PMF and sunny day dam breach scenarios for Northwest Oklahoma City Sludge Lagoon. Times to peak stage for 75% PMF breach scenario at modeled bridges, as well as points of interest are shown. Figure courtesy of U.S. Geological Survey.

B10 Stanley Draper Lake

A link to higher resolution pdf versions of the inundation maps was included below. Inundation map pdfs are provided by the US Geological Survey.

http://pubs.usgs.gov/sir/2015/5052/downloads/sir2015-5052_Appendix11.pdf

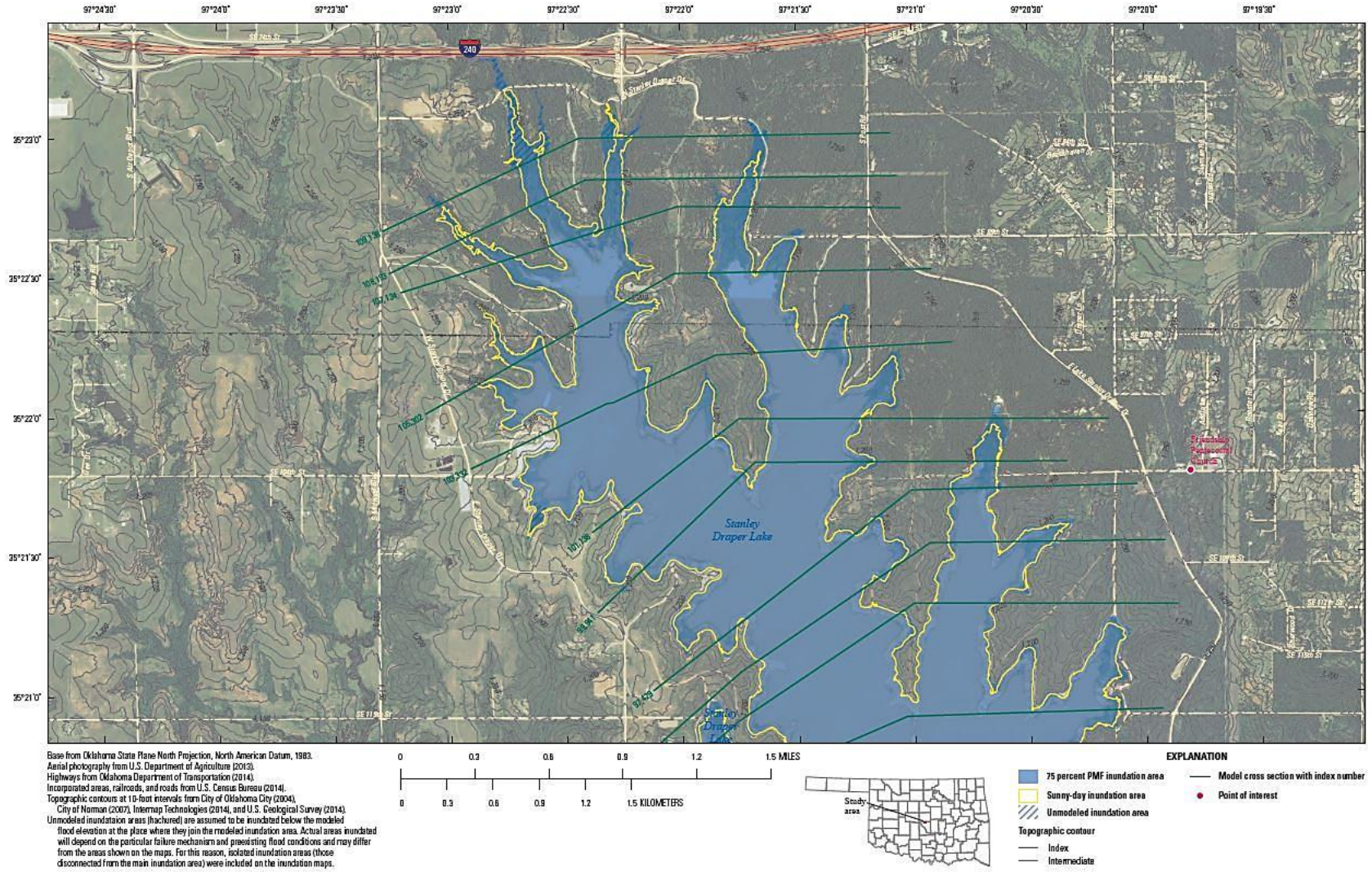

Figure B.10.1. Inundated area for Stanley Draper Lake. Map of the inundated areas for both 75% PMF and sunny day dam breach scenarios for Stanley Draper Lake. Times to peak stage for 75% PMF breach scenario at modeled bridges, as well as points of interest are shown. Figure courtesy of U.S. Geological Survey.

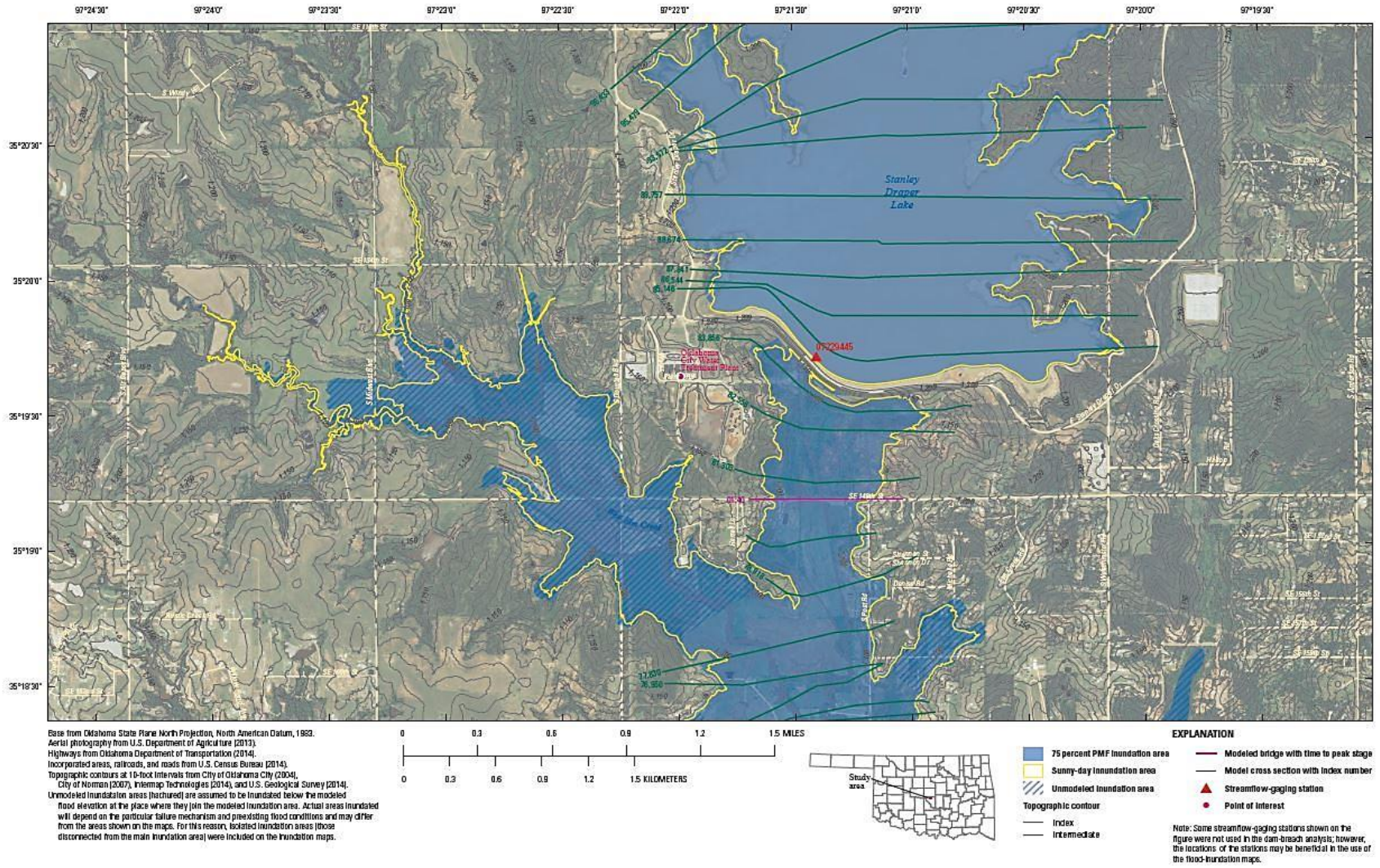

Figure B.10.2. Inundated area for Stanley Draper Lake. Map of the inundated areas for both 75% PMF and sunny day dam breach scenarios for Stanley Draper Lake. Times to peak stage for 75% PMF breach scenario at modeled bridges, as well as points of interest are shown. Figure courtesy of U.S. Geological Survey.

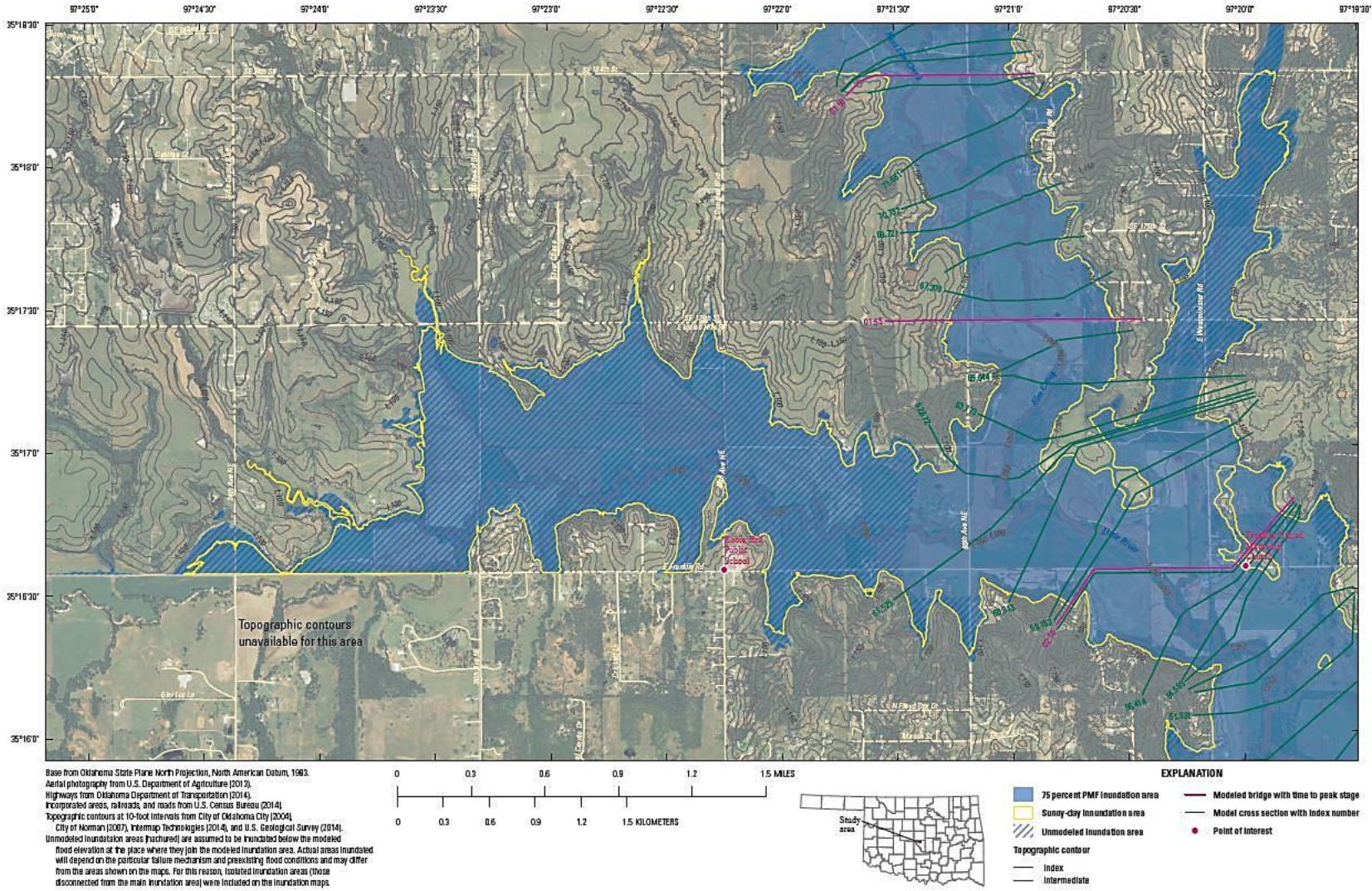

Figure B.10.3. Inundated area for Stanley Draper Lake. Map of the inundated areas for both 75% PMF and sunny day dam breach scenarios for Stanley Draper Lake. Times to peak stage for 75% PMF breach scenario at modeled bridges, as well as points of interest are shown. Figure courtesy of U.S. Geological Survey.

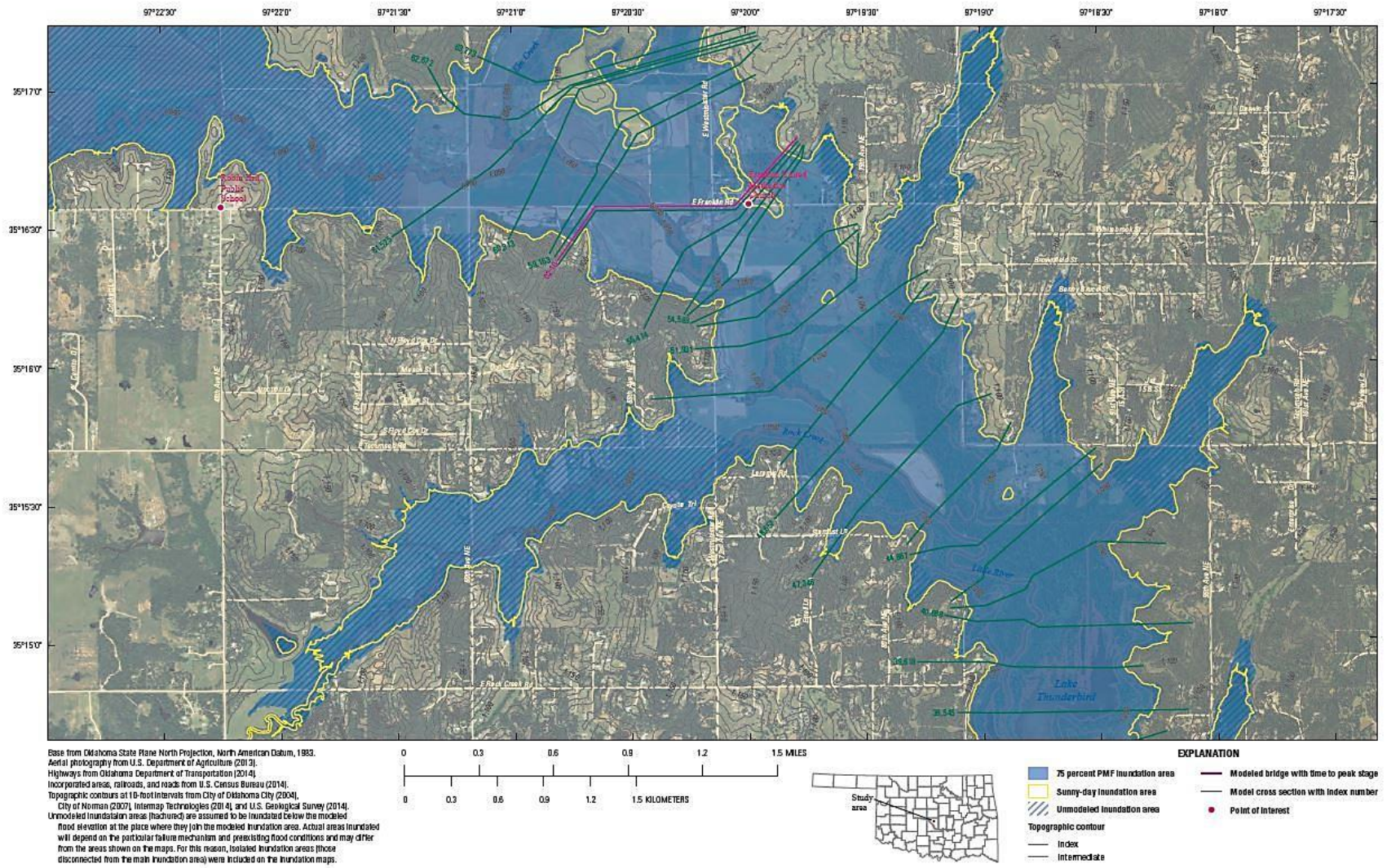

Figure B.10.4. Inundated area for Stanley Draper Lake. Map of the inundated areas for both 75% PMF and sunny day dam breach scenarios for Stanley Draper Lake. Times to peak stage for 75% PMF breach scenario at modeled bridges, as well as points of interest are shown. Figure courtesy of U.S. Geological Survey.

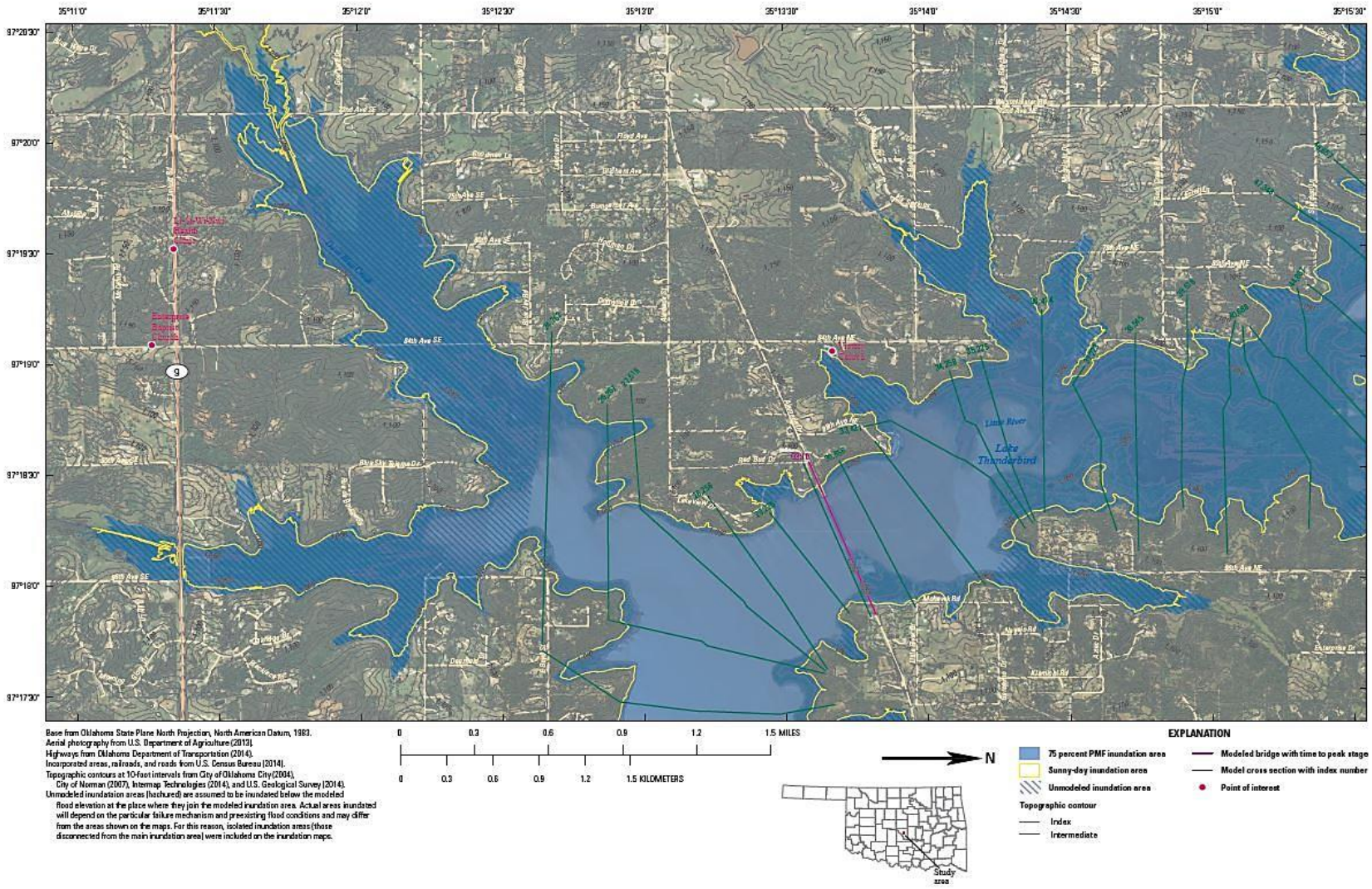

Figure B.10.5. Inundated area for Stanley Draper Lake. Map of the inundated areas for both 75% PMF and sunny day dam breach scenarios for Stanley Draper Lake. Times to peak stage for 75% PMF breach scenario at modeled bridges, as well as points of interest are shown. Figure courtesy of U.S. Geological Survey.

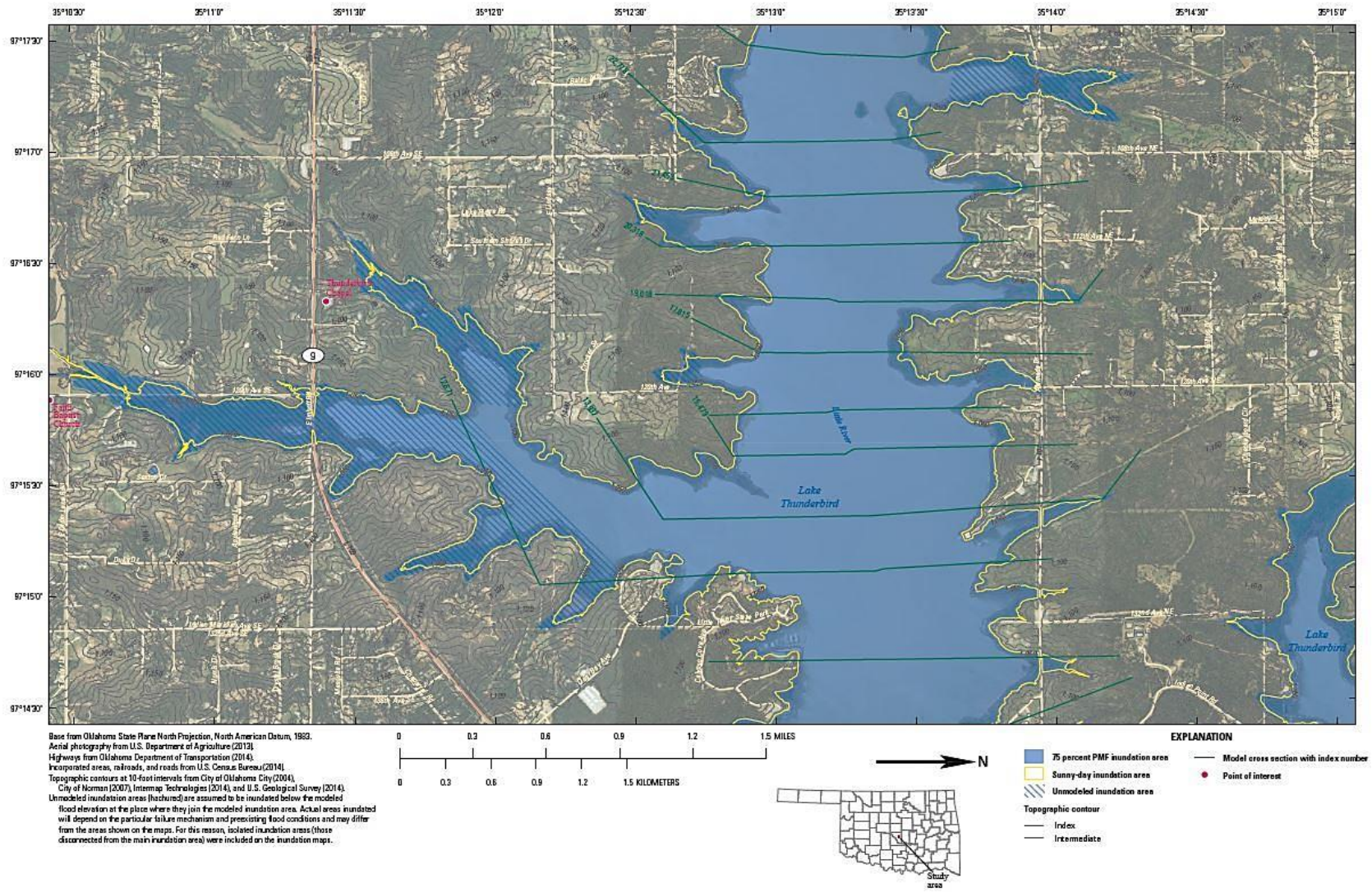

Figure B.10.6. Inundated area for Stanley Draper Lake. Map of the inundated areas for both 75% PMF and sunny day dam breach scenarios for Stanley Draper Lake. Times to peak stage for 75% PMF breach scenario at modeled bridges, as well as points of interest are shown. Figure courtesy of U.S. Geological Survey.

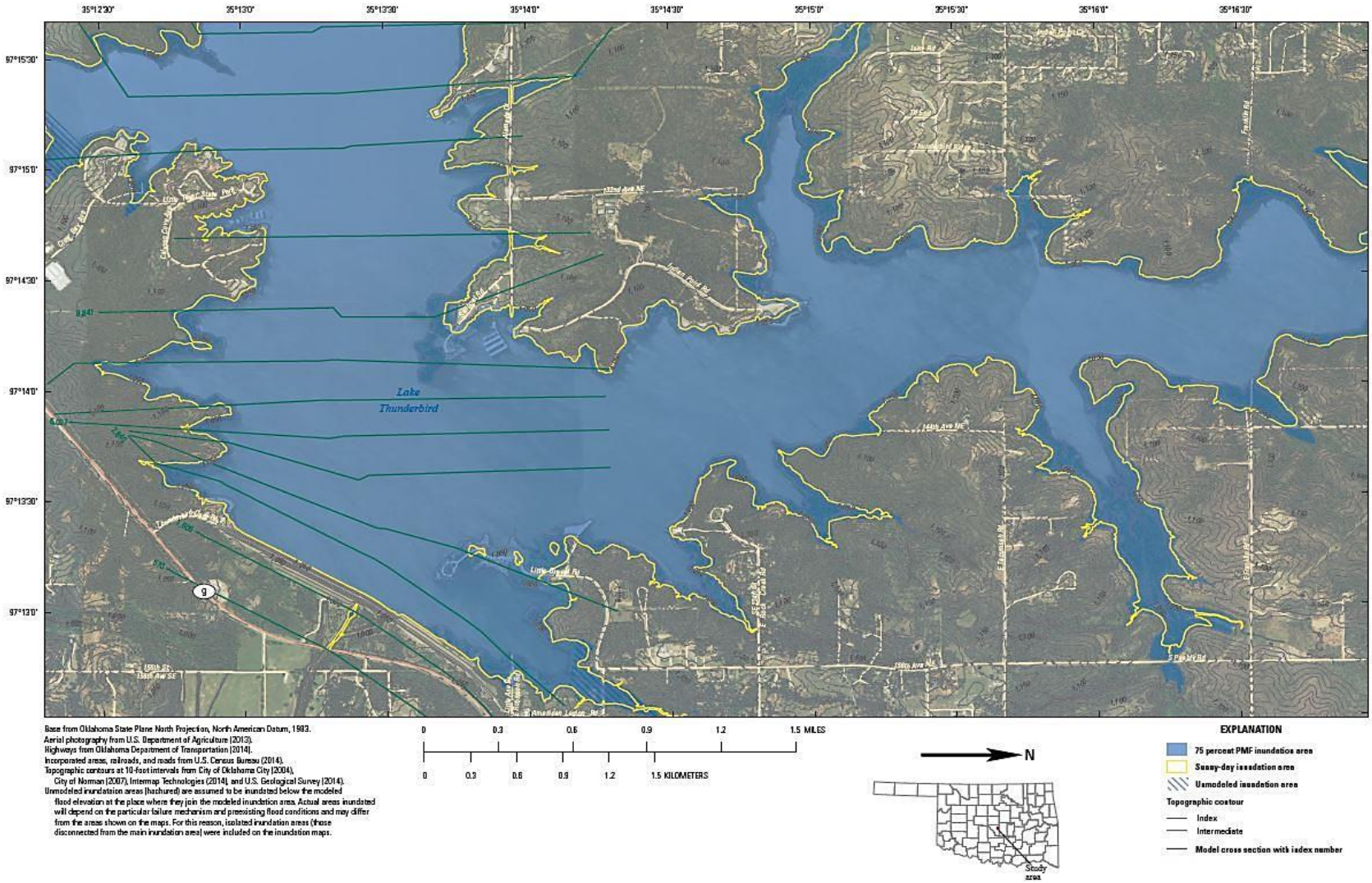

Figure B.10.7. Inundated area for Stanley Draper Lake. Map of the inundated areas for both 75% PMF and sunny day dam breach scenarios for Stanley Draper Lake. Times to peak stage for 75% PMF breach scenario at modeled bridges, as well as points of interest are shown. Figure courtesy of U.S. Geological Survey.

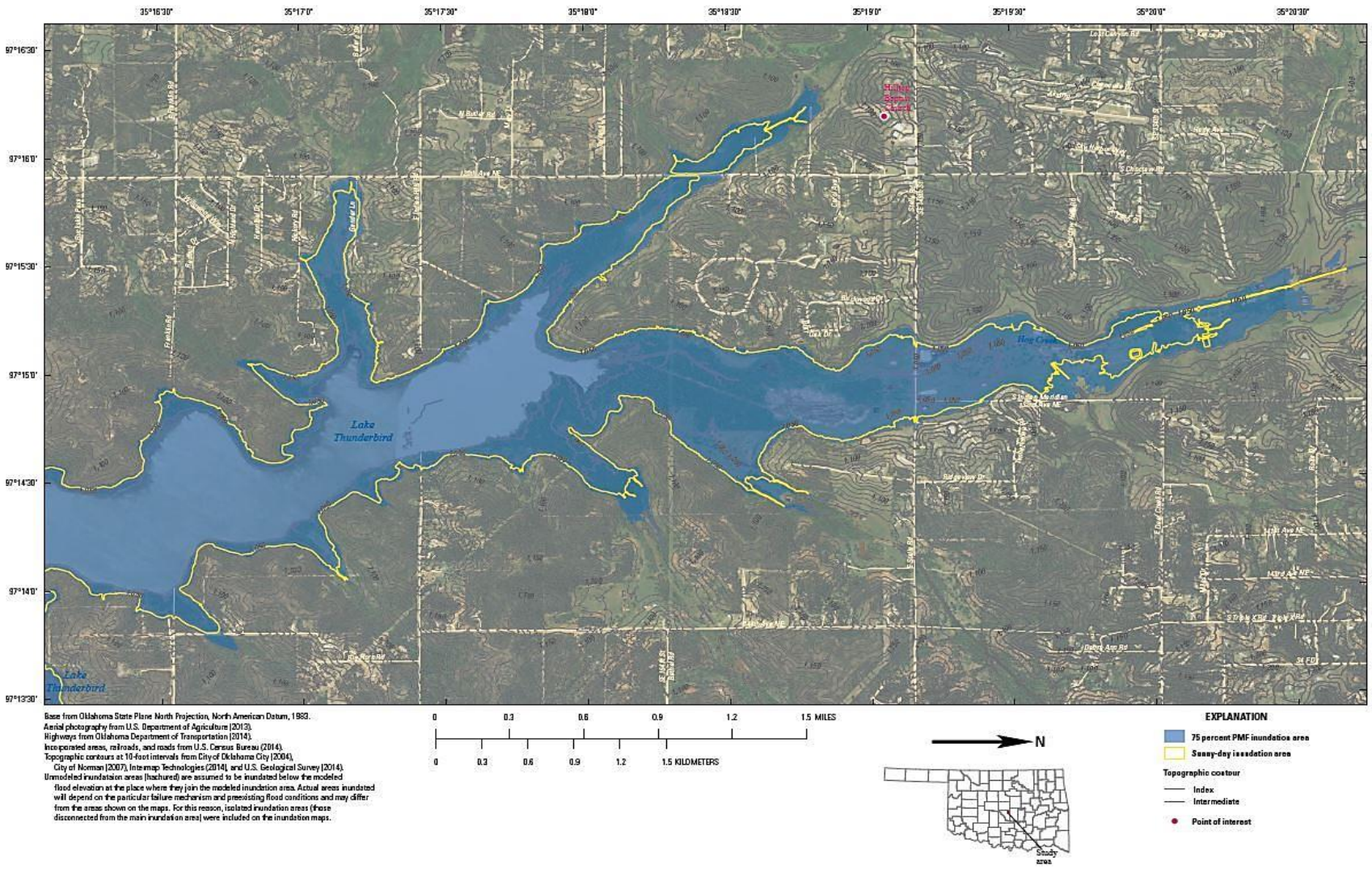

Figure B.10.8. Inundated area for Stanley Draper Lake. Map of the inundated areas for both 75% PMF and sunny day dam breach scenarios for Stanley Draper Lake. Times to peak stage for 75% PMF breach scenario at modeled bridges, as well as points of interest are shown. Figure courtesy of U.S. Geological Survey.

B11 Will Rogers Park Holding Pond

A link to higher resolution pdf versions of the inundation maps was included below. Inundation map pdfs are provided by the US Geological Survey.

http://pubs.usgs.gov/sir/2015/5052/downloads/sir2015-5052_Appendix12.pdf

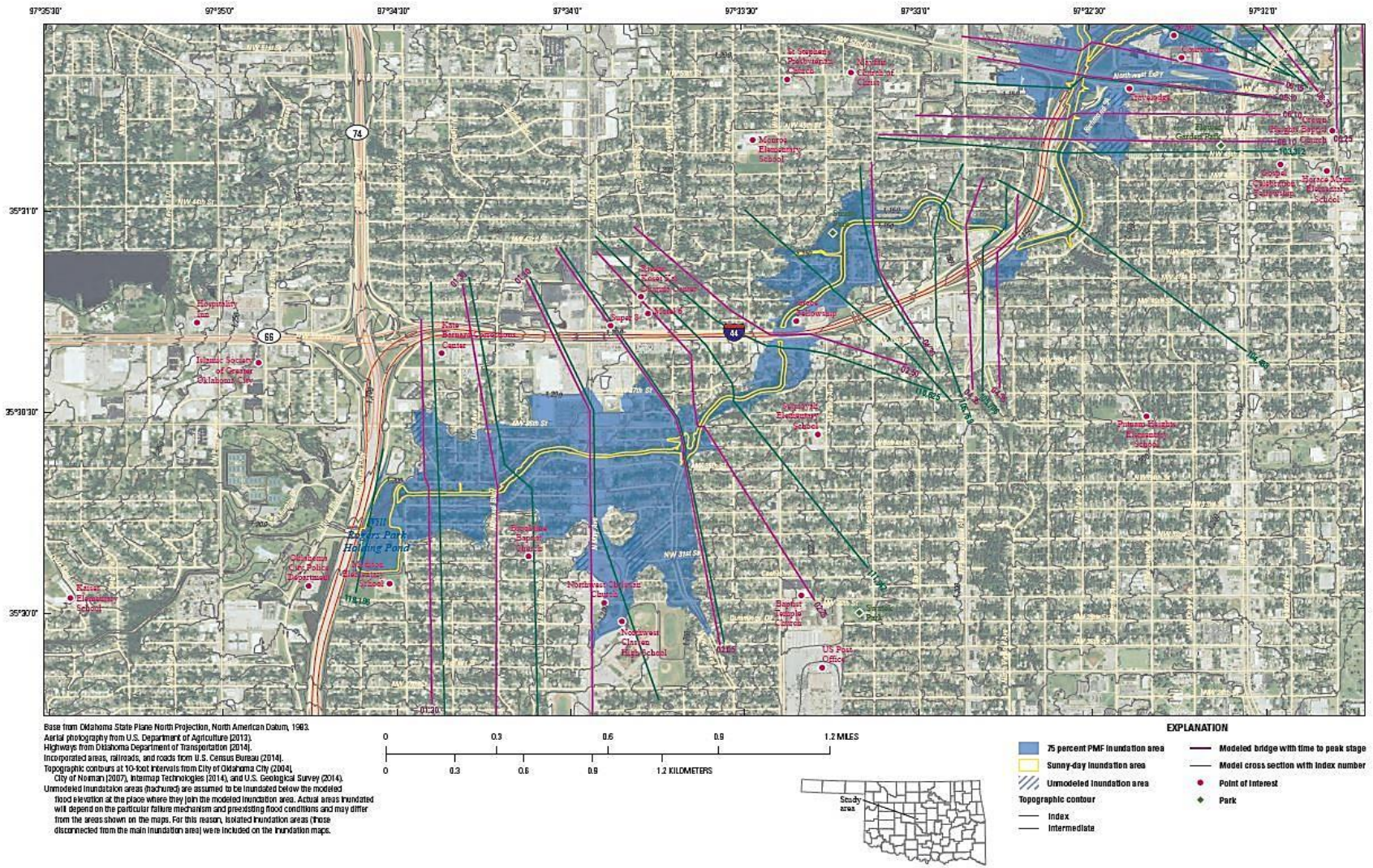

Figure B.11.1. Inundated area for Will Rogers Park Holding Pond. Map of the inundated areas for both 75% PMF and sunny day dam breach scenarios for Will Rogers Park Holding Pond. Times to peak stage for 75% PMF breach scenario at modeled bridges, as well as points of interest are shown. Figure courtesy of U.S. Geological Survey.

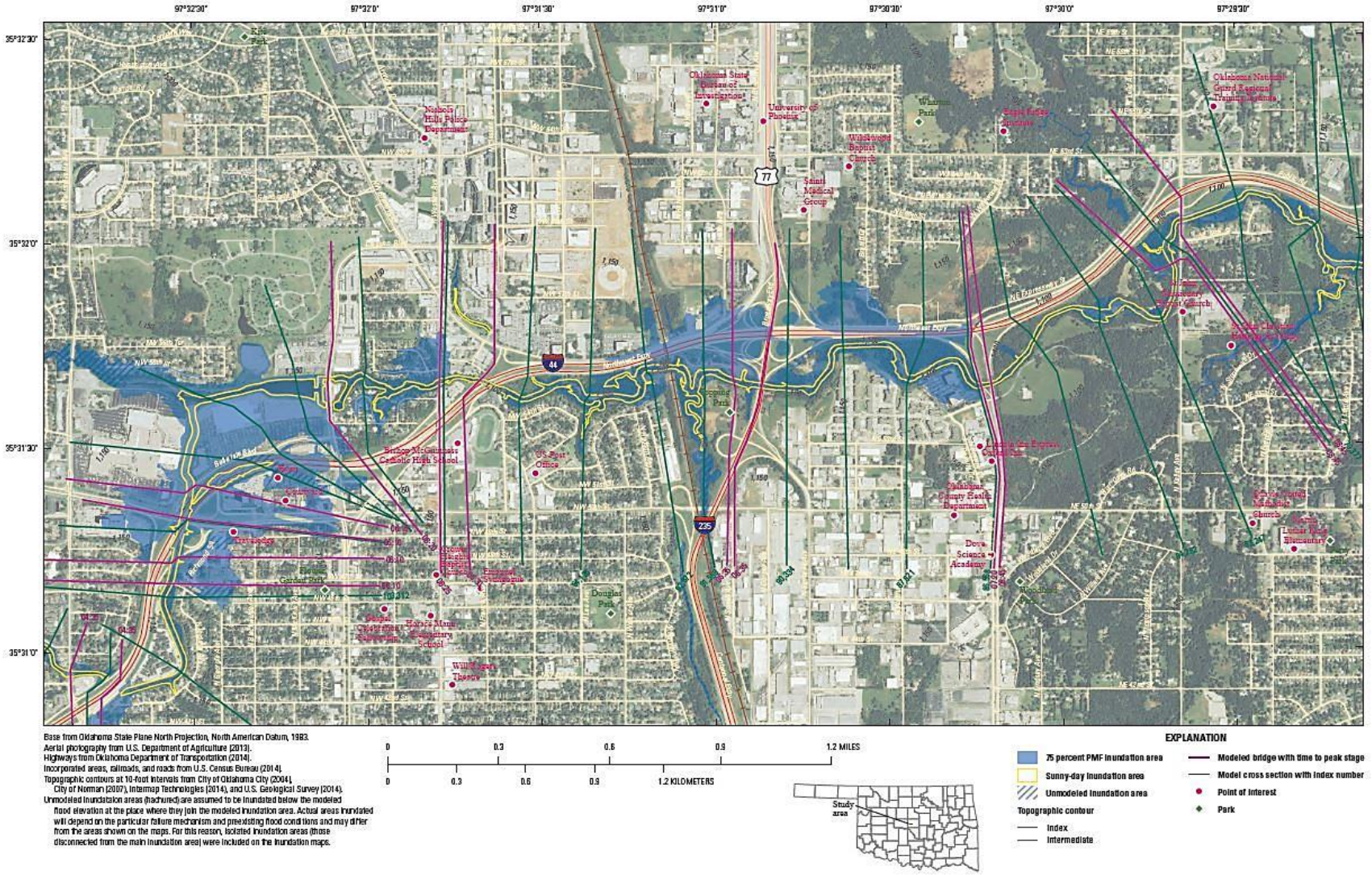

Figure B.11.2. Inundated area for Will Rogers Park Holding Pond. Map of the inundated areas for both 75% PMF and sunny day dam breach scenarios for Will Rogers Park Holding Pond. Times to peak stage for 75% PMF breach scenario at modeled bridges, as well as points of interest are shown. Figure courtesy of U.S. Geological Survey.

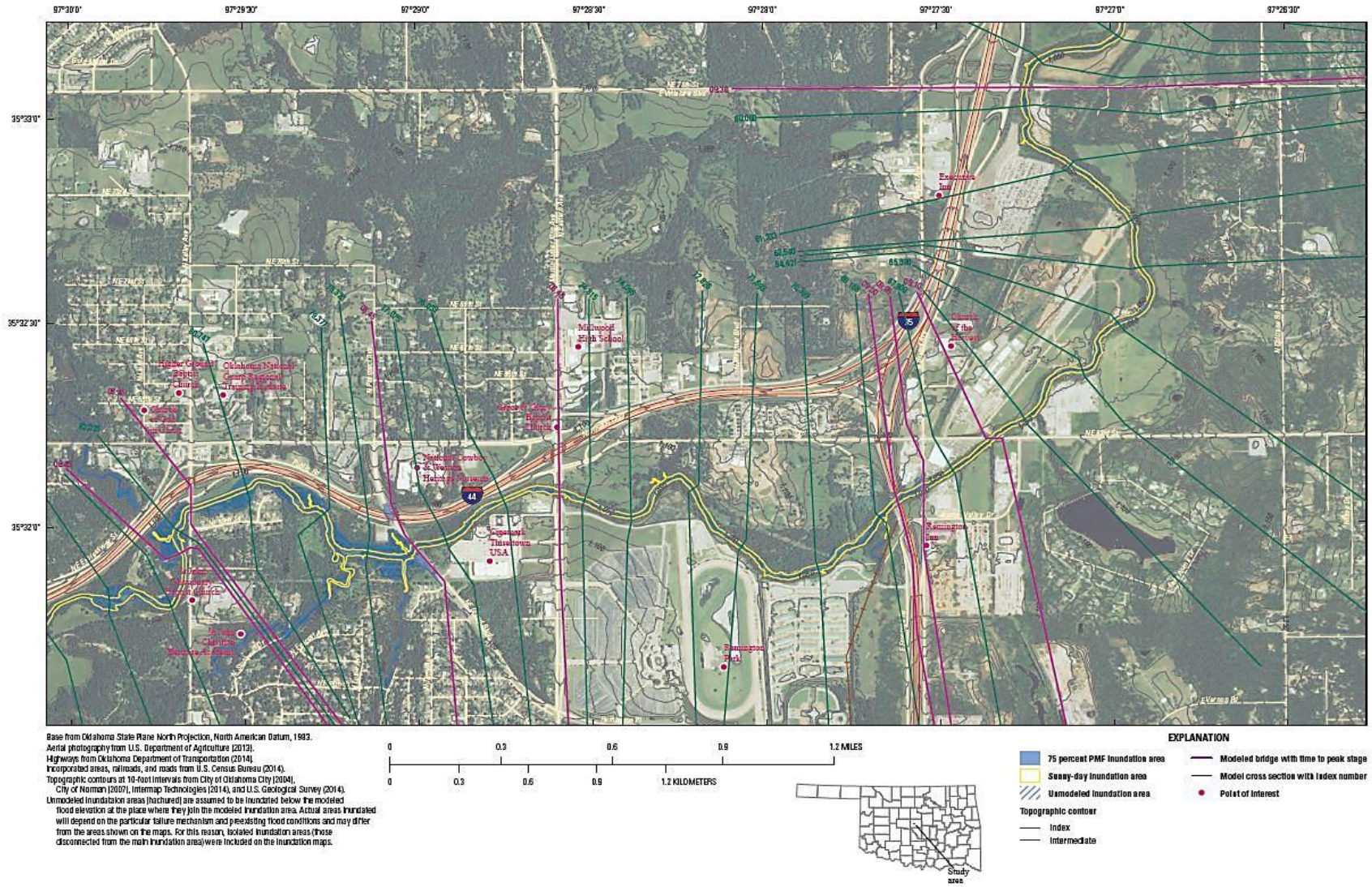

Figure B.11.3. Inundated area for Will Rogers Park Holding Pond. Map of the inundated areas for both 75% PMF and sunny day dam breach scenarios for Will Rogers Park Holding Pond. Times to peak stage for 75% PMF breach scenario at modeled bridges, as well as points of interest are shown. Figure courtesy of U.S. Geological Survey.

VITA

Molly Shivers

Candidate for the Degree of

Master of Science

Thesis: DAM BREACH STUDY AND INUNDATION MAPPING OF ELEVEN DAMS OWNED BY OKLAHOMA CITY, OK

Major Field: Environmental Science

Education:

Completed the requirements for the Master of Science in Environmental Science at Oklahoma State University, Stillwater, Oklahoma in May, 2016

Completed the requirements for the Bachelor of Science in Engineering Physics-Mechanical Engineering at University of Central Oklahoma, Edmond, Oklahoma in 2011

Experience:

2011-Present US Geological Survey

Hydrologist, *Oklahoma Water Science Center*

Collect surface water data

Compute, monitor, and review surface water data records

Author scientific reports pertaining to water related topics

Collect survey data related to water levels

Perform surface water measurements at flood stages and low flow stages for record and report purposes

2008-2011 US Geological Survey

Student Hydrological Technician, *Oklahoma Water Science Center*

Assist in the collection of surface water data

Assist in the collection of water quality samples and data

Assist in the collection of survey data related to water levels